The internal versus external dynamics in building the Andes (46°30'–47°30' S) at the Patagonia slab window, with special references to the lower Miocene morphotectonic frontline: a review

Jacques Bourgois, Jose Frutos, Maria Eugenia Cisternas

The internal versus external dynamics in building the Andes (46°30′–47°30′S) at the Patagonia slab window, with special references to the lower Miocene morphotectonic frontline: A review

Jacques Bourgois, Jose Frutos, Maria Eugenia Cisternas

PII: S0012-8252(21)00323-8

DOI: https://doi.org/10.1016/j.earscirev.2021.103822

Reference: EARTH 103822

To appear in: *Earth-Science Reviews*

Received date: 9 July 2020

Revised date: 7 September 2021

Accepted date: 26 September 2021

Please cite this article as: J. Bourgois, J. Frutos and M.E. Cisternas, The internal versus external dynamics in building the Andes (46°30′–47°30′S) at the Patagonia slab window, with special references to the lower Miocene morphotectonic frontline: A review, *Earth-Science Reviews* (2021), https://doi.org/10.1016/j.earscirev.2021.103822

The Internal versus external dynamics in building the Andes (46°30'-47°30' S) at the Patagonia slab window, with special references to the lower Miocene morphotectonic frontline: a review

Jacques Bourgois[a,*] jacques.bourgois@sorbonne-universite.fr, **Jose Frutos**[b], **and Maria Eugenia Cisternas**[c]

[a] *Sorbonne-Université, CNRS-INSU, Institut des Sciences de la Terre Paris, ISTeP, F-75005 Paris, France.*

[b] *SanJuan de Luz 4060, Providencia, Santiago, Chile.*

[c] *Instituto de Geologia Economica Aplicada, Universidad de Concepcion, Chile.*

[*] **Corresponding author at:** Dr Jacques Bourgois Université Pierre et Marie Curie, Institut des Sciences de la Terre Paris, ISTeP, 4 place Jussieu, Tour 46-00, 2ème étage, 75252 Paris Cedex 05 – France.

Abstract

New fieldwork and tectonic analysis has been carried out along the Andean morphotectonic frontline between 46°30' and 47°30'S. The right lateral transtensional Marques-Zeballos Pass fault system (MZPRS) controlled the 800-1200 m uplift of the Andes at 16.1-18.1 Ma. Our data and analysis indicate that there was no lower Miocene contractile event along the Andean morphotectonic frontline. The Main Andean Thrust (MAT), which is deeply rooted in the upper crust is a retroarc thrust dipping 10-15° westward, and provides evidence for major crustal shortening at ~120 Ma. At that time the arc volcanic strata of the Ibañez Fm (148-178 Ma) was transported eastward above the rift volcanic Quemado Fm (144-179 Ma), which lies unconformably on the Deseado basement massif.

The geologic records from the fieldwork together with the available data allow us to identify the processes controlling the dynamic evolution of the two main topographic features of the studied Andean segment. (1) Upward convection originating from the subducted South Chile Ridge -1 segment (SCR -1) is dynamically sustaining the high topography of the North Patagonian Icefield (4070 m at the Mt San Valentin, ~2 km higher than the Southern South Volcanic Zone). This, together with the locus of maximum moisture being at 47°S during glacial events has resulted in producing the two largest glacial lobes of Patagonia. (2) The 180 km long, E-W trending antiformal arch structure of the Mt Zeballos Ridge (MZR, a hinge zone trending N-S along the MZPRS) straddling the Andes and the Foreland is proposed to be the morphological "twin" of the South American Plate Moho Plateau (SAM MOHO P). The SAM MOHO P controls the location of both the MZPRS and the MZR boundaries location through time. The Patagonia Slab Window and SAM asthenospheric dynamics (upward and corner flows, respectively) and their in-depth interaction appear to control the morphotectonic evolution of the whole studied segment through a powerful feedback loop between tectonics, morphology, and climate, at least for the past 3-4 Myr.

Keywords: Slab window, Patagonia, Andean frontline, orogenesis, morphotectonic, uplift dynamics

1. Introduction

The internal dynamics related to the Patagonian Andes uplift may originate from two deeply different processes, internal or external: that is, tectonic, climatic or both. One of the main targets of this paper is to disentangle the processes at the origin of the dynamics of the Andean uplift, focusing on the past ~30 Myr of the segment extending from 46°30' to 47°30'S.

The Patagonian Slab Window (PSW, Table S2, acronyms) developed in relation to the South Chile Ridge subduction during the past 13—14 Myr (Dickinson and Snyder, 1979; Leslie, 1986; Cande and Leslie, 1986; Thorkelson and Taylor, 1989; Mpodozis et al., 1985; Flint et al., 1994; Bourgois and Michaud, 2002; Breitsprecher and Thorkelson, 2009; Russo et al., 2010a and b; Russo, 2012; Bourgois et al., 2016a; Rodriguez and Russo, 2020) and has been considered to play a major role in controlling the upper plate structure and backarc volcanism (Ramos and Kay, 1992; Bourgois et al., 1996; Gorring et al., 1997, 2001, 2003; Brown et al., 2004; Lagabrielle et al., 2004; Ramos, 2005; Guivel et al., 2006). The studied segment of the Andes located above the PSW (Fig. 1) exhibits widespread uplift, and its origin is strongly debated. From carbon and oxygen isotope analysis, Blisniuk et al. (2005) documented 1 km surface uplift of the Andes at ~16.5 Ma, based on the onset of aridity in the eastern foreland. The most likely reason invoked for this surface uplift is the underthrusting of foreland continental sediments associated with the onset of the lower Miocene Patagonian Fold and Thrust belt. The inverted unroofing sequence in foreland sediment (Ramos and Kay, 1992; Lagabrielle et al., 2004; Guillaume et al., 2013; Ronda et al., 2019; Encinas et al., 2019) supports this assumption. The studied segment is recognized as the northern continuation of relations described south of 49°S some 200 km along strike to the south (Ramos, 1989; Fosdick et al., 2011 and 2013; Ghiglione et al., 2016, 2019) and north of 46°S approximately 60 to 100 km to the north (Folguera and Iannizzotto, 2004; Folguera and Ramos, 2011; Butler et al. 2020). However, the main shortening event is generally accepted as having occurred at ~16—17 Ma, which was approximately 9—12 Myr after the onset of PSW development along the studied segment at 5—7 Ma.

Glaciations have been suggested as a significant control on the origin of mountain building (e.g., Montgomery, 1994; Berger et al., 2008; Whipple, 2009). In the Andes, dynamic processes would have acted in two different ways. (1) Thomson et al. (2010) presented low

temperature thermochronological data from the Patagonia Andes. From 38° to 49° S the data suggest a marked acceleration in erosion coeval with the onset of major glaciations at 5—7 Myr ago (Caldenius, 1932; Mercer, 1976; Mercer and Sutter, 1982; Coronato et al., 2004; Rabassa et al., 2005). From 49° to 56° S, much lower erosion rates exist despite the strongest glacial conditions there since the latest Miocene. Thomson et al. (2010) thus concluded that the southern Patagonian Andes grew and increased in elevation due to regional glacial protection. (2) Near latitude 50° S, Clague et al. (2020) noted the high elevations of upper Pliocene tills relative to Middle and Late Pleistocene moraines in the area of glacial lakes. These moraines are coeval with the increasing intensity of glaciations over the past 3.7 Myr. They argued that a series of Lower and Middle Pleistocene glacial lobes formed and deepened the great glacial lake trenches, while high meseta remained high above the glacial lakes. This is the "till meseta paradox" as discussed in Kaplan et al. (2009) and Anderson et al. (2012). They suggested that the volume of ice involved in the late Pliocene advances would have been smaller than that sourced from the Andes during the Middle and Late Pleistocene resulting in renewed uplift of the Andes.

Recently, using 10 Be dating on dropstones along General Carrera-Buenos Aires (GCBA) lake, studies (Bourgois et al., 2016 b and c, and Bourgois, 2019) quantified the magnitude of regional glacial rebound. The lake area uplifted at a rate between 15 and 33.5 $mm.yr^{-1}$ during the past 7.9 ± 1.1 ka. Between 2003 and 2006, GPS measurements were conducted in an area located between 48° and 49°30'S (Dietrich et al., 2010). These documented a vertical uplift rate of 39 $mm.yr^{-1}$ on the same order of magnitude as those documented at GCBA Lake.

This paper focuses on detailed fieldwork conducted along the eastern front of the Andes (46°30' to 47°30'S) extending from GCBA to Cohrane-Pueyrredon (CP) lakes. A review of previous studies and ideas integrated with new tectonic and morphological analyses allows us to reconstruct the dynamic evolution of this key area for the past ~30 Myr. Two main issues

are identified. (1) The relative role of external (repeated glacial) events and internal (PSW development) geodynamic processes in constructing the Andes is evaluated for the past 5—7 Myr. The E-W trending Mt Zeballos Ridge (MZR) located between the overdeepened GCBA and CP glacial lake trenches (GCBAGL and CPGL trenches hereafter) are pervasive morphotectonic features (Fig. 2). Local glacial faulting has influenced the evolution of the orogen for the past ~400 kyr. (2) An 800—1200 m high scarp defines the Andean morphotectonic frontline. This N-S trending morpho-structural element cuts across the E-W trending MZR together with its bordering GCBAGL and CPGL trenches. Major transtensional relay ramps and associated overlapping faults of early Miocene age characterize the tectonic signature of this Andean frontal zone.

2. Background

2.1. Geologic framework

The Andes east of the NPI show volcanic and sedimentary rocks with ages ranging from Paleozoic to Holocene (Fig. S1). A regional main unconformity (MU1) separates the Mesozoic-Cenozoic rock sequences from the underlying Paleozoic metamorphic basement. This includes the Andes and Andean foreland, which developed to the east. Geologic units and formations extending throughout this area are abundantly described (more details in File S1, Fig. S1, S2, and S3).

In the study area (Fig. 3), shallow marine deposits of the Austral Basin exhibiting typical oyster beds and associated marine faunas of lower Miocene age exist. These have been found (Fig. S4) in two different situations, including the El Chacay Fm along the foothills of the Andes and the Guadal Fm West of the Andean front (in the MCC and CB). Along the foothill zone (46°30’ to 48°S) the El Chacay Fm (Fig. 4) has been dated at 18.1 to 20.3 Ma (Cuitiño et al., 2015). These data compliment a 22.4 ± 0.7 Ma age (Blisniuk et al., 2005) for the

underlying fluvial deposits of the Centinela Fm and a maximum age of 16.05 ± 0.4 Ma age for the overlying fluvial deposits of the Santa Cruz Fm (Boutonnet et al., 2010). Along the Zeballos Pass and to the north (east of the Meseta de Chile Chico), the lower Miocene unit exhibits the following sequence from base to top: the fluvial deposits of the Centinela Fm, shallow marine El Chacay-Guadal Fm, red fluvial sediment of the Rio Jeinimeni Fm, and grey fluvial deposits of the Zeballos Pass Fm. In the Cosmelli Basin (Flint et al., 1994; De la Cruz and Suarez, 2006; Encinas et al., 2019), the fluvial sediment of the Pampa Castillo Fm (Fig. 4) overlying the oyster beds –i.e., the Guadal Fm– along the Cosmelli Basin, provide an 18.7 ± 0.3 Ma age (Folguera et al., 2018). This is in good agreement with the 19.8 ± 0.4 Ma age from the Guadal Fm (Encinas et al., 2019). Compared with the foothill area, the regression in the Cosmelli Basin area occurred from 0.5 to 0.9 Myr earlier. The maximum age for the fluvial deposits overlying the El Chacay-Guadal Fm is 14.5 to 18.1—18.7 Ma (Fig. 4). The onset of basaltic volcanism that characterizes the foreland area is 14.5—16.5 Ma in age (Boutonnet et al., 2010). Along the study area, several volcanic pulses in the MCC and MLBA exist (Fig. 4 and Table S1). These are coeval with glacial episodes, at least during the past 5—7 Ma. Mt Zeballos (MZ), the highest point (2700 m) of the study area, is a major volcano (1.7—4 Ma) located west of the MLBA (foreland area).

2.2. Patagonia slab window (PSW)

In a recent review paper, Bourgois et al. (2016a) provided the up-to-date constraints on the geodynamic and tectonic evolution of the Chile Triple Junction (CTJ) area. In addition to evidence regarding ophiolite, volcanic flows (Forsythe et al., 1986; Bourgois et al., 1993; Lagabrielle et al., 1994), and adakite-like emplacement during the Pliocene-Quaternary, ridge-jump events and microplate differentiation related to the subduction of the South Chile Ridge 0 (SCR 0) and SCR-1 segments have been documented (more details File S2).

Additionally, Bourgois et al. (2016a) documented kinematic inconsistences in the

development of the Patagonia slab window. A 110 km westward jump for the SCR-1 spreading segment occurred at ~6.5 to 6.8 Ma, which allows locating the SCR-1 segment beneath the NPI.

Although they are morphologically unconnected, the north-south trending NPI and South Patagonia Icefield (SPI, Fig. 1) are aligned, suggesting a possible common origin. Whereas high volcanoes are the backbone of the SPI, no volcanic edifice exists along the NPI. The Upper Cretaceous Andean batholith intruding Paleozoic metamorphic basement is the backbone of the NPI, which coincides with a volcanic gap (Fig. 1; DeLong et al., 1978, 1979; Ramos and Kay, 1992; Kay et al., 1993). Adakite volcanic flows from the Austral Volcanic Zone (AVZ) bear the partial melting signature of the subducted Antarctic slab edge (Stern et al., 1984; Martin, 1987; Stern and Kilian 1996; Sigmarsson et al., 1998). The ridgeline of the SPI follows the western boundary of the Patagonia slab window at depth (Fig. 1). As it crosses the Esmeralda FZ from south to north, the subducted Antarctic slab edge is bent westward toward the Golfo de Penas coastline (Russo et al., 2010 a and b; Bourgois et al., 2016 a), suggesting slab tearing at depth. Combining the common conversion point (CCP) stacking method with H-k crustal thickness estimates, Rodriguez and Russo (2020) provided a crustal thickness map for the forearc-backarc area of the CTJ region extending from 43°30' to 48°30'S. This key work is discussed in greater detail in Section 4.2.1.1.

2.3. Paleoclimatic background (more details in File S3**)**

Recently, Clague et al. (2020) documented 14 glacial events spanning the 1.1—3.7 Ma period. These events included the Great Patagonian Glaciation (GPG), which occurred prior to 1 Ma (Kaplan et al., 2009), during OIS 30—34 (1.016 to 1.168 Ma, Rabassa et al., 2005). After the GPG, succeeding glaciations were less extensive. Detailed studies have been conducted along the GCBA (Singer et al., 2004; Kaplan et al., 2004, 2005; Douglass et al., 2006) and CP (Hein et al., 2009, 2010, 2011) glacial lakes that allow reconstruction of the

precise chronology and evolution of the main frontal moraines during the past ~1 Myr.

During the LGM at 19—27 ka the Patagonian ice cap extended 1800 km along the Andes (Hollin and Schilling, 1981; Porter et al., 1992). From Cape Horn at 56°S to Chiloe Island at 42°S, the ice field totally covered the Andes from the Argentinean Andean piedmont to the Pacific shoreline. The last glaciation ended with massive collapse of ice lobes during the Antarctic Cold Reversal (ACR) at 12.9 to 14.5 ka (Bourgois et al., 2016; Bourgois 2019). Since that time, the ice cap retreated to its present distribution, restricted to the NPI and SPI.

Therefore, along the studied segment, between 46°30' and 47°30'S, we infer that the succession of glacial-interglacial cycles exhibited two different periods: (1) a glacial period with low river output to the Pacific, water being mainly drained to the Atlantic in response to a several km thick ice cap accumulation, and (2) a warmer period during which the ice cap retreat allowed the Patagonian Andean piedmont to be drained toward the Pacific Ocean crossing the Andes (Fig. 2).

Along the NPI, the precipitation maximum coincided with the maximum elevation of the Andes during glacial periods (Fig. 1). This resulted in hosting the most prominent glacial lobes. Accordingly, the GCBA and CP glacial lakes are the deepest in the Patagonian Andes. The corresponding trenches afford excellent exposures of the deepest structures of the "Andean fold and thrust belt".

2.4. Morphological framework

Along the 44°30'-49°30'S Andean segment, the first-order morphotectonic elements exhibit a complex organization (Figs. 1 and 2) including a western area (west of ~73°W) with major relief trending north-south and an eastern area with major glacial lakes oriented in an approximately east-west trending direction, normal to the dominant structural grain.

The western area consists of two main morphotectonic units: (1) the Chiloe Block, bounded to the west by the subduction front, is moving northward at a rate of 6.5 mm.yr-1

along its eastern boundary (Wang et al., 2007), which is the right lateral-transtensional Liquine Ofqui fault system (LOFS, Fig. 1; Cembrano et al., 2000; Thomson, 2002). The evolution of the Golfo de Penas pull-apart basin (GPPB, Fig. 1) located in the wake of the Chiloe Block constrains the onset of the LOFS. The associated northward drifting of the Chiloe Block began during the middle Eocene (Forsythe and Nelson, 1985; Bourgois et al., 2016a), long before the onset of the SCR collision at 13—14 Ma. At current rates, the Chiloe Block would have moved ~260 km to the north during the past 40 Myr, accommodating part of a northward component of NAZ-SAM plate convergence. (2) The NPI (4070 m) located along the PSW-induced volcanic gap (DeLong and Fox, 1977; Ramos and Kay, 1992; Kay et al., 1993) is in the southward projection of the Southern South Volcanic Zone (SSVZ, D'orazio et al., 2003) and the northward projection of the Austral Volcanic Zone (AVZ, Fig. 1; Stern and Kilian, 1996). The SSVZ, NPI and AVZ comprise the north-south trending morphological backbone of the Patagonian Andes. This north-south trending alignment of the highest local relief exhibits two major anomalies: (i) north of the NPI, an abrupt decrease in relief exists at the latitude of the Chile Triple Junction (46°09' S; Bourgois et al., 2000), and (ii) south of the NPI, a 100—150 km long depressed zone exists between the NPI and SPI. Both anomalies might have resulted (Georgieva et al., 2016) from partitioning of oblique plate convergence due to the SCR collision, which in turn might have induced the northward translation of the NPI tectonic block dragged by the northward moving Chiloe Block (Fig. 1).

East of 73°W, an east-west trending pervasive morphological segmentation characterizes this segment of the Andes (Fig. 2). This includes the deep trenches (Murdie et al. 1999) of the GCBA and CP glacial lakes at 550 and 350 m below sea level respectively, and the MZR elongated ridge. Both the GCBA and CP lakes and the MZR extend more than 100 km on either side of the Andean morphotectonic frontline. The GCBA and CP lakes belong to the same Rio Baker watershed that drains the Andean foreland bypassing the Andes toward the

Pacific. The LGM frontal moraine controls the Pacific-Atlantic divide (Willett et al., 2020) between the Rio Baker (Pacific) and Rio Deseado (Atlantic) watersheds (Fig. 2). The Andean morphotectonic frontline, as defined by Colwyn et al. (2019), shows no significant morphologic signature as it crosses the GCBAGL and CPGL trenches (Fig. 3). The ~2 km deep trenches excavated by the GCBA and CP glacial lobes are potential windows into the deep structure of what is commonly called the "Andean fold and thrust belt". The Andean morphotectonic frontline crosses the MZR following the deep Rio Jeinimeni glacial valley and then connects southward to the Rio Zeballos-Rio Ghio valleys (Fig. 3), referred to as the Zeballos Pass corridor hereafter. These areas including the MCC eastern front are deeply obscured by lateral ice lobe scars, screes, moraines, tills, and lake sediment. Although scarce, localized outcrops expose key tectonic features that allow reconstruction of the regional geodynamic evolution.

2.5. Previous studies

2.5.1. Ibañez and Quemado Fms

Because they clearly have similar ages, volcanic flows of the Ibañez Fm (Chile) are commonly considered to be an internal equivalent of the Quemado Fm (Argentina). Between Las Posadas Lake and the southern MLBA (Fig. 3), the acidic lavas of the Quemado Fm exhibit flat lying beds intensely fractured by vertical faults and joints. To the north (Fig. S3), the volcanic tuffs of the Upper Rio Tarde Fm unconformably overlie the Quemado Fm, documenting a depositional hiatus of 32 Myr. In contrast, the Ibañez Fm located west of the Andean morphotectonic frontline (Fig. 2) exhibits a cover of marine sediments (Fig. S1), including the Toqui, Katterfeld, and Apeleg Fms (120—145 Ma, Chile) and the Springhill, Rio Mayer, and Rio Belgrano Fms (~122—140 Ma, Argentina). Moreover, the calc-alkaline volcanic strata (i.e., subduction-induced) of the Ibañez Fm and the acidic lava and volcaniclastic rocks formed under a rifting regime (i.e., Gondwana breakup) of the Quemado

Fm originated in different geodynamic environments (see below). The Andean frontline in recent times therefore defines a sharp boundary between two domains exhibiting major differences in their evolution prior to ~120 Ma. Contrasting histories together with the contrasting morphologic signature of the Ibañez and Quemado Fms suggest that they were juxtaposed by convergent tectonic motion. Whenever in contact, the Ibañez and Quemado Fms tectonic deformation styles (see below) are discordant and in tectonic contact, and show an unconformity prohibiting a direct stratigraphic relationship from being established between them. Below, our geologic analysis indicates that convergence between the foreland (Quemado Fm) and Andean (Ibañez Fm) sequences occurred at ~120 Ma (Fig. S2).

2.5.2. Lower Miocene Fold and Thrust Belt

Most previous work along the studied segment has described or implicitly considered that a fold and thrust belt of lower Miocene age exists at the front of the Andes. Thrust faults associated or not associated with deep-seated detachments are regarded as thin-skinned structures, which began developing during the Aptian-Albian and continued throughout the Late Cretaceous and Tertiary. A westward-dipping detachment related to the Jurassic tensional event was inverted during Andean deformation, as concluded in the work of Ramos (1989). His work underlies the core of most subsequent interpretations of the central Patagonian Andes, such as those by Gianni et al. (2015), Rojas Vera et al. (2015), Cuitiño et al. (2015), and Ghiglione et al. (2016). Following Echaurren et al. (2016), major detachments at depth may control the age and mechanism building of the orogen.

Along these lines, Ronda et al. (2019) presented kinematically restored cross-sections of the study area. Emerging structures branching downward to deep-seated (5—10 km) contractional decollements include the Lago Posadas and Zeballos Pass front zones together with the El Bagual, Sierra Colorada, and Jeinimeni faults (Fig. S5). These are the key sites commonly cited in support of the main contractional tectonic event of lower Miocene age

thought to control the main Andean uplift. Because one of the main targets of this paper is to disentangle the processes in the origin of the dynamics of Andean uplift during the past ~25—30 Myr, detailed fieldwork including mapping and tectonic analyses was conducted along each of these structures.

3. Fieldwork and data

3.1. Lago Posadas, Pueyrredon, and Cochrane lake area

This area exhibits the main thrust fault systems (Fig. 3) proposed to be key structures of the "Andean fold and thrust belt" (Ronda et al., 2019). Two of these fault systems include (1) the Furioso River thin-skinned structure (h Fig. S5) described as a tectonic wedge thrusting Paleozoic basement to the west over the Cretaceous sediment (97—140 Ma) to the east; (2) the El Bagual fault, which forms the i boundary (Fig. S5) to an unnamed tectonic wedge located between Colorada Range and Pueyrredon Lake. Our tectonic analysis of these two structures reveals major discrepancies with previous interpretations. These results rise from geological evidence at two different scales, regional and local.

3.1.1. Andean frontline from Lago Posadas to Cochrane lakes

Ronda et al. (2019) described the western boundary of what they called the "Furioso River Thin-Skinned Structure" (FRTSS, Fig. 5) as a thrust fault (point e, Fig. S5). This fault was proposed to be located along the regional unconformity between the Paleozoic metamorphic basement and Quemado Fm (Fig. S5). In addition, Ghiglione et al. (2015) and Barberon et al. (2015) described the same Paleozoic metamorphic basement thrusting eastward over the Quemado Fm. Along the Rio Oro (Fig. 5); no evidence exists (Fig. 6) in support of these putative observations. At this site, the Ibañez Fm (Fig. S6) unconformably overlies the Paleozoic metamorphic basement (MU1). In the same area, Ronda et al. (2019) described the eastern boundary of the FRTSS as a westward-dipping thrust fault (point h Fig. S5) bounding

the Ibañez Fm (instead of the Quemado Fm, see above) over the Springhill, Belgrano and Rio Tarde Fms.

Detailed mapping and reconstructed cross-sections of this area (Figs. 5 and 6) show a different structural organization. Along the Rio Oro (Fig. S6), the Paleozoic metamorphic basement lies unconformably beneath its volcanic-sedimentary cover (Ibañez, Springhill and Belgrano Fms) dipping 70—80° eastward. These steeply dipping beds are part of an asymmetrical frontal fold (Figs. 7 and 8), which exhibits a long flat inward flank and a short steeply dipping outward flank. To the east, the Upper Cretaceous Rio Tarde Fm, which unconformably overlies Lower Cretaceous beds (i.e., Springhill, Belgrano and Ibañez Fms) dips gently (3—4°) eastward (CC', Fig. 8). Along the FRTSS, no evidence exists for the Rio Tarde Fm together with its lower Miocene sedimentary cover underthrusting westward beneath the Andes (i.e., relief west of the Andean morphotectonic frontline, Fig. 2). Conversely, the westward projection of bedding allows the inference that these strata overlapped the Andean relief before being removed by erosion (Fig. S7). We interpret the locally steep dip of the Rio Tarde Fm as it approaches the Andean morphologic frontline to be related to north-south trending normal faults (Figs. 7 and 8) following the Rio Furioso. To the north (Fig. 5), along the Chile-Argentina border, the Jurassic Quemado Fm is underthrust beneath the Paleozoic metamorphic basement of the Andes. South of this area, the western and eastern shores of Pueyrredon Lake expose different rock facies: the Paleozoic metamorphic basement of the Andes to the west and the Quemado Fm to the east. The low dip (5—7° to the west) of the Quemado Fm projected westward suggests that the underthrust strata exposed along cross-section AA' (Fig. 6) extend southward to Las Posadas Lake. We assume that the underthrusting of the Quemado Fm beneath the Paleozoic basement exists at depth beneath the FRTSS. The Rio Tarde Fm thus lies unconformably over the Quemado Fm on one side and once overlapped Paleozoic basement on the other side that has since been

eroded away. The Rio Tarde Fm therefore seals the MAT that separates the Paleozoic metamorphic basement of the Andes from the Quemado Fm (foreland area). Available ages place the contractional deformation after 120—122 (youngest Ibañez-Quemado) and before 118—120 Ma (oldest Rio Tarde). The most likely age for the MAT is thus ~120 Ma.

3.1.2. El Bagual fault system

Ronda et al. (2019) proposed that the north-south trending El Bagual fault system (Fig. S8) is one of the main structures belonging to the lower Miocene "Frontal Thrust and Fold Belt of the Andes" (Fig. S5). They claimed that two associated antithetic faults (A and B Fig. S5) of the El Bagual fault system are connected downward to a main detachment at a depth of 5—6 km. More accurately, they described the El Bagual fault as a reverse fault dipping westward (B, Fig. S5). The following addresses questionable points arising from these interpretations.

The El Bagual fault system (Figs. 3 and S8) is an ~22 km long structure. It trends north south, extending from the southern access of the Zeballos Pass corridor to the Las Posadas Lake area (Fig. 3). This fault system is located 13 to 15 km east of the MAT, which extends along Pueyrredon Lake. The El Bagual fault system separates a western block from an eastern block lowered by several hundred meters. At a closer look, the El Bagual fault system consists of two major unconnected segments of slightly different orientation. From north to south, it includes the S1 and S2 segments (Fig. S8).

The S1 segment of the El Bagual fault system (Fig. S9) is ~12 km long extending from 47°10'21"S-71°49'30"W to 47°17'22"S-71°48'19"W. Trending north south, it dips 75—85° to the east. The S1 segment (Figs. S9 and S10) exhibits two subsegments S1A and S1B. The S1A subsegment exhibits structures indicating right lateral transtensional movement, such as right-stepping extensional bends, releasing bends and a tensional gash (Figs. S11 and S12). Since an intrusive body (Figs. S9 and S10) seals the S1A and S1B subsegments no direct connection exists between them. It is proposed that the corresponding intrusive material fills a

releasing bend along the right-lateral El Bagual fault S1 segment. The infilling volcanic material belongs to the Quemado Fm. We infer that no major displacement along the El Bagual fault S1 segment has occurred since 144—179 Ma. Moreover, a thick volcanic flow of the Quemado Fm seals the fault at the southern tip of the S1 segment, reinforcing our interpretation that it is mainly Mesozoic in age (Fig. S9).

The S2 segment of the El Bagual fault system (Fig. S13) is ~10 km long extending from 47°18'44"S-71°47'42"W to 47°23'28"S-71°47'16"W. It exhibits two subsegments S2A and S2B, from north to south. The S2B subsegment is a normal fault. A volcanic flow seals its northern tip in a similar way to that described for the S1B subsegment (southern tip). Subsegment S2A connects southward to a horst structure, and the eastward normal fault (i.e., subsegment S2B) is an approximate extension of the S2A subsegment. To the south the horst structure branches off into a complex graben structure.

3.1.3. Inferences

The Lago Posadas, Pueyrredon, and Cochrane lake area exhibits the following evidence: (1) the El Bagual fault system, which has evolved through tensional or transtensional tectonic events, is older than 144 Ma; (2) the Jurassic Quemado Fm (foreland area) underthrusts beneath the Paleozoic metamorphic basement of the Andes, and this major crustal thrust is the MAT; (3) the Rio Tarde Fm (~118 Ma) is sealing the MAT; (4) no evidence exists for the MAT involving sequences of lower Miocene age; and (5) the MAT is related to the major shortening event that allowed the Quemado and Ibañez Fms to be close to one another at present. The Quemado Fm was underthrust beneath the Ibañez Fm at approximately 120 Ma.

3.2. Southern Zeballos Pass corridor

The El Bagual fault system is in the southern prolongation of the north-south trending glacial corridor of the Zeballos Pass (Fig. S8). A flat glacial valley trending approximately east-west located east (Fig. 9) of the Paso Roballos border crossing (Chile-Argentina border)

separates the flat-lying volcanic beds of the Quemado Fm to the south from the north-south trending corridor heading toward the Zeballos Pass (Fig. 9). The Paso Roballos fault divides the lower Zeballos Pass corridor into western and eastern blocks. Strong bending of volcanic breccias along the fault (Figs. S14 and S15) indicates a dip-slip component toward the downthrown eastern block. Field mapping suggests a right-lateral component along this transtensional fault. To the north (i.e., north of the area covered by Fig. 9), the upper Zeballos Pass corridor extends to the Rio Ghio spring area, where it is covered by thick glacial sediment accumulations.

3.2.1. Paso Roballos and lower Zeballos Pass areas

The downthrown block located east of the Paso Roballos fault (Figs. 9, 10, and S15) shows the regional stratigraphic succession (foreland area) and the tectonic style of the local deformation (Fig. S3). The subhorizontal pyroclastic flows of the upper Rio Tarde Fm (97—112 Ma) disconformably overlie volcanic breccias of the El Quemado Fm (144—179 Ma) along the MU2 unconformity with a 32 Myr hiatus. Upsection another hiatus of ~20 Myr separates the Upper Rio Tarde Fm and Eocene basalt (45—57 Ma). These two formations are nearly horizontal and exhibit no angular discordance. Upward, the Oligocene-Miocene section exposed along the Zeballos Pass corridor exhibits the stratigraphic succession described above (Fig. 4). The main point to be highlighted (DD', Fig. 10) is the presence of the shallow marine El Chacay Fm (Fig. S4), indicating that this area, close to the Andean morphotectonic frontline, was at sea level between 18.1 and 20.3 Ma.

The stratigraphic accumulation (Fig. S3) described above is located at the eastern end of cross-section CC' (Fig. 10). To the west, a wedge of the Ibañez Fm (Y, Fig. 9) is trapped between the Upper Rio Tarde and the underlying El Quemado Fm. We assume that the Ibañez Fm wedge is a tectonic sheet. The tectonic organization shown in cross-sections BB', CC', and DD' (Fig. 10) is similar to that documented along Pueyrredon Lake, where the Rio Tarde

Fm is sealing the ~120 Ma MAT (Figs. 5 to 8). Imbricate thrusts and rock slices underline the MAT.

The Paso Roballos and Estancia Lago Bertrand transtensional faults (Fig. 9) bound a triangle-shaped wedge (in map view) located at the toe of the morphological frontline of the Andes (Sierra del Parque de Jeinimeni). This wedge shows the nearly horizontal El Quemado Fm (144—179 Ma) beneath folded Andean sequence strata (Ibañez Fm covered by shallow marine rocks of Berriasian to Lower Aptian age, ~120 to 145 Ma, Fig. S1). Indeed, the upper tectonic unit (Andean sequence) exhibits an antiform structure trending NW-SE, which is located between cross-sections AA' and BB' (Fig. 9). This indicates that tectonic denudation occurred underneath the upper unit. A tectonic decollement exists between the Quemado Fm (foreland sequence) and the overlying Ibañez Fm (Andean sequence). This decollement is considered the northward prolongation of the MAT identified along Pueyrredon Lake (Fig. 5, and AA' Fig. 6).

3.2.2. Active tectonics in the upper Chacabuco valley

The right lateral displacement of Pleistocene deposits by 2170 m identified along the Valle-Chacabuco fault (Figs. S16 and S17) makes establishing geological correlations between the Pueyrredon Lake (Fig. 5) and Paso Roballos-lower Zeballos Pass (Fig. 9) areas challenging (more details in File S4).

3.2.3. Alto Rio Ghio

3.2.3.1. Transtensional Andean frontline

One of the main geological features of the Alto Rio Ghio area is a pervasive sequence of sandstone beds, the Jeinimeni Fm, extending from one side to the other of the Zeballos Pass corridor (Figs. 11, S18, and S19). These beds trend NW for approximately 6 km and exhibit no interruption between Cerro Lapiz southeastward to the Sierra del Parque Jeinimeni. Only a north-south trending fault paralleling the Alto Rio Ghio River (Fig. 3) left-laterally offsets the

Rio Jeinimeni Fm (Fig. 11). East of the RN41 road, the Oligocene-Miocene sediments exhibit an almost complete sequence, which includes the Centinela, El Chacay, Rio Jeinimeni, and Zeballos Pass Fms, from base to top (Fig. 4). These formations show a local gently dipping homocline structure (Figs. S18 and S19). Bedding, which strikes N50°W, dips 20—25° toward the NE (cross-section DD', Fig. 9), and includes a prominent marker horizon of the shallow marine fauna (oysters and large numbers of shells) characteristic of the 18.1—20.3 Ma El Chacay Fm. Two thick sandstone beds that overlie the El Chacay Fm at the base of the Rio Jeinimeni Fm are key markers in the section. These two sandstone beds extend west of the Alto Rio Ghio River to the base of the Sierra del Parque Jeinimeni (point X, Fig. 11) coming into contact against the volcanic material of the Ibañez Fm. The fault at the slope break bounding the lower Miocene deposits and volcanic ash flows follows the Andean morphotectonic frontline (Fig. S19). Upslope, lower Miocene beds dipping 45° to the NE are displaced along an inferred fault located at the slope break: the transtensional Argentina-Chile Border fault 1 trending N25°E. Additionally, these lower Miocene beds rest above volcanic beds of the Ibañez Fm dipping 60° toward the NE. Moreover, to the west, the lower Miocene beds abut the Ibañez Fm at 1700 m elevation. Another fault should exist at this site: the Argentina-Chile Border fault 2. In the point X area (Fig. 11), no evidence exists for the lower Miocene beds undertnrusting beneath the Andean morphotectonic frontline.

A 1000—1500 m high cliff characterizes the Andean morphotectonic frontline extending from the upper Chacabuco Valley (Roballos pass area, 550 m in elevation, point X Fig. 9) to the area of point X (1500 m in elevation, Fig. 11). Three faults trending N25—30°E control the scarp. From S to N, these faults include the Estancia Lago Bertrand fault, Argentina-Chile Border fault 1, and Argentina-Chile Border fault 2. These three faults geometrically define an array of en echelon faults, allowing tectonic deformation to be relayed in a left-stepping sense. One of these faults, Estancia Lago Bertrand, is transtensional, exhibiting an E-W trending

extensional component (Fig. S20). We assume that tectonic deformation is transferred northward along Argentina-Chile Border faults 1 and 2. These rocks associated with the Estancia Lago Bertrand fault exhibit an en echelon fault arrangement. We propose that these faults are part of a right-lateral ramp system controlling this segment of the Andean morphotectonic frontline (see below).

3.2.3.2. Glacial deposits

The Alto Rio Ghio Valley is an ablation till plain edged on either side by steep rock-glacial tongues (Fig. S21). The relationship between these glacial formations and the volcanic basement suggests an age older than 4—6 Ma for the depression of the Zeballos Pass corridor (more details in File S5).

3.2.3.3. Inferences

It is accepted that the ~120 Ma MAT identified along Pueyrredon Lake extends along the lower Zeballos pass area. The Rio Tarde Fm unconformably overlies the Jurassic sequences that were tectonically deformed before ~120 Ma. The western boundary of the lower Zeballos Pass corridor exhibits lower Miocene beds (foreland) coming into contact with the Jurassic Ibañez Fm through a right-lateral relay ramp system located along the Andean morphological frontline. The Miocene beds are resting above the Jurassic Ibañez volcanic flows. No evidence exists for the Miocene beds underthrusting beneath the Andean front. The Upper Zeballos Pass corridor exhibits extensive glacial deposits. In the Alto Rio Ghio area, mafic dikes intruding into the Zeballos Pass Fm constrain a maximum age of 2.12 ± 0.45 Ma for the glacial deposits. Basaltic lava flows with an age older than 4.32 ± 0.23 Ma (Fig. S22) suggest that the depression of the alto Rio Ghio (Fig. S23) probably existed at that time

3.3. North Zeballos Pass corridor

North of the Zeballos pass, the Zeballos Pass corridor extends to the Rio Jeinimeni (Figs. 12 and 13). Thick ash flow deposits and major landslides heavily blanket the east and west sides of the corridor, respectively.

3.3.1. East Zeballos Pass corridor

Mt Zeballos (2726 m) located east of the Zeballos Pass corridor is the highest summit of a major volcano, Mt Zeballos Volcano. The associated volcanic flows and ash together with intrusive plugs have been extensively studied (Fig. 12). Mt Zeballos exhibits the morphology of a deeply eroded volcano, in which hypabyssal roots intrude older rocks, including the lower Miocene sediment of the Zeballos Pass Fm (Fig. S2d).

From the age compilation (Table S1), the MLBA volcanic accumulation exhibits three main volcanic complexes, including the Mt Zeballos volcanic complex (1.7—4 Ma), Cerro Overo (4.5—8 Ma), and Cerro Plomo (7.5—14.5 Ma) from youngest to oldest (Fig. 4). Glacial deposits including till regressive moraines that bound flat areas of polygonal and kettle morphologies cover the NW area of the MLBA (east of cross-section DD', Figs. 12 and 13). One of the pervasive morphological signatures is a dense network of small volcanic cones (ages ranging from 0.33 ± 0.01 to 1.39 ± 0.04 Ma; Brown et al., 2004; Table S1) scattered on the MLBA. The area covered by glacial deposits exhibits none of these small volcanic cones, which were removed by glacial erosion. This suggests a younger age for the frontal recessional moraines and subsequent remains from ice retreat. These glacial deposits covering the northwest area of the Meseta are assumed to be younger than ~1 Ma.

3.3.2. West Zeballos Pass corridor, Rio Lincoln fault

West, the Zeballos Pass corridor contains the deeply excavated Rio Lincoln valley (Fig. 14). Here, we see the only well-exposed relationship between the basement rock of the Sierra del Parque Jeinimeni and the lower Miocene Zeballos Pass Fm. At the RN41 bridge crossing the Rio Lincoln, the eastern morphological front of the range exhibits basalt flows of the

Ibañez Fm dipping 40—45° (DD', Figs. 13, and 14A). Upsection, following RN41 southward, the roadcut shows three ~10 m thick basalt flows, which increase in dip from 50 to 85° from west to east. Farther east, these basalt flows have a sedimentary cover dipping almost vertically. This detrital, well-stratified sequence is composed of 1 to 3 m-thick beds of sandstone. Sandstone beds assigned to the Lower Cretaceous (Apeleg Fm) are almost vertical. A few tens of meters to the east, the roadcut exposes the horizontal beds of the Zeballos Pass Fm. Both the Lower Cretaceous and Zeballos Fm outcrops extend downward from the road to the riverbed of Rio Lincoln with the same dip (Figs. 14B and C). At the riverbed, only 20—25 m separates the two formations, the Zeballos Pass Fm shows the same almost horizontal dip, and the Lower Cretaceous sequence remains almost vertical. The Zeballos Pass Fm layers projected to the west come in perpendicular contact with the Lower Cretaceous beds (Fig. 14 C). At this site, the Lower Cretaceous beds and Zeballos Pass Fm exhibit no significant internal tectonic deformation. No evidence for a fault exists. Hence, we interpret the contact to be a major unconformity. Moving southward, uphill toward the Zeballos pass, the western side of the RN41 road cuts through younger detrital sequences of the Zeballos Pass Fm. These beds remain almost horizontal (Fig. S25) and progressively onlap onto the Lower Cretaceous beds and then come into contact with the Ibañez Fm at the elevation of the Zeballos pass. Most likely, the Zeballos Pass Fm sediment (at least the upper section) appears to seal the Andean morphotectonic frontline. The fault bounding the Andes remains at depth beneath the lower Miocene sediment (i.e., the Zeballos Pass Fm) including along the Rio Lincoln riverbed (Fig. 14).

3.3.3. Rio de Las Nieves (W of Meseta de Chile Chico)

To the north, on the Chilean side (point X, Fig. 12), De la Cruz and Suarez (2008) proposed a major east-verging thrust fault located along the Rio de Las Nieves. The Ibañez Fm of the MCC was proposed to underthrust beneath the Ibañez Fm of the Sierra del Parque

de Jeinimeni. At point X, the almost vertical volcanic breccia of the Ibañez Fm from the Sierra del Parque Jeinimeni connects eastward to almost horizontal beds of the MCC (EE', Figs. 12 and 13). The general structure is an asymmetrical monoclinal fold exhibiting a short vertical limb associated with a long subhorizontal limb. This structure is similar to that existing along Rio Lincoln (DD', Fig. 13). A major anticline with an axis following the eastern side of the Sierra del Parque de Jeinimeni extends northward to the Chilean border, crossing the Rio Jeinimeni. This structure must involve a major decollement at depth ascribed to the MAT at ~120 Ma (previously identified at Cochrane Lake, see AA', Fig. 6). The Rio Lincoln fault inferred at depth along the Rio Lincoln area does not appear to extend to the north as a significant structure. No evidence exists for this fault extending along the Rio de las Nieves on the Chilean side, north of the Rio Jeinimeni.

3.3.4. Rio Jeinimeni segment (S of Meseta de Chile Chico)

Along the segment following the Rio Jeinimeni between the Rio de Las Nieves confluence and the Jeinimeni fault, the Mesozoic and Cenozoic sequences of the MCC gently dip southward (FF', Fig. 13). The Divisadero Fm (Rio Jeinimeni right bank, Fig. S2) unconformably overlies the Ibañez Fm and the Lower Cretaceous complex (Rio Jeinimeni left bank). Upsection to the south, the Divisadero Fm disconformably overlies Cenozoic volcanic-sedimentary cover, including the Lower Basalt, Ligorio Marquez Fms, and lower Miocene complex, which include the shallow marine sediment of the El Chacay Fm. It is proposed that this segment, trending N45-N55°E, is a ramp structure connecting the Rio Lincoln and Jeinimeni faults. Because the area along cross-section FF' (Figs. 12 and 13) is heavily covered by glacial sediment, the inferred ramp decollement has not been identified in the field. In any case, this area shows the so-called foreland sediment of lower Miocene age overlying the Andes (southward extension of the MCC south of the Jeinimeni River). At this site, no evidence exists showing that these foreland sediments underthrust the Andes.

3.4. Meseta de Chile Chico area

The Andean morphotectonic frontline along the eastern edge of the MCC (Figs. 15 and 16) exhibits different morphological signatures. To the south, it exhibits a scarp with elevations ranging from 1200 to 1400 m. To the north, the Andean front zone lowers from 500 m in elevation to 200 m toward the GCBA Lake shoreline. At Chile Chico, the Andes frontline extends northward below lake level (i.e., below 201 m in elevation). The MCC has been studied extensively. The main basic studies include those from Charrier et al. (1979), Espinoza et al. (2005), and Guivel et al. (2006). The sketch map (Fig. 15) is modified from the Chile Chico-Rio de Las Nieves Sernageomin map n°11 (De la Cruz and Suarez, 2008).

3.4.1. ~120 Ma Main Andean Thrust (MAT)

As in the Pueyrredon Lake area, the Chile Chico area is characterized by major volcanic activity that occurred during the Late Jurassic and Early Cretaceous. Elsewhere in Chilean Patagonia, the corresponding volcanic flows have been assigned to a single unit, the Ibañez Fm. In the Chile Chico area, dissimilarities in morphological signatures, tectonic style, and internal deformation allow the characterization of part of the Ibañez Fm as belonging to the Quemado Fm. The area west of Chile Chico exhibits an E-W trending major glacial scar fringing the MCC to the north (see locations in Figs. 3 and 15, and BB' Fig. 16). This main morphological boundary extending from Chile Chico to Lago Verde is located at approximately 46°35'S. North of this boundary is a low area characterized by a roche moutonnée morphology that was excavated by the GCBA ice lobe during the LGM. This deeply eroded area exhibits Upper Jurassic volcanic flows in thick effusive units that are alternatively red and green in color (Fig. 17). Major faults trending N20 to 30°E divide the area into five strips (Fig. 15) extending from the GCBA Lake shoreline to the E-W trending scar at 46°35'S. These strips and associated faults show no prolongation south of the morphological limit at 46°35'S. The strip located northwest of Chile Chico (Fig. 17) exhibits

the general signature of an almost horizontal stack of volcanic flows. Toward the SW, the dip of volcanic flows steepens gradually, reaching 20—25° close to the morphological limit at 46°35'S. In this area, bedding of volcanic flows strikes N20—30° W, making an angle of 60—70° with the E-W glacial scar bounding the MCC at 46°35'S. South of this scar, the MCC exhibits less organized volcanic ash flows of the Ibañez Fm. These ash flows exhibit two contrasting tectonic deformation styles, including a major frontal fold trending N15°E (DD' and EE', Fig. 16) and N-S trending faults, such as the Pedregoso fault (Fig. 15). These tectonic structures do not extend north of the morphological limit at 46°35'S.

The morphological limit bordering the MCC to the north follows a major tectonic boundary between the upper and lower tectonic units (Figs. 15 and 16). The lower part contains the Quemado Fm, and the upper part contains the Ibañez Fm. Compositional dissimilarities between these two tectonic units are similar to those described above, reflecting their different geodynamic origins: subduction-related (Ibañez Fm) versus Gondwana-breakup (Quemado Fm). A dike dated at ~95—115 Ma (Fig. 15) seals the main fault bounding the upper and lower units. This main fault is older than 95 Ma. It is the trace of the MAT identified in the Pueyrredon Lake area.

3.4.2. Jeinimeni fault zone

The N-S Jeinimeni fault zone (Fig. 18) bounding the MCC to the east is commonly accepted as being the Andean morphotectonic frontline. It is a major tectonic boundary. Indeed, the shallow marine El Chacay Fm of lower Miocene age is identified on either side of the fault at elevations ranging from 1300—1600 m to 300—500 m in the MCC and foreland areas, respectively. The northern segment of the Jeinimeni fault zone exhibits a maximum elevation of 1000 m. Southward; the fault trace diminishes in elevation, crossing the Rio Jeinimeni at 550 m. The Jeinimeni fault zone is inferred to be subvertical because of its linear map trace. Cross-sections CC', DD', and EE' (Fig. 16) show the structural relationship

between the MCC and the foreland area. Between DD' and EE', the Jeinimeni fault zone cuts across older tectonic structures of the MCC. These include a NNW-trending fold involving the Ibañez Fm and its shallow marine sedimentary cover of Lower Cretaceous strata (EE' Fig. 16). This suggests that no relationship exists between the tectonic origin of this specific fold of the MCC and the Jeinimeni fault zone. As proposed above, folding is likely associated with the main contractional event at ~120 Ma, while the fault is lower Miocene in age. Moreover it should be noted that the Jeinimeni fault zone shows no extension north of the Arroyo Marques.

The Arroyo Quebrada Honda exhibits the highly tectonized segment of the Jeinimeni fault zone (Figs. 18 and S26). To the west, the across-fault segment exhibits a stack of almost vertical imbricated tectonic sheets of the Ibanez Fm that are also exposed along Quebrada Chica. The N-S striking faults, which bound these tectonic slivers, are poorly exposed. However, sparse exposures have allowed the identification of two right-lateral strike-slip faults with striations with low pitches (<5—10°). In the same way, a clear dip-slip fault was identified with steep pitches of striations of ~80°. East of the highly tectonized segment, a tectonic lens exhibits volcanic-detrital sediment containing shallow marine faunas (B, Fig. 18). These indicate the 18.1—20.3 Ma El Chacay Fm was involved in the penetrative deformation of the highly tectonized segment of the Jeinimeni fault zone; therefore, the fault zone had motion that is younger than 18.1—20.3 Ma. The area in the middle of the Jeinimeni fault zone exhibits a steeply east-dipping stack of tectonic lenses, including units derived from the Centinela and Ligorio Marquez Fms (Figs. 4 and S1).

Immediately east of the highly tectonized segment of the Jeinimeni fault zone, the riverbed exposes three detrital beds of the Zeballos Pass Fm dipping 80° to the east (A and C, Fig. S26). At this site, the Zeballos Pass Fm exhibits no penetrative tectonic deformation. A contrast in the tectonic style thus exists on either side of the fault bounding the penetratively

deformed Jeinimeni fault zone to the west and the Zeballos Pass Fm detrital sequences to the east.

At less than 100 m to the east of the fault zone, the northern bank of the Arroyo Quebrada Honda River exhibits several mega sequences of the Zeballos Pass Fm dipping 3—5° to the east. An open knee fold (A and B, Fig. S26) allows connecting these gently dipping beds to the steeply dipping beds along the Jeinimeni fault zone.

The tectonic analysis of this area suggests that deformation along the Jeinimeni fault zone occurred in at least two phases. (1) The first phase was associated with a major right lateral transtensional tectonic phase after deposition of the El Chacay Fm. Most of the 800—1000 m uplift of the MCC (see above) probably occurred at that time. (2) As a result of (1), the accumulation of the fluvial Rio Jeinimeni and Zeballos Pass Fms was restricted to the foreland area. A moderate tensional tectonic phase occurred subsequent to Jeinimeni and Zeballos Pass deposition.

3.4.3. Chile Chico fault zone

The Chile Chico fault extends north and south of Chile Chico in an area mainly obscured by fluvioglacial deposits (Fig. 19). Toward the north, the fault morphological relief follows the rectilinear GCBA Lake shoreline. In map view (Fig. 17) the fault zone shows an elongated array of tectonic lenses with lengths varying from hundreds of meters to kilometers. The general trend of the fault traces are N20°W. The coastline cliff north of Chile Chico exposes 150 to 300 m of bare rock. Glacial polishing and striations obscure previous tectonic imprints, including fault planes and their potential kinematic indicators. The subhorizontal, thick volcanic flows of the Quemado Fm exhibit the tectonic style described above. This tectonic signature suggests that the fault developed in a tensional tectonic stress regime. South of Chile Chico, the fault zone is concealed beneath a GCBA Lake terrace (Fig. 19). Along the inferred trace of the Chile Chico fault zone, a 1 km-long vertical dike crops out (Fig. S27). De

la Cruz and Suarez (2008) suggested a 102—111 Ma age for this specific dike. Their estimate was based on a pervasive dike swarm that characterizes the Lago Verde area ten to twenty km west of Chile Chico. This dike swarm exhibits a mean age similar to that of the Chile Chico dike (Fig. 15). We suggest that the Chile Chico dike is a tectonic sliver involved in the Chile Chico fault rather than a post-tectonic feature.

3.4.4. Arroyo Marques relay ramp

South of Chile Chico, the Andean morphotectonic frontline shows a 4—5 km westward reentrant (Fig. 19). This reentrant coincides with the end of the Chile Chico and Jeinimeni fault zones to the south and north, respectively. The Arroyo Marques and Arroyo La Horqueta rivers drain this area, carving deep enough through the LGM glacial deposits to expose subglacial bedrock. At point X (Fig. 19A), the Arroyo Marques River shows subvertical beds of Eocene basalt faulted above the horizontal Quemado Fm. This basalt, located at the exact limit between the Andes and foreland area, is equivalent in age to the Lower Basalt Fm (MCC, the Andes) and the Posadas basalt (foreland). Following the Arroyo Marques River downstream, the left bank exposes the Centinela Fm, and the overlying 18.1—20.3 Ma El Chacay Fm dipping 45—50° toward N130°E (Fig. S28A). At the same site, the right bank exposes the Zeballos Pass Fm dipping gently to the south. Since the Lower Basalt and the lower Miocene Fms exhibit a regionally flat dip (i.e., throughout the MCC and foreland areas), their steep dip in areas X and Y (Fig. 19) is clearly associated with local tectonic structure. The tilted beds of the El Chacay Fm exhibit subpenetrative tectonic features localized in mudstone layers. Stretching features in these strata document a dip-slip component of movement toward the foreland area (Fig. S28B). The highly deformed zone exhibiting southward bedding steepening is 100—150 m thick. It appears to be associated with a major detachment dipping toward the foreland. Approximately 100 m to the south, the right bank of the Arroyo Marques River exhibits the flat lying Zeballos Pass Fm, showing no evidence for

significant internal tectonic deformation, including in mudstone layers. Projecting the bedding toward the left bank places the upper Zeballos Pass Fm in contact with the steeply dipping beds of the El Chacay Fm. This suggests two possibilities for the contact. (1) The upper sequence of the Zeballos Pass Fm unconformably overlies the previously deformed El Chacay Fm, or (2) an E-W trending normal fault (i.e., the El Manzano fault, Fig. 19) following the Arroyo Marques River juxtaposes the downthrown Zeballos Pass Fm to be in steep fault contact with the deformed El Chacay Fm. A mix of these two possibilities best fits the local tectonic constraints. The ~4 km-long zone of tectonic deformation following the Arroyo Marques River exhibits two different phases of faulting: an older one inducing almost penetrative tectonic features into the steeply tilted El Chacay Fm and related strata and a more recent one cutting across the previously tilted bed, faulting it against the Zeballos Pass Fm. The evolution of the Arroyo Marques fault zone thus appears to exhibit similarities with the two phases of deformation associated with the Jeinimeni fault zone. A main tectonic event occurred after deposition of the El Chacay Fm. Subsequently, all or part of the Zeballos Pass Fm with an age younger than 18.1 Ma escaped the penetrative deformation of the El Chacay Fm. Finally, the Zeballos Pass Fm was juxtaposed against the El Chacay Fm along a normal fault that accentuated the MCC uplift. These similarities in association with structural relationships suggest that the Arroyo Marques River segment is a relay ramp (Arroyo Marques ramp) connecting the overlapping Chile Chico and Jeinimeni fault zones. The right-lateral transtensional kinematics of the Arroyo Marques ramp system is derived from the transtensional deformation identified along the Jeinimeni fault zone and Arroyo Marques detachment kinematics.

Finally, no evidence exists showing the Cenozoic foreland sequences underthrusting the Andes. As in all areas described to the south, the Arroyo Marques ramp area shows lower Miocene sequences resting above the Andean sequences, not in the footwall of major thrust

structures. No major E-W convergence occurred between the foreland area and the Andes after the accumulation of the 34—57 Ma Lower Basalt Fm.

4. Discussion

The intricate morphology of the study area records superimposed major tectonic, climatic and geodynamic events that are difficult to decipher. The detailed fieldwork conducted along the Andean morphotectonic frontline has allowed us to synthesize previously acquired data and our own observations in a coherent regional context. PSW development in the wake of SCR subduction has induced major geodynamic reorganizations over the last 6 Myr. The tectonic uplift event at ~16.5 Ma is also a major step in reconstructing the proto-Andes. In parallel, water routing of the main drainage networks has persisted over time, at least from the early to middle Miocene. Moreover, regional drainage has been controlled through episodic cold events during the past 5—7 Myr. The following presents the external and internal geodynamic events and their signatures from the youngest to the oldest after first appraising the permanence of the drainage.

4.1. Water routing through time

The Rio Baker and the adjacent Rio Simpson watersheds drain large parts of the Andean foreland area and cross the Andes to their terminations along the Pacific coast (Figs. 2 and 20). These are antecedent drainage systems older than the uplift of the proto-Andes at ~16.5 Ma, which is a conservative statement. A key observation is that outflow from ice margin lakes in the foreland occurred toward the Atlantic during glacial periods. Conversely, end-moraines prevented outflow of the GCBA and CP glacial lakes to the Atlantic during the ice recession periods, the outflow occurring toward the Pacific. It is generally accepted that this pattern of drainage has been maintained throughout the Late Cenozoic glaciations (i.e., the past 5—7

Myr) during which a minimum of 24 cold events have occurred (Rabassa and Clapperton, 1990; Rabassa et al., 2005; Clague et al., 2020).

The Rio Simpson watershed (Fig. 20), located north of the PSW northern boundary (Fig. 1), potentially provides a model for the morphotectonic evolution of the Rio Baker watershed prior to SCR subduction. We suggest that the two watersheds may have evolved similarly before 5—6 Ma under the same climatic dynamics and tectonic regime. Additionally, the outlet channels of the Rio Baker and Rio Simpson watersheds (i.e., the Baker Canal and the Simpson Canal, respectively) exhibit morphological similarities. The Rio Simpson watershed connects to the Canal Simpson channel (45°30'07"S-72°08'17"W) along the eastern edge of the Patagonian batholith at 150 m in elevation. Because the Patagonian batholith is an ~1500 m high mountain ridge, the Canal Simpson channel lies along an antecedent drainage route to the Pacific Ocean. Similarly, the Canal Baker fjord crosses the high ridge of the Patagonian batholith at Caleta Tortel (47°47'44"S-73°35'05"W) at sea level.

Based on fission track analysis, Thomson et al. (2001) documented a 4 to 9 km total amount of denudation along the E-W trending 100 km-long Canal Baker fjord (Fig. 20). Although discussed by Christeleit et al. (2017), we consider that the pulse of denudation migrated from W to E along the fjord from the Pacific coastal area at 23—30 Ma until 14—18 Ma at Caleta Tortel. We consider the regressive incision at the riverbed of the Canal Baker fjord to be the response to the wave-like pulse of unroofing. This allowed the canal Baker to remain at a low elevation over time when crossing the high relief of the Patagonian batholith. At 14—18 Ma, as a minimum age, the Canal Baker was thus an active channel draining water from a catchment basin that extended east of Caleta Tortel. In turn, the Rio Baker watershed could be considered a model for the Rio Simpson watershed during the Miocene. We infer that the drainage of both the Rio Baker and Rio Simpson watersheds began flowing toward the Pacific at 14-18 Ma. By then, a river network flowing to the Pacific drained a wide area

east of the Patagonian batholith (backarc area) extending from 45 to 49°S. This drainage imprint has apparently persisted over time and has survived major subsequent geodynamic events, both external and internal, until the present. River and glacial lobe locations were inherited from a former drainage network dating back to the lower Miocene.

4.2. PSW development and glaciations, over the past 5—7 Myr

Two major geodynamic and climatic events likely influenced the regional morphology from the late Miocene (Messinian) to Holocene. These are the PSW development at depth and the alternation of climatic conditions from glacial to interglacial. A pervasive morphoclimatic signature was the repeated growth of large ice lobes that carved the deep trenches along the GCBA and CP glacial lakes (Figs. 2 and 3). Additionally, aggradation of Mt Zeballos Volcano (western MLBA, 1.7—4 Ma) and Pico Sur basaltic flows (MCC, 3.6—5.7 Ma) contributed to the construction of the E-W trending MZR.

4.2.1. Internal processes

4.2.1.1. Internal dynamics west of 73°W

The SCR-1 segment (Fig. 21 A and B) has been located at depth beneath the N-S trending NPI (3000—4000 m in elevation). This statement was inferred independently through tomographic (Russo et al., 2010 a and b) and kinematic (Bourgois et al., 2016 a) methods. This allows the inference that asthenospheric material flows upward along an area located just below the NPI at depth. We suggest that this asthenospheric flow dynamically sustains the high topography of the NPI. Indeed, the Mt San Valentin area in the northern part of the NPI is ~2000 m higher than the SSVZ basement located less than 20 km northward. Considering that both the NPI and SSVZ exhibit the same Patagonian Batholith granitic basement, no differential response originating from the upper crust seismic velocity and/or density structure is expected along orogenic strikes. Along the studied segment, we propose that the main

process controlling uplift of the Andes west of 73°W is dynamic topography originating from mantle convection along the SCR-1 segment at depth.

Mixing the common conversion point (CCP) stacking method with H-k crustal thickness estimates, Rodriguez and Russo (2020) provided a crustal thickness map for the forearc-backarc area of the CTJ region extending from 43°30' to 48°30'S. They documented an overall northward thickening of the crust from 32—33 km at 47°30'S to 37—38 km at 45°S. The crustal depth contours strike E-W, perpendicular to the N-S trending Andes. The increase in buoyancy resulting from hot SCR subduction would result in greater subduction erosion and thinning of the overriding plate south of CTJ at 46°09'S (Bourgois et al., 1996; Rodriguez and Russo, 2020). This is consistent with the fact that the NPI area is far the isostatic equilibrium because the crust is 3 km thinner than to the north, predicting that it should be lower. In this area, dynamic topography is likely the main cause of the excess elevation associated with Mt San Valentin (4070 m). However, the 2 km-high topographic step associated with Mt San Valentin is also located above a very complex system at depth. It is situated both above the Tres Montes FZ-SCR-1 junction and the westward projection of the 5 km-high step bounding the South American plate MOHO Plateau (SAM MOHO P hereafter) to the north (Fig. 21, see next section).

Using shear wave splitting, Russo et al. (2010a) examined asthenospheric mantle flow in the vicinity of the PSW. North of the subducted SCR, upper mantle flow beneath the Nazca slab is predominantly trench parallel. South of the triple junction, the upper mantle flows ENE-WSW parallel to the subducted Taitao FZ. PSW development abruptly interrupts the trench-parallel mantle flow accommodating the westward retreat of the Nazca slab and the rapid westward motion of South America over the past 50 Myr (Russo and Silver, 1994, 1996; Silver et al., 1998; Anderson et al., 2004). The Taitao and closely adjacent Tres Montes FZ parallel to the northern PSW boundary (Fig. 1 and 21) are strong barriers to the upper

mantle flow direction. These lower plate structures, deeply seated in the mantle, induced segment asthenospheric flow, which in turn appears to control segmentation in the upper plate. Because it developed over the last 4—5 Myr, the present effects of PSW development provide a uniformitarian developmental model, not only for the forearc area (Bourgois et al., 2016a) but also for the arc and backarc areas.

4.2.1.2. Internal dynamics east of 73°W

Each of the 4 CCP stacking profiles (A, B, C, and D, Fig. 21A) exhibits 2 specific points where the MOHO is shallower by approximately 5 km, from 35 to 30 km (Rodriguez and Russo, 2020). Along each of the profiles, a sharp jump in MOHO elevation occurs at 46°30' and 47°05'S. Projecting the sharp jump points from one profile to another defines an E-W trending strip of uplifted MOHO, the SAM MOHO P (see above), which is 70 km wide and 120 km long, from N to S and E to W, respectively. Interestingly, the SAM MOHO P exhibits a morphological mirror image. This is the E-W trending MZR (Figs. 2 and 3), which overlays the SAM MOHO P with an almost perfect fit from 71°30' to 72°30'W. Additionally, the N and S boundaries of the SAM MOHO P have their own morphological signatures; that is, the GCBAGL and CPGL trenches between 70°30' and 72°30'W. Both in space and time, similarities in the evolution of the Canal Baker and Canal Simpson exist. These are outlets for Rio Baker and Rio Simpson, respectively. This allows us to contemplate similarities in their watersheds. This substantiates the lower Miocene age incision of main valleys on either side of the MZR (i.e., the Rio Baker watershed to the N and to the S) as proposed above. Therefore, it is suggested that the SAM MOHO P could have also had a role in the morphological evolution during the past 14—18 Myr or more, the incision age of the valleys and location being controlled by its boundaries at depth. The SAM MOHO P together with its MZR morphological signature thus defines a major segmentation in the Andes. As discussed below,

this segmentation likely dates back from the Main Andean tectonic event at ~120 Ma (see below).

The E-W trending MZR is 180—200 km long, straddling the foreland area and the Andes. MZR extends from east of the MLBA to the Cosmelli Basin (CB, Figs. 2 and 21) in the west. Roughly, the MZR lengthwise profile exhibits a topographic arch, which culminates at Mt Zeballos Volcano (~2700 m, foreland area). To the east, the MLBA plateau basalt dips gently eastward from 2000—2200 m to less than 1000 m elevation, while the Sierra del Parque Jeinimeni dips to the west and slopes westward from the Andean morphotectonic frontline (2000—2200 m) to the Cosmelli Basin at ~1000 m (average elevation between 201 m and 1400 m for the shallow marine Guadal Fm of Burdigalian age). The 1.7—4 Ma Mt Zeballos Volcano erupted along the hinge zone of the MZR arch. We suggest that tension stresses normal to the MZR arch hinge have localized volcanic material migration near the crest of the arch.

The arch deformation of the SAM MOHO P could result from a higher coupling between the SAM and Nazca asthenosphere (cf. Fig. 21B) at the western end of the SAM MOHO P. Eastward mantle flow migration with a downward component could result predominantly from the SAM asthenospheric corner flow joining the upward flow from the SCR-1 Nazca diverging drift. This assumption could find its morphological signature in the forced subsidence recorded along the Cosmelli Basin (Fig. 20). Indeed, the shallow marine Guadal Fm of early Miocene age crops out along the GCBA shoreline at 201 m in elevation (Fig. S29). At this location the shallow marine sediment is close to its initial depositional elevation although it is located 70—80 km in the interior of the Andes. The SAM MOHO P bending related to the MZR arch structure is expected to produce a particular depth-dependent tectonic response. The midcrustal converters resolved in the data acquired by Rodriguez and Russo (2020) document the juxtaposition of rocks of distinct seismic velocities and/or densities or

varying physical states, including a possible partial melt. This midcrustal discontinuity (~15 to 21 km depth) may act as a strain guide for decollement or ductile shearing detachment. Lateral flow drained along the midcrustal converters could likely mitigate the upper crust tectonic response from Moho deformation, which would dampen part of the 2 to 3 km gap between the SAM MOHO P uplift and MZR topography

4.2.2. External processes

4.2.2.1. Glacial rebound

Basic field data and ages for calculating glacial isostatic rebound along GCBA Lake have been provided. At Longitude 72°30'W, the lake area has uplifted at a rate of 15 to 33.5 mm.yr-1 during the past ~7.9 ± 1.1 kyr (Bourgois et al. 2016b). Because this rate is on the same order of GPS measurements along an SPI transect (Dietrick et al., 2010), it was inferred that most of the calculated 135 m of rebound originated from ice loss in the GCBA Lake area. The area in which the uplift rebound rate has been calculated is located just N of the Cosmelli Basin axis (Figs. 2, 20, and 21). At this site, the shallow marine Guadal Fm of early Miocene age (Fig. 4) crops out along the southern GCBA shoreline (Flint et al., 1994) at ~201 m elevation (Fig. S29). This site is located close to the coupling zone at the convergent SAM plate and the NAZ plate asthenosphere flows at depth (C, Fig. 21B) and therefore has been dynamically pulled down by the sinking forces in the asthenosphere. The area has thus been under opposite forces during the last deglaciation: tectonic subsidence from below and uplift from glacial rebound from above. Consequently glacial rebound as previously calculated for this specific site is likely underestimated.

4.2.2.2. Water and volcanic flow divide

At a larger scale of time, Thomson et al. (2010), Tomkin and Roe (2007), and Clague et al. (2020) inferred a leading factor for glaciations in constructing the Andes. The most significant ice lobe incisions of Patagonia include the GCBAGL and CPGL trenches. The sinuous

drainage divide (Fig. 2) between the Atlantic and Pacific oceans follows lateral scars of ice lobes connecting eastward to the terminal moraines (Fig. S30). Ages of these moraines range from 1.1 Ma (GPG moraine) to 14—24 ka (Menuco-Fenix moraines). Moraine accumulations controlling the divide are climatically induced. Additionally, lateral scars connect westward to the Andean morphotectonic frontline that follows the Zeballos Pass corridor. Thus, the water divide was both tectonically and climatically controlled at least during the past 1.1 Myr. This situation has more likely prevailed for the past 5—7 Myr.

Two N-S trending alignments of dike and plug intrusions with ages ranging from 1.7 to 4 Ma follow the western side of the Zeballos Pass corridor and the eastern edge of the MCC. These are related to the Mt Zeballos (MLBA) and Pico Sur (MCC) volcanic complexes, which flow from these zones to the east and west, respectively. They follow the hinge zone of the MZR arch structure that has controlled the topographic divide of effusive products, at least for the last ~10—11 Myr.

4.2.2.3 Meseta till paradox (Clague et al., 2020)

Meseta basalt flows in the Lago Viedma area (49°30'S) have provided information regarding landscape evolution (Clague et al., 2020). As in the study area, Pliocene-Pleistocene volcanic flows originating from the front of the Andes dip gently to the east. The general morphological situation at the Lago Viedma transect (49°35'S) is similar to that at the MLBA. Westward, the foreland volcanic sequences are truncated via erosion in steep cliffs along the sides of the MLBAGL and CPGL trenches. Clague et al. (2020) called the presence of older hills >1000 m above Pleistocene glacial valleys the "till meseta paradox". Following Kaplan et al. (2009) and Anderson et al. (2012), they argued that lateral erosion over time would explain the high elevations of the upper Pliocene tills imbricated into the western end of basalt flows from foreland mesetas. Conversely, the long sequence of end moraines since the GPG at 1.1 Ma remains at a low elevation. Because older moraine remains were removed,

they inferred that a smaller ice volume was involved before the Early Pleistocene. During the Early and Middle Pleistocene, the major glacial lobes overdeepened great valleys, placing older tills and basalt flows at higher elevations than the lake floor at present. Therefore, the high elevation of old moraines from basalt mesetas could have originated from differential erosion related to more significant ice accumulation since the GPG.

At the MLBA northwestern scar (Fig. S30 for location), Mercer and Sutter (1982) described interbedded glacial tills and basalt flows in structural situations similar to those described by Clague et al. (2020). At 1500 m in elevation (i.e., 1300 m above lake level at present) they documented a glacial till overlying a basalt flow with an average age of 7.03 ± 0.11 Ma, which is in turn covered by a basalt flow dated at 4.63 ± 0.07 Ma (average age). It was suggested that this area, located close to the hinge zone of the MZR arch, was tectonically uplifted during the past 5—6 Ma due to PSW development (see above and Fig. 21). The MLBA area clarifies the "till meseta paradox" as described by Clague et al. (2020). Tectonic uplift contributed to the high elevation of upper Miocene-Pliocene tills frequently interstratified with meseta basalt flows. Overdeepening of the valley floor was therefore a likely response to tectonic uplift allowing the glacial trenches to remain at low elevations over time.

4.2.2.4. Volcanism during glaciations at the Andean frontline

Mt Zeballos volcano (2726 m), located just east of the Andean morphotectonic frontline, is a major cone (1.7—4 Ma) resting on a previously eroded surface down to the lower Miocene sequence in the Zeballos pass (more details in File S6).

4.2.3. Tectonic-climatic feedback loop

4.2.3.1. Glacial protection concept

West of 73°W, the dynamic uplift sustaining the high relief of the NPI sustained the icefield location over time. The locus of westerlies and maximum moisture at 47°S during

glacial events (Fig. 1) and the high elevation of the NPI area produced the highest rates of ice accumulation along the NPI. This resulted in the accumulation of the most prominent ice sheet during glacial periods. Consequently, the NPI has provided the most prominent glacial lobes from Patagonia, including those extending along the GCBAGL and CPGL (Fig. 2). At GCBA Lake the most extended glacial lobe dates back to the GPG at ~1.1 Ma (Fig. S30). Additionally, the GCBA and CP glacial lobe locations were influenced by the SAM MOHO P and related structures at depth (see above). In other words, PSW development induced the high relief of the NPI, which in turn localized maximum ice accumulation. The location of the NPI at the latitude of maximum moisture resulted in large glacial lobes protruding hundreds of kilometers across the Andes and the foreland during glacial events. The studied segment thus provides a basic example of a geodynamic-tectonic-climatic feedback loop.

Thomson et al. (2010) argued for reduced late Cenozoic erosion in the Andes south of 49°S despite stronger glacial conditions. They concluded that the southern Patagonian Andes benefited from regional glacial protection inducing growth of the orogen. This concept is questionable along the studied segment. The crustal structure and asthenospheric dynamics were identified as prominent factors controlling the tectonic evolution of the Andes for the past 5—7 Myr. Along the studied segment, a part of the active tectonic response to climatic cooling remains an elusive concept. As argued above, the erosion response to climatic variations passes through feedback loops basically controlled by internal dynamics. Additionally, glacial protection varied over time in an alternating regime with more than 24 glacial events since the late Miocene. No glacial protection existed for wide areas across the Andes during the warm interglacial periods. Although substantial, only the NPI and the San Lorenzo massifs representing 10—15% of the Andean segment between 46°30'-47°30'S benefit from potential permanent glacial protection over time. Glacial protection, as proposed by Thomson et al. (2010), could only be applied locally.

4.2.3.2. Water routing diverted

The Rio Baker spillway for the GCBAGL is located just above the western margin of the SAM MOHO P at depth (Fig. 21A). Additionally, Rio Baker is located 50 km east of SCR-1 at depth, which makes this area prone to collecting ice accumulations from major ice lobes originating from the NPI. Although SCR-1 and the SAM MOHO P produce opposing vertical forces, it is accepted that the nearby downward forces originating from the SAM asthenospheric corner flow induce predominant tectonic control in the overlying Rio Baker area. Another point to be considered is that the internal and external dynamic processes evolve differently over time. The SCR-1 and SAM asthenospheric flows are relatively uniform in time. In contrast, the climatic signal evolves as a sinusoidal waveform of varying frequency and amplitude. In the Rio Baker area, ice loading adds to the downward forces during glacial periods, as discussed above.

As considered above, broad morphological similarities between the Rio Simpson and Rio Baker watersheds exist. The Rio Simpson provides a model for the morphotectonic evolution of the Rio Baker watershed prior to SCR subduction (i.e., prior the onset of the NPI uplift). Because the GCBAGL and CPGL are located on either side of the MZR, we speculate that these two major lakes drained separately before PSW development using different outlets: the Canal Baker for the CPGL and the Rio Bayo for the GCBAGL (Fig. 20). The dramatic uplift of the NPI area would have diverted the GCBAGL drained waters from W to S, subsequently captured by the CP outlet at ~3—4 Ma (Bourgois et al., 2019; Bourgois et al., 2016b and 2016c). Subsidence forces produced from the SAM asthenosphere corner and glacial loading would also have facilitated GCBAGL outlet relocation from Rio Bayo to the Rio Baker channel. A particular ice loading-unloading step was likely a key time period for the CP Lake watershed to capture and incorporate the GCBA Lake watershed, together forming the Rio Baker watershed in its present configuration. The forced subsidence resulting from SAM and

NAZ asthenospheric flows at depth would have induced GCBAGL waters to flow southward, connecting then to the Canal Baker. This may represent another feedback loop between tectonics, morphology and climate.

The potential feedback loops identified in the study area make it difficult to quantify the prevailing factors of internal versus external processes in controlling the morphologic and drainage dynamics over time. However, it should be noted that building of the high relief, including the NPI and MZR, appears to be mainly controlled by asthenosphere dynamics and deep crustal structures, respectively.

4.3. From 5—7 to 25—30 Ma

A major shortening event associated with fold and thrust belt development during the lower Miocene is the commonly accepted compressional tectonic event inducing the onset of Andean orogenesis and uplift. Supported by stable isotopic data, Blisniuk et al. (2005) have documented more than 1 km of surface uplift at ~16.5 Ma. The detailed fieldwork conducted along the Andean morphotectonic frontline (46°30'-47°30'S) does not support this model for the origin of the lower Miocene Andean uplift.

4.3.1. From 18.1 to 25—30 Ma

From 20.3 to 25—30 Ma, the continental environment of the backarc area was that of a plain with a low hill relief landscape drained by meandering rivers. East of 72°10'W, the shallow marine El Chacay Fm transgression flooded these lowlands at 20.3 Ma (Fig. 22). This age is significantly younger than the 23.4 ± 1 Ma age reported for the transgression of the Guadal Fm west of 72°10' W (Cosmelli Basin, Fig. 4). The ~2 Myr gap for the transgression recorded on either side of the Sierra del Parque de Jeinimeni may have been related to the sources from which the marine transgression would have originated: south of 49°S and north of 41°S for the El Chacay and Guadal Fms, respectively (Fig. S4; Aragon et al., 2013). The onset of the MMCO deformations dated at 17—18 Ma is too young to be related to the

transgression of either the Guadal or El Chacay Fms. The Farallon-Aluk spreading center collision with the South American plate during the Paleogene time (Somoza, 1998; Lonsdale, 2005) was associated with the development of a large slab window that lasted 30 Myr (Kay et al. 2002, 2004, 2007; Aragon et al., 2011). The inward detached slab of the subducted Aluk plate may have induced subsidence along the Patagonian Atlantic coastal area. Subsequently, a marine transgression developed southward, reaching the Cosmelli Basin area by the early Miocene.

The shallow marine El Chacay and Guadal Fms indicate that at least 50% of the study area was near sea level during the early Miocene (Fig. 22). At 46—48°S paleontological studies (Frassinetti and Covacevich, 1999) showed that no connection existed between the Atlantic and Pacific at that time. Along the study area, the Cosmelli Basin recorded the maximum extension of Atlantic waters to the west. These were less than 100 km from Caleta Tortel between 19.8 ± 0.4 and 23.4 ± 1.0 Ma. Because the eastward erosion along the canal Baker established a connection between the Pacific and a lowland area east of the Patagonian batholith (see above), it is inferred that the Caleta Tortel area was at Pacific sea level at 14—18 Ma (Thomson et al., 2001). Most likely, the eastward regressive erosion along the canal Baker reached the Caleta Tortel area 0.5 to 1 Myr after the regression onset of Atlantic waters from the Cosmelli Basin. This suggests that Atlantic waters have never reached the Pacific Ocean at ~47°S.

4.3.2. From 16.1—16.9 to 18.1 Ma

4.3.2.1. Early Miocene tectonic events

Along the MZR, the Atlantic-Pacific drainage divide follows the Andean morphotectonic frontline and is tectonically controlled (see above). Between GCBA Lake and the upper Chacabuco Valley to the north, the Andean morphotectonic frontline consists of an arcuate array of right stepping of right-lateral transtensional faults (Fig. 22). Faults are 15 to 30 km

long, striking from N10°W along the Chile Chico fault (Fig. 15) to the north to N30°E at the Argentina Chile border fault system (ACBFS, Fig. 11) to the south. The zigzag shape shown in map view is related to an ~100 km long relay ramp system that connects transtensional STEP fault segments, including the Chile Chico, Jeinimeni, Rio Lincoln, and Argentina-Chile Border faults, from north to south. Here, we designate them basic elements of an en-echelon ramp system, the Marques-Zeballos Pass ramp system, MZPRS. The right-stepping ramp zone results in a 22—24 km westward displacement of the Andean morphotectonic frontline between Chile Chico and the upper Chacabuco valley. The 2 to 2.5 km of material erosionally removed at the GCBAGL and CPGL trenches has opened access to the three-dimensional structure in the northward and southward prolongations of the MZPRS (i.e., the Andean morphotectonic frontline). To the north, the southern valley wall of the GCBAGL trench exposes the transtensional Chile Chico fault vertically, and its traces cut across contours down to the GCBA Lake shoreline. South of the Zeballos Pass corridor, the Pleistocene left-lateral Eastern Spur fault (Fig. 9) masks the lower Miocene ramp system. However no clear continuation of the MZPRS has been identified crossing the upper Chacabuco Valley. It is proposed that the deformation associated with the MZPRS along the MZR has been transferred eastward onto the Colorada Range fault (not described in this work, Fig. 22).

The right-lateral transtensional MZPRS evolved through two tectonic phases. The first induced shallow marine El Chacay Fm regression and was associated with the main orogenic pulse. At the MCC, most of the 800—1200 m uplift recorded by the El Chacay Fm occurred at that time, shaping the morphotectonic frontline of the proto-Andes. Subsequently, the fluvial Rio Jeinimeni and Zeballos Pass Fms accumulated outward of the MZPRS. These accumulations of fluvial sediment unconformably overlie the phase 1 tectonic features and were subsequently involved in a second tectonic phase. This phase 2 tectonic pulse was associated with moderate displacement. Although not firmly defined throughout the MZPRS,

part of the upper Zeballos Pass Fm overlaps phase 1 and 2 tectonic features and associated relief. The phase 1 tectonic event thus occurred after 18.1 Ma (the end of the shallow marine deposition) and before the accumulation of the Jeinimeni and Zeballos Pass Fms (before 16.1—16.9 Ma). Phase 2 tectonic activities are younger than 16.1 Ma (the younger age obtained for the Zeballos Pass Fm). This is in fairly good agreement with the ~16.5 Ma onset of the >1 km uplift proposed by Blisniuk et al. (2005).

From the upper Chacabuco Valley southward to Las Posadas Lake, the lower Miocene sediment was removed along the CPGL trench. South of Posadas Lake, no significant fault has been identified disrupting the original unconformity of the El Chacay Fm. (Figs. 7, 8, and 22). The Burdigalian transgression flooded a peneplain that evolved since the end of the Aptian, after the main contractional tectonic event at ~120 Ma. South of the upper Chacabuco Valley, a large dome structure is the main signature of the Andes at present. In this area, the basaltic volcanic flows of the MLBA and Lago Posadas areas (14.5 Ma and younger) top across the tectonic features shaping the lower Miocene Andean morphotectonic frontline. Between 46°30' and 47°30'S, no evidence documents the commonly accepted lower Miocene compressional tectonic event. No lower Miocene Andean Fold and Thrust Belt in the commonly accepted meaning is documented.

4.3.2.2. Uplift dynamics

The right-lateral transtensional displacement occurring along the MZPRS is the primary structure accommodating the ~800—1200 m uplift of the Andes at ~16.1—18.1 Ma. The uplift dynamics related to this event is thus not due to contractile tectonics. The MZPRS defines the boundary between a western Andean block and an eastern foreland block. The Andean block has moved right-laterally along an ~N25°W direction relative to the foreland block. The divergence between blocks is associated with a dip-slip component striking NW-SE. Rupture at the block boundaries accommodated the uplift of the Andean block. The post-

MU2 volcanic-sedimentary sequences that unconformably overlie the MCC are almost undeformed (i.e., almost horizontal) including the Lower Basalt (34—57 Ma), El Chacay (18.1—20.3 Ma), and the Upper Basalt (7—16 Ma) Fms. This suggests that the MCC behaved as a nondeforming block during the Burdigalian tectonic event. The Andean block extending westward to the Cosmelli Basin exhibited the same tectonic behavior over time (De la Cruz and Suarez, 2006 and 2008). The tectonic deformation was concentrated along the Andean morphotectonic frontline, suggesting relatively passive uplift of the Andean block. This block, including the Sierra del Parque Jeinimeni and MCC, extends westward to the major fault bounding the Cosmelli Basin to the east (Fig. 2).

Olbertz et al. (1997) suggested that trench migration relative to upper mantle flow is the decisive factor controlling slab geometry relative to absolute plate velocities (Pardo-Casas and Molnar, 1987). Subsequently Schellart (2008) explored three existing geodynamic models that attempt to explain how trench migration velocity controls overriding plate deformation. In any available global reference frame, he showed that Peru-Chile trench migration should induce shortening in the Andes for all explored models.

Indeed, the three main geodynamic mechanisms proposed to explain Andean orogenesis, including uplift and growth during slab flattening (Horton, 2018; Gianni et al., 2018; Hu et al., 2016; Ramos and Folguera, 2009; Oncken et al., 2006; Ramos et al. 2002; Pennington, 1981), slab anchoring in the lower mantle (Quinteros and Sobolev, 2013; Faccenna et al., 2017; Chen et al., 2019), and trench-parallel retrograde flow along the subducting subslab asthenosphere interface (Russo and Silver, 1994, 1996; Silver et al., 1998; Anderson et al., 2004), all predict horizontal shortening in the Andes. Horizontal subduction favors compression far from the trench, above the asthenospheric wedge and steeply dipping segment of the subducting slab (Jordan et al., 1983, 2010), such that slab flattening is a driving mechanism that would control the width of the Andes (Martinod et al., 2020). The three geodynamic mechanisms often

proposed thus offer no satisfactory explanation inference for the 800—1200 m uplift of the studied Andean segment occurring under a transtensional stress regime during the Burdigalian.

The Andean segment at approximately 40°S was proposed to have evolved under an extensional setting in the Eocene, Oligocene and early Miocene time (Aragon et al., 2011, 2013). At that time, a large slab window –here called the Neuquén slab window– evolved in response to Farallon-Aluk spreading center subduction up to approximately 23 Ma. As at the PSW, ridge collision would have been associated with a magmatic hiatus along the arc axis. The detachment of the subducting Aluk plate would have resulted in extension and uplift in the overriding backarc area. The extensional tectonic regime is considered to have extended from the arc area to the Andean foreland. The Andean morphotectonic frontline was proposed to be a major normal fault (Aragon et al., 2011, 2013). Inward, continental crust deformation is heterogeneous within the backarc area, with thin extended crust isolating a thick solid nondeforming crustal block in the main Andes. Decompression initiated in the upper mantle from the detached slab at depth resulted in major volcanic activity in these two settings. Subsequently, the subducting plate decoupled completely, inducing additional uplift of the crustal bloc due to upward asthenospheric flow.

The evolution of the Andean segment at ~40°S proposed by Aragon et al. (2013) for the Eocene-Oligocene time exhibits similarities with the evolution of the studied segment for the 16.1—18.1 Ma period. In particular, the Neuquén slab window model considers the uplift of the Andean frontline to have been related to a tensional tectonic regime.

The proposed evolution for the studied segment is as follows: (1) at 23.4 ± 1 Ma, coupling between the SAM and Aluk slab at depth would have controlled subsidence and transgression of Atlantic waters to the Cosmelli Basin; (2) at 20.3 Ma, transgression of the Austral Basin originating from 49°S reached the Las Posadas Lake area (Fig. S4); (3) at 19 Ma, the Aluk slab detached at depth, which would have induced the regression of the Guadal Fm from the

Cosmelli Basin area; (4) regression of the Austral Basin from Las Posadas Lake occurred at 18.1 Ma, 0.9 Myr after that in the Cosmelli Basin; (5) the Aluk slab completely detached just after 18.1 Ma, allowing decoupling of the Andean block from the foreland area along the MZPRS; and (6) a tensional tectonic adjustment subsequently occurred until 16.1 Ma, at a maximum.

Russo et al. (2010a and b) showed that PSW development diverted the Nazca subslab mantle flow, rotating it from northward to eastward. This flow rotation toward the east likely resulted in horizontal stretching in the overriding backarc area. Accepting that the Neuquén slab window development induced such a dynamic rotation of the mantle flow at depth, it is possible that the trench-parallel retrograde model played a role in the Burdigalian tectonic evolution of the study area.

Similarities in the tectonic evolution of the ~40° and 46°30'-47°30'S Andean segments suggest a common causality for tensional stress inducing passive uplift along the Andean morphotectonic frontline. The Neuquén slab window development provides a geodynamic mechanism in agreement with the tectonic regime, inferred from synextensional volcanism analyses at ~40°S and from fieldwork and analysis in the study area near the modern CTJ. It is proposed that the MZPRS break-up may have originated from the Neuquén slab window migrating southeastward to the study area.

4.3.3. From 6 to 16.1 Ma

The upper sequence of the fluvial Zeballos Pass Fm (16.5 ± 0.5 Ma, Fig. S25) is proposed as sealing the Andean morphotectonic frontline associated with the passive uplift of the proto Andes along the MZPRS. In the Zeballos Pass area, the Cerro Plomo basalt (14.48 ± 0.17 Ma) unconformably overlies the Zeballos Pass Fm, with both formations being flat lying. The lava flow seals a paleosurface topping the fluvial sediment, suggesting that no major tectonic deformation occurred between their formations. Subsequently, most of the study area was

covered by volcanic flows that shaped the accumulation of the large MLBA and MCC Plateau basalts from the middle Miocene to Holocene. These stacks of basalt flows exhibit no significant tectonic deformation in terms of faulting and folding. Most magmatic products originated from a N-S-trending strip that follows the MZPRS. Basaltic magma flowed on either side of the Andean morphotectonic frontline and on either side of the MZR hinge arch (Fig. 21B). We infer that a tectonic zone of weakness could have prompted the ascent of magma from a deep-rooted crustal tear in the SAM MOHO P. This tear would have evolved over time in the wake of crustal weakness originating from the lower Miocene MZPRS.

4.4. Main contractional event at ~120 Ma

Tectonic style and age

The Andean morphotectonic frontline south of the upper Chacabuco Valley is deeply eroded along the valley floor of the CPGL trench (Figs. 2 and 22). Along this segment, the CP glacial lobe removed the volcanic-sedimentary deposits down to the Quemado Fm. The lower Miocene sediments and the underlying sequences, including the Centinela, Posadas basalt Fm of Eocene age, and Rio Tarde Fms, were removed. The Colorada Range (Fig. 22) is a monadnock (butte temoin) documenting that the volcanic-sedimentary cover above the MU2 unconformity extended out of the CPGL trench. Inward, the excavated corridor of the CPGL trench crosses the Andean morphotectonic frontline. Between the upper Chacabuco valley and CP Lake, the Quemado Fm underthrusts beneath the metamorphic basement of the Andes along an E-verging thrust, the so-called MAT (Figs. 5 and 22). The MAT is deep-rooted in the upper crust. At this site, the MAT is a shear thrust dipping 10—15° westward documenting major crustal shortening.

A main knee fold is often exposed along the Andean morphotectonic frontline (Figs. 6, 8, and 13). This knee fold is very dissymmetric, exhibiting a lengthy inward flat limb, an axial surface dipping 45° westward, and a short outward almost vertical limb. The fold axis trend

N-S, and the wavelenght is 15—18 km. East of Lago Posadas, folding involves the metamorphic basement. Along the MCC eastern front, a symmetrical fold exists (Fig. 16). Basal truncation of this fold has been documented at the GCBA southern valley side (W of Chile Chico).

The segment close to Lago Posadas shows that the volcanic-sedimentary layers (16—118 Ma) gently tilt eastward (Figs. 5 to 8) unconformably overlying the MAT that bounds an inward Andean block from a foreland block to the east. Because the Andean block involves shallow marine formations (Fig. S1) with ages ranging from 120 to 145 Ma, the MAT is younger than 120 Ma. The age of the MAT is well constrained at ~120 Ma.

MAT dynamics

The complex rifting history of SW Gondwana was recently reassessed (Loveccchio et al., 2020). They provided a reconstruction of the South Atlantic during the final stage at 121 Ma. For the previous Jurassic stages of rifting history, the study area was located west of an elongated crustal wedge, here called the Malvinas/Falkland Wedge (Fig. S31). The Weddell Sea and the Aguilhas-Malvinas (Falkland) FZ bound this wedge to the south and to the north, respectively. The North Malvinas, San Jorge Gulf and Rio Mayo basins are local extensional structures associated with the evolution of the northern boundary of the Malvinas/Falkland Wedge. All of these structures are located hundreds of km, north of the study area. To the west, the Patagonian batholith granite documents active subduction of the proto-Pacific beneath the Malvinas/Falkland Wedge. This Patagonian volcanic arc would have been associated with a backarc basin development in the northward extension of the Rocas Verdes Basin (Stern and De Wit, 2003; Barberon et al., 2015; Ghiglione et al., 2015). The traces of this basin include the Apeleg and Rio Belgrano Fms in the study area (Fig. S1). Together with the Katterfeld and Toqui (Chile) and Rio Mayer and Springhill Fms (Argentina), these shallow marine sequences accumulated on the calc-alkaline volcanic breccias of the Ibañez

Fm (i.e., volcanic flows associated with the Patagonian batholith). The closure of the "Ibañez" backarc basin at ~120 Ma was associated with east-verging MAT development. At that time, the arc and backarc material was transported eastward above the Gondwana breakup acidic lavas of the Quemado Fm, which flowed onto the Deseado massif basement. Crustal thickening related to the ~120 Ma MAT would have amplified the uplift isostatic response of the proto-Andes during the Burdigalian transtensional tectonic event.

Rodriguez and Russo (2020) proposed five scenarios to explain southward crustal thinning from 55 to 30 km along profiles A, B, C, and D in Fig. 21A. Two of these events were related to Paleozoic tectonic events; one was related to the Mesozoic rifting of Gondwana, and the last two propose thermal or mechanical erosion related to Cenozoic SCR subduction. Since crustal thickening likely existed in relation to the main crustal shortening at ~120 Ma MAT, we favor the last two scenarios, allowing subsequent crustal thinning.

5. Conclusions

5.1. Internal dynamics

Patagonia Slab Window

1) The reconstructed PSW development for the past 5—6 Myr provides a "uniformitarian" model for arc and backarc areas. Signatures associated with ridge subduction beneath the continental basement are identified. This complements the model previously published for the forearc area (Bourgois et al., 2016a). An evolutionary model for a near complete transect from the subducting ridge area (Chile Triple Junction) to the Andes foreland is proposed. This includes tectonic, volcanic and morphological signatures together with the associated crustal and asthenospheric dynamics.

2) The 2 km excess topography at Mt San Valentin (NPI) is dynamically sustained from upward convection originating from the SCR-1 ridge segment at depth.

3) Lower plate structures, such as the Taitao and Tres Montes FZs, induced a major asthenospheric segmentation that controls the first-order segmentation of the upper plate. These relationships should open new perspectives for the Eurasian plate boundary during the early Andean stages of the Tethys.

Eastern Andes segmentation

4) The SAM MOHO P crustal structure controls the first-order E-W-trending MZR morphological feature. This structure lies astride the foreland Andes boundary and introduces a first-order segmentation into the eastern Andes. Two different modes for Andean segmentation are possible, subduction- and foreland-controlled.

5) The SAM MOHO P boundaries at depth control the location of major glacial lake trenches bordering the MZR (GCBAGL and CPGL to the north and to the south, respectively). The drainage location is inscribed in morphological records since the early Miocene, as inferred from the Rio Baker watershed evolution over time.

6) The Neuquen slab window that controlled the MZPRS location and age introduced weaknesses in the upper crust during the lower Miocene. This in turn forced the SAM MOHO P/MZR bending to be located along the MZPRS. This weakness zone is proposed to have drained the volcanic products from below during PSW development during the past 6—7 Myr.

Lower Miocene dynamics of the Andes

7) The 100 km-long, right-lateral transtensional MZPRS controls the Andean morphotectonic frontline as it crosses the MZR. This ramp system, which has favored a rupture of coupling between the Andes and the foreland, was responsible for the ~800—1200 m uplift of the Andes at ~16.1—18.1 Ma. The uplift dynamics related to this event were not due to contractional tectonics.

8) The MCC and Sierra del Parque de Jeinimeni behaved as a nondeforming blocks during the Burdigalian tectonic event. Transtensional tectonic deformation was concentrated along the MZPRS at the Andean morphotectonic frontline, suggesting passive uplift of the Andes.

9) The three main geodynamic mechanisms proposed to explain Andean orogenesis, uplift and growth during slab flattening, slab anchoring, and trench-parallel retrograde flow, were associated with horizontal shortening in the Andes. They provide no satisfactory explanation for the transtensional stress state identified along the MZPRS during the Burdigalian.

10) At 40°S, the Neuquén Slab Window model (Aluk slab) is considered to be the controlling factor for the tensional tectonic regime of the Andean frontline during the lower Miocene and Oligocene (Aragon et al., 2011, 2013). Neuquén slab window development provides a geodynamic mechanism in agreement with the tectonic regime inferred from synextensional volcanism at ~40°S and from fieldwork and tectonic analysis at 46°30'-47°30'S. It is proposed that the MZPRS break-up would have originated from the Aluk slab migrating southeastward to the study area.

Main Andean contractional event at ~120 Ma

11) The MAT is a deep rooted upper crustal structure dipping 10—15° westward, documenting a major crustal shortening event at ~120 Ma. The MAT is the main contractile event identified along the studied segment.

12) The MAT represents the closure of the backarc basin associated with proto-Pacific subduction beneath the Patagonian continental basement. The Patagonian batholith together with the arc volcanic material of the Ibañez Fm records the trace of the subduction zone. The Ibañez Fm was transported eastward above the Quemado Fm, which accumulated onto the Deseado massif basement of Paleozoic age. Volcanic strata of the Quemado Fm resulted from Atlantic rifting.

13) Part of the inherited SAM MOHO P crustal structure was likely incorporated into the

Andes during the main shortening event at ~120 Ma. Its foreland segment has been located west of the Andean frontline since that time.

5.2. External dynamics

1) The tectonic response to climatic variations may be present through feedback loops between climate, morphology, and tectonics. The internal dynamics, however, appear as a result of the prevailing factors balancing and controlling the impacts of the external processes, at least for the past 5—7 Myr. Along the studied segment the role of the active tectonic response to climatic cooling remains an elusive concept at the Myr time scale.

2) The "till meseta paradox", as described by Clague et al. (2020), is clarified for the MLBA. Tectonic uplift related to PSW development contributed to the high elevation of upper Miocene-Pliocene tills interstratified with high standing basalt flows.

3) Rivers and glacial lobe patterns were inherited from a former drainage network dating back to the early Miocene or earlier (antecedent network).

Acknowledgments

Funding from the Institut National des Sciences de l'Univers (France) was at the origin of this research. The Evaluation-Orientation de la Coopération Scientifique-Comision National de Investigacion Cientifica y Tecnologia program funded this work through several projects. These include two field campaigns in the Taitao and Tres Montes Peninsulas and the CTJ expedition with the R/V L'Atalante. We acknowledge Carlos Pallares for informal and extensive discussions on Patagonian Andes. We appreciate constructive and extensive comments and revisions done by Brian Wernicke that helped us to improve an earlier version of the manuscript. We are grateful for the help from the ESR Managing Editor Gillian R. Foulger. Thanks to Guidetta Fellin and Mark Brandon for specific comments. J. B. is grateful to the Université Pierre et Marie Curie (Sorbonne-Université) and the Centre National de la

Recherche Scientifique (France). SERNAGEOMIN (Villarica, Chile) and the Universidad de Concepcion (GEA) have provided logistical support for fieldwork. We are also grateful for assistance from Parque Patagonia.

Disclosure statement

Authors are reporting no potential conflict of interest.

Conflict of interest

None.

References

Anderson, M.L., Zandt, G., Triep, E., Fouch, M., and Beck, S., 2004, Anisotropy and mantle flow in the Chile-Argentina subduction zone from shear wave splitting analysis: Geophysical Research Letters, v. 31, L23608, doi: 10.1029/2004GL020906.

Anderson, R.S., Duhnforth, M., Colgan, W., and Anderson, L., 2012, Far-flung moraines: exploring the feedback of glacial erosion on the evolution of glacier length: Geomorphology, v. 179, p. 269-285.

Aragon, E., Pinotti, L., D'Eramo, F., Castro, A., Rabbia, O., Coniglio, J., Demartis, M., Hernando, I., Cavarozzi, C.E., and Aguilera, Y.E., 2013, The Farallon-Aluk ridge collision with South America: implications for the geochemical changes of slab window magmas from fore- to back-arc: Geoscience Frontiers, v. 4, p. 377-388, http://dx.doi.org/10.1016/j.gsf.2012.12.004

Aragón, E., D`Eramo, F., Castro, A., Pinotti, L., Brunelli, D., Rabbia, O., Rivalenti, G., Varela, R., Spackman, W., Demartis, M.L., Cavarozzi, C.E., Aguilera, Y., Mazzucchelli, M., and Ribot, A., 2011, Tectono-magmatic response to major convergence changes in

the north Patagonian suprasubduction system: the Paleogene subduction-transcurrent plate margin transition: Tectonophysics, v. 509, p. 218-237.

Barberon, V., Ronda, G., Leal, P.R., Sue, C., and Ghiglione, M.C., 2015, Lower Cretaceous provenance in the northern Austral basin of Patagonia from sedimentary petrography: Journal of American Earth Sciences, v. 64, p. 498-510. doi.org/10.1016j.jsames.2015.08.014.

Berger, A.L., Gulick, S.P.S., Spotila, J.A., Upton, P., Jaeger, J.M., Chapman, J.B., Worthington, L.A., Pavlis, T.L., Ridgway, K.D., Willems, B.A., and McAleer, R.J., 2008, Quaternary tectonic response to intensified glacial erosion in an orogenic wedge: Nature Geoscience, v. 1, p. 793-799, doi:10.1038/ngeo334

Blisniuk, P.M., Stern, L.A., Chamberlain, P., Idleman, B., and Zeitler, P.K., 2005, Climatic and ecologic changes during Miocene surface uplift in the southern Patagonian Andes: Earth Planet. Sc. Letters, v. 230, p. 125-142.

Bourgois, J., Cisternas, M.-E., and Frutos, J., 2019, Comments on: "Glacial lake evolution and Atlantic-Pacific drainage reversals during deglaciation of the Patagonia ice sheet" by Thorndycraft et al. [Quat. Sci. Rev. 203 (2019), 102e127]: Quat. Sc. Rev., https://doi.org/10.1016/j.quascirev.2019.03.036

Bourgois, J., Lagabrielle, Y., Martin, H., Dyment, J., Frutos, J., and Cisternas, M.E., 2016a, A review on forearc ophiolite obduction, adakite-like generation, and slab window development at the Chile Triple Junction area: uniformitarian framework for spreading-ridge subduction: Pure and Applied Geophysics: v. 173, p. 3217-3246, DOI: 10.1007/s00024-016-1317-9.

Bourgois, J., Cisternas, M.E., Braucher, R., Bourles, D., and Frutos, J., 2016b, Geomorphic records along the General Carrera (Chile)-Buenos Aires (Argentina) glacial lake (46-

48°S), climate inferences and glacial rebound for the past 7-9 ka: The Journal of Geology, v. 124, p. 27-53, DOI: 10.1086/684252.

Bourgois, J., Cisternas, M.E., Braucher, R., Bourles, D., and Frutos, J., 2016c, Geomorphic records along the General Carrera (Chile)-Buenos Aires (Argentina) glacial lake (46-48°S), climate inferences and glacial rebound for the past 7-9 ka, A Reply: The Journal of Geology, v. 124, p. 637-642, DOI: 10.1086/687551.

Bourgois, J., and Michaud, F., 2002, Comparison between the Chile and Mexico triple junction areas substantiates slab window development beneath northwestern Mexico during the past 12-10 Myr: Earth Planet. Sci. Lett., v. 201, p. 35-44.

Bourgois, J., Guivel, C., Lagabrielle, Y., Calmus, T., Boulègue, J., and Daux, V., 2000, Glacial interglacial trench supply variation, spreading-ridge subduction, and feedback controls on the Andean margin development at the Chile triple junction area (45-48°S): J. of Geophys. Res., v. 105, p. 8355-8386.

Bourgois, J., Martin, H., Lagabrielle, Y., Le Moigne, J., and Frutos, J., 1996, Subduction-erosion related to spreading-ridge subduction: Taitao peninsula (Chile margin triple junction area): Geology, v. 24, p. 723-726.

Bourgois, J., Lagabrielle, Y., Le Moigne, J., Urbina, O., Janin, M-Ch., and Beuzard, P., 1993, Preliminary results of a field study of the Taitao ophiolite (southern Chile): implications for the evolution of the Chile triple junction: Ofioliti, v. 18, p. 113-129.

Boutonnet, E., Arnaud, N., Guivel, C., Lagabrielle, Y., Scalabrino, B., and Espinoza, F., 2010, Subduction of the South Chile active spreading ridge: a 17 Ma to 3 Ma magmatic record in central Patagonia (western edge of Meseta del Lago Buenos Aires, Argentina): J. of Volcanology and Geothermal Res., v. 189, N° 3-4, p. 319-339. doi: 10.1016/j.jvolgeores.2009.11.022

Breitsprecher, K., and Thorkelson, D.J., 2009, Neogene kinematic History of Nazca-

Antarctic-Phoenix Slab windows beneath Patagonia and Antartic Peninsula: Tectonophysics, v. 464, p. 10-20.

Brown, L.L., Singer, B.S., and Gorring, M.L., 2004, Paleomagnetism and 40Ar/39Ar chronology of lavas from Meseta del Lago Buenos Aires, Patagonia: Geochem. Geophys. Geosyst., v. 5 (1), Q01H04, doi:10.1029/2003GC000526.

Butler, K.L., Horton, B.K., Echaurren, A.,, Folguera, A., and Fuentes, F., 2020., Cretaceous-Cenozoic growth of the Patagonian broken foreland basin, Argentina: chronostratigraphic framework and provenance variations during transitions in Andean subduction dynamics: Jour. South Amer. Earth Sc., v. 97, doi.org/10.1016/j.jsames.2019.102242.

Caldenius, C., 1932, Las glaciaciones cuaternarias en Patagonia y Tierra del Fuego: Anales, Direccion General de Geologia y Mineria, Buenos Aires, v. 95, 150 p.

Cande, S.C., and Leslie R.B., 1986, Late Cenozoic tectonics of the southern Chile trench: J. of Geophys. Research, v. 92, p. 495-520.

Cembrano, J., Schermer, E., Lavenu, A., and Sanhueza, A., 2000, Contrasting nature of deformation along an intra-arc shear zone, the Liquine–Ofqui fault zone, southern Chilean Andes: Tectonophysics, v. 319, p. 129–149.

Charrier, R, Linares, E., Niemeyer, H. and Skarmeta, J., 1979, K-Ar ages of basalt flows of the Meseta Buenos Aires in Southern Chile and their relation to the Southeast Pacific triple junction: Geology, v. 7, p. 436-439.

Chen, Y-W., Wu, J., and Suppe, J., 2019, Southward propagation of Nazca subduction along the Andes: Nature, v. 565, p. 441.

Christeleit, E. C., Brandon, M. T., Shuster, D. L., 2017. Miocene development of alpine glacial relief in the Patagonian Andes, as revealed by low-temperature thermochronometry : Earth Planet. Sci. Lett. v. 460, p. 152–163.

Clague, J.J., Barendregt, R.W., Menounos, B., Roberts, N.J., Rabassa, J., Martinez, O.,

Ercolano, B., Corbella, H., and Hemming, S.R., 2020, Pliocene and Early Pleistocene glaciation and landscape evolution on the Patagonian Steppe, Santa Cruz Province, Argentina: Quat. Sci. Rev., v. 227, doi.org/10.1016/j.quascirev.2019.105992.

Colwyn, D.A., Brandon, M.T., Hren, M.T., Hourigan, J., Pacini, A., Cosgrove, M.G., Midzik, M., Garreaud, R.D., and Metzger, C., 2019, Growth and steady state of Patagonian Andes: Amer. J. of Sci., v. 319, p. 431-472, DOI 10.2475/06.2019.01.

Coronato, A.M.J., Martinez, O., and Rabassa, J., 2004, Glaciations in Argentine Patagonia, Southern South America, In: Ehlers, J., Gibbard, P. (Eds.). Quaternary glaciations: Extent and chronology. Part III: South America, Asia, Africa, Australia, and Antarctica: Quaternary Book Series. Elsevier, Amsterdam, p. 49-67.

Cuitiño, J.I., Ventura Santos, R., Muruaga, P.J.A., and Scasso, R.A., 2015, Sr-stratigraphy and sedimentary evolution of early Miocene marine foreland deposits in the northern Austral (Magallanes) Basin, Argentina: Andean Geology, v. 42, N°3, doi: 10.5027/andgeoV42n3-a05

Dal Molin, C., Márquez, M., and Malsenabe, B., 1998, Hoja Geológica 4571-IV Alto Río Senguerr, Provincia del Chubut 1: SEGEMAR, Escala 1:250,000.

De Iuliis, G., Brandoni, D., and Scillato-Yané, G.J., 2008, New remains of Megathericulus patagonicus Ameghino, 1904 (Xenarthra, Megatheriidae): information on primitivefeatures of megatheriines: J. Vertebr. Paleontol. V. 28, p. 181–196.

De la Cruz, R., and Suarez, M., 2006, Geologia del area Puerto Guadal-Puerto Sanchez, Region Aisen del General Carlos Ibañez del Campo, Servicio Nacional de Geologia y Mineria, Carta geologica de Chile, Serie Geologia Basica, N° 95; 58 p., 1 mapa escala 1:100 000, Santiago.

De la Cruz, R., and Suarez, M., 2008, Geología del area Chile Chico-Rio de las Nieves, Region del General Carlos Ibañez del Campo: Servicio Nacional de Geología y Minería, Carta Geológica de Chile, Serie Geología Básica, N° 112, 67 p., 1 mapa escala

1:100,000, Santiago.

DeLong, S.E., and Fox, P.J., 1977, Geological consequences of ridge subduction, In Island arc, deep sea trenches, and back-arc basins, Maurice Ewing Ser., v. 1 (ed. Talwani, M. and Pitman III, W.C.) (AGU Washington D.C.), p. 221–228.

DeLong, S.E., Fox, P.J., and MacDowell, F.W., 1978, Subduction of the Kula Ridge at the Aleutian Trench: Geol. Soc. of Am. Bull., v. 89, p. 83-95.

DeLong, S.E., Schwarz, W.M., and Anderson, R.N., 1979, Thermal effects of ridge subduction, Earth Planet. Sc. Lett., v. 44, p. 239–246.

Dickinson, W.R., and Snyder, W.S., 1979, Geometry of subducted slabs related to San Andreas Transform: Journal of Geology, v. 87, p. 609-627.

Dietrich, R., Ivins, E. R., Casassa,G., Lange, H.,Wendt, J., and Fritsche, M., 2010, Rapid crustal uplift in Patagonia due to enhanced ice loss: Earth Planet. Sci. Lett., v. 289, p. 22–29.

D'Orazio, M., Innocenti, F., Manetti, P., Tamponi, M., Tonarini, S., Gonzalez-Ferran, O., Lahsen, A., and Omarini, R., 2003, The Quaternary calc-alkaline volcanism of the Patagonian Andes close to the triple junction: geochemistry and petrogenesis of volcanic rocks from the Cay and Maca volcanoes (45°S, Chile): Jour. South Am. Earth Sci., v. 16, p. 219–24.

Douglass, D. C., Singer, B. S., Kaplan, M. R., Mickelson, D. M., and Caffee, M. W., 2006, Cosmogenic nuclide surface exposure dating of boulders on last-glacial and late-glacial moraines, lago Buenos Aires, Argentina: interpretative strategies and paleoclimate implications: Quat. Geochronol., v. 1, p. 43–58.

Echaurren, A., Folguera, A., Gianni, G., Orts, D., Tassara, A., Encinas, A., Gimenez, M., and Valencia, V., 2016, Tectonic evolution of the north Patagonian Andes (41°–44°S) through recognition of syntectonic strata: Tectonophysics, v. 677-678, p. 99–114.

Encinas, A., Folguera, A., Riffo, R., Molina, P., Fernandez Paz, L., Litvak, V.D., Colwyn, D.A., Valencia, V.A., and Carrasco, M., 2019, Cenozoic basin evolution of the Central Patagonia Andes: Evidence from geochronology, stratigraphy, and geochemistry: Geoscience Frontiers, v. 10, p. 1139-1165, https://doi.org/10.1016/j.gsf.2018.07.004.

Espinoza, F., Morata, D., Polve, M., Lagabrielle, Y., Maury, R.C., Guivel, C., Cotten, J., Bellon, H., and Suarez, M., 2007, Bimodal back-arc alkaline magmatism after ridge subduction: Pliocene felsic rocks from Central Patagonia (47.S): Lithos, v. 101, p. 191-217.

Espinoza, F., Morata, D., Polvé, M., Maury, R., Cotten, J., Bellon, H., Guivel, C., Lagabrielle, Y., Suarez, M., and Rossello, E., 2006, Mio-Pliocene magmatic variability in the central Patagonia back-arc region (47°5′S), paper presented at Backbone of the Americas, Patagonia to Alaska. Geol. Soc. of Am., Mem., Mendoza, Argentina.

Espinoza, F., Morata, D., Pelleter, E., Maury, R.C., Suarez, M., Lagabrielle, Y., Polvé, M., Bellon, H., Cotten, J., De la Cruz, R., and Guivel, C., 2005, Petrogenesis of the Eocene and Mio-Pliocene alkaline basaltic magmatism in Meseta Chile Chico, Southern Patagonia, Chile: evidence for the participation of two slab windows: Lithos, v. 82, p. 83-96, doi:10.1016/j.lithos.2004.09.024.

Faccenna, C., Oncken, O., Holt, A.F., and Becker, T.W., 2017, Initiation of the Andean orogeny by lower mantle subduction: Earth Planet. Sci. Lett., v. 463, p. 189–201.

Flint, S.S., Prior, D.J., Agar, S.M., and Turner, P., 1994, Stratigraphic and structural evolution of the Tertiary Cosmelli basin and its relationship to the Chile triple junction: Journal of the Geological Society of London, v. 151, p. 251-268.

Folguera, A., and Iannizzotto, N.F., 2004, The Lagos La Plata and Fontana fold-and-thrust belt: long-lived orogenesis at the edge of western Patagonia: Journal of South America Earth Sciences, v. 16, p. 541-566.

Folguera, A., and Ramos, V.A., 2011, Repeated eastward shifts of arc magmatism in the Southern Andes: a revision to the long-term pattern of Andean uplift and magmatism: Journal of South America Earth Sciences, v. 32, p. 531-546.

Folguera, A., Encinas, A., Echaurren, A., Gianni, G., Orts, D., Valencia, V., and Carrasco, G., 2018, Constraints on the Neogene growth of the central Patagonian Andes at the latitude of the Chile Triple Junction (45-47°S) using U/Pb geochronology in synorogenic strata: Tectonophysics, v. 744, p. 134-154.

Forsythe, R.D, and Nelson, E., 1985, Geological manifestations of ridge collision: evidence from the Golfo de Penas-Taitao basin, Southern Chile: Tectonics, v. 4, p. 477-495.

Forsythe, R.D., Nelson, E., Carr, M.J., Kaeding, M.E., Hervé, M., Mpodozis, C.M., Sofia, M.J., and Harambour, S., 1986, Pliocene near trench magmatism in Southern Chile: a possible manifestation of ridge collision: Geology, v. 14, p. 23-27.

Fosdick, J.C., Romans, B.W., Fildani, A., Bernhardt, A., Calderon, M., and Stephan, A.G., 2011, Kinematic evolution of the Patagonian retroarc fold-andthrust belt and Magallanes foreland basin, Chile and Argentina, 51°30'S: Geol. Soc. Am. Bull., v. 123, p. 1679-1698, doi : 10.1130/B30242.1.

Fosdick, J.C., Grove, M., Hourigan, J.K., and Calderón, M., 2013, Retroarc deformation and exhumation near the end of the Andes, Southern Patagonia: Earth Planet. Sc. Lett., v. 361, p. 504–517.

Frassinetti, D., and Covacevich, V., 1999, Invertebrados fosiles marinos de la Formacion Guadal (Oligocene superior-Mioceno inferior) en Pampa Castillo, region de Aisen, Chile: Servicio Nacional de Geologia y Mineria Boletin, v. 51, 96 p., Santiago.

Georgieva, V., Melnick, D., Schildgen, T.F., Ehlers, T.A., Lagabrielle, Y., Enkelmann, E., and Strecker, M.R., 2016, Tectonic control on rock uplift, exhumation, and topography above an oceanic ridge collision: Southern Patagoniaz Andes (47°S), Chile: Tectonics,

v. 35, doi:10.1002/2016TC004120.

Ghiglione, M.C., Ronda, G., Rodrigo J. Suárez, J.R., Aramendía, I., Barberón, V., Ramos, M.E., Tobal, J., García Morabito, E., Matrinod, J., and Christian Sue, C., 2019, Structure and tectonic evolution of the South Patagonian fold and thrust belt: coupling between subduction dynamics, climate and tectonic deformation: Andean Tectonics, Elsevier, Chapter 4, p. 675-698. https://doi.org/10.1016/B978-0-12-816009-1.00024-1

Ghiglione, M.C., Ramos, V.A., Cuitiño, J., and Barberon, V., 2016, Growth of the Southern Patagonian Andes (46-53°S) and their relation to subduction processes, A. Folguera et al. (eds.) Growth of the Southern Andes: Springer Earth System Sciences, p. 201-240, DOI 10.1007/978-3-319-23060-3_10.

Ghiglione, M.C., Naipauer, M., Sue, C., Barberon, V., Valencia, V., Aguirre-Urreta, B., and Ramos, V.A., 2015, U-Pb zircon ages from the northern Austral basin and their correlation with the Early Cretaceous exhumation and volcanism of Patagonia: Cretac. Research, v. 55, p. 116–128. Doi.org/10.1016j.cretres.2015.02.006.

Gianni, G. M., Echaurren, A., Fennell, L., Navarrete, C., Quezada, P., Tobal, J., and Folguera, A., 2018, Cretaceous orogeny and marine transgression in the Southern Central and Northern Patagonian Andes: aftermath of a large-scale flat-subduction event? In A. Folguera, et al. (Eds.), The Evolution of the Chilean-Argentinean Andes : Cham, Switzerland: Springer, p. 279–316.

Gianni, G., Navarrete, C., Orts, D., Tobal, J., Folguera, A., and Gimenez, M., 2015, Patagonian broken foreland and related synorogenic rifting: the origin of the Chubut Group Basin: Tectonophysics, v. 649, p. 81–99.

Gorring, M., Singer, B., Gowers, J., and Kay, S., 2003, Plio-Pleistocene basalts from the Meseta del Lago Buenos Aires, Argentina: evidence for asthenosphere-lithosphere interactions during slab-window magmatism: Chemical Geology, v. 193, p. 215-235.

Gorring, M., and Kay, S., 2001, Mantle processes and sources of Neogene slab window magmas from Southern Patagonia, Argentina: Journal of Petrology, v. 42, p. 1067–1094, doi:10.1093/petrology/42.6.1067.

Gorring, M.L., Kay, S.M., Zeitler, P.K., Ramos, V.A., Rubiolo, D., Fernandez, M.I., and Panza, J.L., 1997, Neogene Patagonian plateau lavas: continental magmas associated with ridge collision at the Chile triple junction: Tectonics, v. 16, p. 1-17.

Guillaume, B., Gautheron, C., Simon-Labric, T., Martinod, J., Roddaz, M., and Douville, E., 2013, Dynamic topography control on Patagonian relief evolution as inferred from low temperature thermochronology: Earth Planet. Sc. Lett., v. 364, p. 157-167.

Guivel, C., Morata, D., Pelleter, E., Espinoza, F., Maury, R., Polvé, M., Bellon, H., Cotton, J., Benoit, M., Suarez, M., and De la Cruz, R., 2006, Miocene to Late Quaternary Patagonian basalts (46-47° S): Geochronometric and geochemical evidence for slab tearing due to active spreading ridge subduction: J. of Volcan. and Geotherm Research, v. 149, p. 346–370.

Hein, A.S., Dunai, T.J., Hulton, N.R.J., and Xu, S., 2011, Exposure dating outwash gravels to determine the age of the greatest Patagonian glaciations: Geology, v. 39, p. 103–106, doi: 10.1130/G31215.1.

Hein, A. S., Hulton, N. R. J., Dunai, T. J., Sugden, D. E., Kaplan, M. R., and Xu, S., 2010, The chronology of the last glacial maximum and deglacial events in central Argentine Patagonia. Quat. Sci. Rev. 29, 1212–1227, doi:10.1016/j.quascirev.2010.01.020.

Hein, A. S., Hulton, N. R. J., Dunai, T. J., Schnabel, C., Kaplan,M. R., Naylor, M., and Xu, S, 2009, Middle Pleistocene glaciation in Patagonia dated by cosmogenic nuclide measurements on outwash gravels: Earth Planet. Sci. Lett., v. 286, p. 184–197, doi:10.1016/j.epsl.2009.06.026.

Hollin, J.T., and Schilling, D.H., 1981, Late Wisconsin-Weichselian mountain glaciers and

small ice cap: In The Last Great Ice Sheets, edited by G.H. Denton and T.J. Hughes, p.179-220, John Wiley, New York, 1981.

Horton, B.K., 2018, Tectonic Regimes of the Central and Southern Andes: Responses to Variations in Plate Coupling During Subduction: Tectonics, v. 37, p. 402–429.

Hu, J., Liu, L., Hermisillo, A., and Zhou, Q., 2016, Simulation of late Cenozoic South American flat-slab subduction using geodynamic models with data assimilation: Earth Planet. Sc. Lett., v. 438, p. 1–13, http://dx.doi.org/10.1016/j.epsl.2016.01.011

Jordan, T. E., Nester, P. L., Blanco, N., Hoke, G. D., Dávila, F., and Tomlinson, A. J., 2010, Uplift of the Altiplano-Puna plateau: A view from the west: Tectonics, v. 29, TC5007, https://doi.org/10.1029/2010TC002661

Jordan, T. E., Isacks, B. L., Allmendinger, R. W., Brewer, J. A., Ramos, V. A., and Ando, C. J., 1983, Andean tectonics related to geometry of subducted Nazca Plate: Geol. Soc. Amer. Bull., v. 94, p. 341–361.

Kaplan, M.R., Hein, A.S., Hubbard, A., and Lax, S.M., 2009, Can glacial erosion limit the extent of Glaciation?: Geomorphology, v. 103, p. 172-179.

Kaplan, M.R., Douglass, D.C., Singer, B.S., Ackert, R.P., and Cafee, M.W., 2005, Cosmogenic nuclide chronology of pre-Last Glacial Maximum moraines at Lago Buenos Aires, 46°S, Argentina: Quaternary Research, v. 63, p. 301-315.

Kaplan, M.R., Ackert, Jr., Singer, B.S., Douglass, D.C., and Kurz, M.D., 2004, Cosmogenic nuclide chronology of millenial-scale glacial advances during O-isotope stage 2 in Patagonia: Geol. Soc. Amer. Bull., v. 116, p. 321-384.

Kay, S.M., Ardolino, A.A., Gorring, M., and Ramos, V., 2007, The Somuncura Large igneous province in Patagônia: interaction of a transient mantle thermal anomaly with a subducting slab: Journal of Petrology, v. 48 (1), p. 43-77.

Kay, S.M., Gorring, M., and Ramos, V., 2004, Magmatic sources, setting and causes of

Eocene to Recent Patagonian plateau magmatism (36°S to 52°S): Revista de la Asociación Geológica Argentina, v. 59 (4), p. 556–568.

Kay, S.M., Ramos, V., and Gorring, M., 2002, Geochemistry of Eocene plateau basalts related to ridge collision in southern Patagonia. XV-Congreso Gológico Argentino, Actas 3, p. 60-65.

Kay, M.S., Ramos, V.A., and Marquez, M., 1993, Evidence in Cerro Pampa volcanic rocks for slab melting prior to ridge-trench collision in Southern South America: The journal of Geology, v. 101, p. 703–714.

Lagabrielle, Y., Suarez, M., Rossello, E.A., Hérail, G., Martinod, J., Régnier, M., and De la Cruz, R., 2004, Neogene to Quaternary tectonic evolution of the Patagonian Andes at the latitude of the Chile Triple Junction: Tectonophysics, v. 385, p. 211-241.

Lagabrielle, Y., Le Moigne, J., Maury, R.C., Cotten, J., and Bourgois, J., 1994, Volcanic record of the subduction of an active spreading ridge, Taitao peninsula (Southern Chile): Geology, v. 22, p. 515–518.

Leslie, R.B., 1986, Cenozoic tectonics of Southern Chile triple junction migration, ridge subduction, and forearc evolution: PhD thesis, 276 pp., Columbia Univ., New York.

Lonsdale, P., 2005, Creation of the Cocos and Nazca Plates by fission of the Farallon Plate: Tectonophysics, v. 404, p. 237–264.

Lovecchio, J-P., Rohais, S., Joseph, P., Bolatti, N.D., and Ramos, V.A., 2020, Mesozoic rifting evolution of SW Gondwana: a poly-phased, subduction-related, extensional history responsible for basin formation along the Argentinean Atlantic margin: Earth Sc. Review, v. 203, p. 103–138, https://doi.org/10.1016/j.earscirev.2020.103138

Martin, H., 1987, Archean and modern granitoids as indicators of changes in geodynamic processes: Revista Brasileira de Geociencia, v. 17, p. 360–365.

Martinod, J., Gerault, M., Husson, L., and Regard, V., 2020, Widening of the Andes: an interplay between subduction dynamics and crustal wedge tectonics: Earth Sc. Reviews, v. 204, p. 103170, https:doi.org/10.1016/j.earscirev.2020.103170

Mercer, J., and Sutter, J., 1982, Late Miocene-earliest Pliocene glaciation in Southern Argentina: implications for global ice-sheet history: Pal. Pal. Pal., v. 38, p. 185–206

Mercer, J., 1976, Glacial history of Southernmost South America: Quaternary Research, v. 6, p. 125–166.

Montgomery, D.R., 1994, Valley incision and the uplift of mountain peaks: J. Geophys. Research, v. 99, p. 13,913–13,921.

Mpodozis, C.M., Hervé, M., Nasi, C., Soffia, M.J., Forsythe, R.D., and Nelson, E.P., 1985, El magmatismo Plioceno de Peninsula Tres Montes y su relacion con la evolucion del punto triple de Chile Austral: Revista Geológica de Chile, v. 25-26, p. 13–28.

Murdie, R.E, Pugh, D.T., and Styles, P., 1999, A lightweight, portable, digital probe for measuring the thermal gradient in shallow water sediments, with examples from Patagonia: Geo-Marine Letters, v. 18, p. 315–320.

Olbertz D., Wortel, M.J.R., and Hansen, U., 1997, Trench migration and subduction zone geometry: Geophys. Res. Lett., v. 24, p. 221–224.

Oncken, O., Hindle, D., Kley, J., Elger, K., Victor, P., and Schemmann, K., 2006, Deformation of the central Andean upper plate system, facts, fiction, and constraints for plateau models. In: The Andes: Springer, Berlin, Heidelberg, p. 3–27.

Pardo-Casas, F., and Molnar, P., 1987, Relative motion of the Nazca (Farallon) and South American Plates since Late Cretaceous time: Tectonics, v. 6, p. 233–248, https://doi.org/10.1029/TC006i003p0023

Pennington, W.D., 1981, Subduction of the eastern Panama Basin and seismotectonics of northwestern South America: J. Geophys. Res., Solid Earth v. (1978–2012)86 (B11), p.

10753–10770.

Porter, S.C., Clapperton, C.M., and Sugden, D.E., 1992, Chronology and dynamics of deglaciation along and near the strait of Magellan: South America, Sver. Geol. Unders., v. 81, p. 233-239.

Quinteros, J., and Sobolev, S.V., 2013, Why has the Nazca plate slowed since the Neogene?: Geology, v. 41, p. 31–34.

Rabassa, J., Coronato, A.M., and Salemme, M., 2005, Chronology of the Late Cenozoic Patagonian glaciations and their correlation with biostratigraphic units of the Pampean region (Argentina): J. South Amer. Earth Sc., v. 20, p. 81–103, doi:10.1016/j.jsames.2005.07.004

Rabassa, J., and Clapperton, C.M., 1990, Quaternary glaciations of the Southern Andes: Quat. Sc. Reviews, v. 9, p. 153–174.

Ramos, V.A., and Folguera, A., 2009, Andean flat-slab subduction through time: Geol. Soc. (Lond.) Spec. Publ. 327 (1), p. 31–54.

Ramos, V. A., 2005, Seismic ridge subduction and topography: foreland deformation in the Patagonian Andes: Tectonophysics, v. 399(1-4), p. 73–86, doi:10.1016/j.tecto.2004.12.016.

Ramos, V.A., Cristallini, E.O., and Pérez, D.J., 2002, The Pampean flat-slab of the Central Andes: J. South Am. Earth Sci., v. 15 (1), p. 59–78.

Ramos, V.A., and Kay, S.M., 1992, Southern Patagonian plateau basalts and deformation: backarc testimony of ridge collisions: Tectonophysics, v. 205, p. 261-282.

Ramos, V.A., 1989, Andean foothills structure in northern Magallanes basin, Argentina, Amer. Ass. Petrol. Geologists Bull., v. 73, p. 887-903, DOI: 10.1306/44B4A28A-170A-11D7-8645000102C1865D

Rivas, H., Bostelmann, E., Le Roux, J., and Ugalde, R., 2015, Fluvial facies and architecture

of the late middle Miocene, Mayoan, deposits of Chilean Patagonia. In: XIV Congreso Geológico Chileno, Actas, Volume 1, p. 812–815.

Rodriguez, E.E., and Russo, R.M., 2020, Southern Chile crustal structure from teleseismic receiver functions: responses to ridge subduction and terrane assembly of Patagonia: Geosphere, v. 16 (1), p. 378–391, https://doi.org/10.1130/GEOS016921.1.

Rojas Vera, E.A., Mescua, J., Folguera, A., Becker, T.P., Sagripanti, L., Fennell, L., Orts, D., and Ramos, V.A., 2015, Evolution of the Chos Malal and Agrio fold and thrust belts, Andes of Neuquen: Insights from structural analysis and apatite fission track dating: J. South Am. Earth Sc., v. 64, p. 418–433, http://dx.doi.org/10.1016/j.jsames.2015.10.001

Ronda, G., Ghiglione, M., Barberón, V., Coutand, I., and Tobal, J., 2019, Mesozoic-Cenozoic evolution of the Southern Patagonian Andes fold and thrust belt (47°–48°S): Influence of the Rocas Verdes basin inversion and onset of Patagonian glaciations: Tectonophysics, v. 765, p. 83–101.

Russo, R.M., 2012, Source-side shear-wave splitting and upper-mantle flow beneath the Arakan slab, India-Asia_sundaland triple junction: Geosphere, v. 8, p. 158-178, doi: 10.1130/GES00534.1

Russo, R.M., VanDecar, J.C., Comte, D., Mocanu, V.I., Gallego, A., and Murdie, R.E., 2010a, Subduction of the Chile ridge: upper mantle structure and flow: GSA Today, v. 20, p. 4-10, doi:10.1130/GSATG61A.1.

Russo, R.M., Gallego, A., Comte, D., Mocanu, V.I., Murdie, R.E., and VanDecar J.C., 2010b, Source-side shear wave splitting and upper mantle flow in the Chile Ridge subduction region: Geology, v. 38, p. 707–710, doi: 10.1130/G30920.1.

Russo, R., and Silver, P., 1994, Trench-Parallel Flow Beneath the Nazca Plate from Seismic Anisotropy: Science, v. 263, p. 1105–1111.

Russo, R.M., and Silver, P.G., 1996, Cordillera formation, mantle dynamics, and the Wilson

cycle: Geology, v. 24, p. 511–514.

Schellart, W.P., 2008, Subduction zone trench migration: slab driven or overriding-plate-driven?: Physics of the Earth and Planetary Interiors, v. 170, p. 73–88. doi:10.1016/j.pepi.2008.07.040

Sigmarsson, O., Martin, H., and Knowles, J., 1998, Melting of a subducting oceanic crust in Austral Andean lavas from U-series disequilibria: Nature, v. 394, p. 566–569.

Silver, P. G., Russo, R. M., and Lithgow-Bertelloni, C., 1998, Coupling of South American and African Plate motion and plate deformation: Science, v. 279, p. 60–63. https://doi.org/10.1126/science.279.5347.60

Singer, B., Ackert, Jr. R.P., and Guillou, H., 2004, $^{40}Ar/^{39}Ar$ and K/Ar chronology of Pleistocene glaciations in Patagonia: Geol. Soc. Amer. Bull., v. 116, p. 434–450. doi:10.1130/B25177.1.

Somoza, R., 1998, Updated Nazca (Farallon)–South America relative motions during the last 40 My: Implications for mountain building in the central Andean region: Journal of South American Earth Sciences, v. 11, p. 211–215.

Stern, C.R., 2011, Subduction erosion rates, mechanisms, and its role in arc magmatism and the evolution of the continental crust and mantle: Gondwana Research, v. 20, p. 284-308.

Stern, C.R. and De Wit, M.J., 2003, Rocas Verdes ophiolites, southernmost South America: remnants of progressive stages of development of oceanic type crust in a continental margin back-arc basin: Geological Society, London, Special publication, 218(1), p. 665–683.

Stern, C.R., and Kilian, R., 1996, Role of the subducted slab, mantle wedge and continental crust in the generation of adakites from the Andean Austral Volcanic Zone: Contrib. Mineral. Petrol., v. 123, p. 263–281.

Thomson, S.N., Brandon, M.T., Tomkin, J.H., Reiners, P.W., Vasquez, C., and Wilson, N.J., 2010, Glaciation as a destructive and constructive control on mountain building: Nature, v. 467, p. 313-317, doi:10.1038/nature09365

Thomson, S.N., 2002, Late Cenozoic geomorphic and tectonic evolution of the Patagonian Andes between latitudes 42°S and 46°S an appraisal based on fission-track results from the transpressional intra-arc Liquiñe-Ofqui fault zone: Geol. Soc. Am. Bull., v. 114, p. 1159–1173.

Thomson, S.N., Hervé, F., and Stöckhert, B., 2001, Mesozoic-Cenozoic denudation history of the Patagonian Andes (Southern Chile) and its correlation to different subduction processes: Tectonics, v. 20, p. 693–711.

Tomkin, J.H., and Roe, G.H., 2007, Climate and tectonic controls on glaciated critical-taper orogens. Earth and Planet. Sc. Lett., v. 262, p. 385–397, doi:10.1016/j.epsl.2007.07.040

Thorkelson, R.P., and Taylor, R.P., 1989, Cordilleran slab windows: Geology, v. 17, p. 833–836.

Wang, K., Hu, Y., Bevis, M., Kendrick, E., Smalley Jr, R., Barriga Vargas, R., and Lauria, E., 2007, Crustal motion in the zone of the 1960 Chile earthquake: detangling eathquake-cycle deformation and forearc-sliver translation: Geoch. Geophy. Geosys., v. 8 (10), doi: 10.1029/2007GC001721.

Whipple, K.X., 2009, The influence of climate on the tectonic evolution of mountain belts: Nature Geoscience, v. 2, p. 97–104,

Willett, C.D., Ma, K.F., Brandon, M.T., Hourigan, J.K., Christeleit, E.C., Shuster, D.L., 2020. Transient glacial incision in the Patagonia Andes from ~6 Ma to present: Sci. Adv, v. 6: eaay1641.

Caption of Figures

Figure 1. Geodynamics of the studied area. The South Chile ridge is currently subducting at the Chile Triple Junction (46°09'S, Bourgois et al., 2000). Main FZ and segments of the SCR 1 to SCR 3 before subduction, black line; SCR 0 and SCR -1 after subduction at depth, orange dash line) are shown. The purple dash line shows the Patagonia slab window boundaries at depth (Bourgois and Michaud, 2002; Breitsprecher and Thorkelson, 2009; Russo et al., 2010 a and b; Bourgois et al., 2016a). Note that the reentrant of the Patagonia Slab Window boundary at ~48°S branches away from the Austral Volcanic Zone. The SCR -1 segment is located beneath the North Patagonia Icefield. The PSW matches a volcanic gap (DeLong and Fox, 1977; Ramos and Kay, 1992; Kay et al., 1993). Dark blue arrows show the locus of Westerlies and maximum moisture during the Last Glacial Maximum at $\delta^{18}O$ isotope stage 2 and at Present.

CTJ–Chile Triple Junction; FZ–Fracture Zone; LOFS–Liquine-Ofqui fault system; NPI–North Patagonia Icefield; PSW–Patagonia Slab Window; SCR–South Chile Ridge. Stars show volcanos; (AVZ)–Austral Volcanic Zone: A–Aguilera; B–Burnay; L– Lautaro; R–Reclus; V–Viedma. (SSVZ)–Southern South Volcanic Zone: C–Cay; Ch–Chaiten; Co–Corcovado; GPPB–Golfo de Penas pull-apart basin; H–Hudson; M–Maca; Me-Mentolat; Mel–Melimoyu; Mi–Michimahuida; Mu–Murta; Y–Yanteles. White color shows icefield. Locations of Fig. 2, 3, 20, 21A, and 22 are shown. Color refers to the online version.

Figure 2. Morphological frame of the studied area. Most significant ice lobe incisions of Patagonia include the General Carrera-Buenos Aires and Chocrane-Pueyrredon glacial lakes. These incisions are the best potential sites for excavating gashes into the Andean morphotectonic frontline commonly accepted as the morphological signature of the so-called Lower Miocene Andean fold and thrust belt. V-shaped incision notching the Andean morphological front must expose the fold and thrust belt entering inward along glacial lake

trenches, if exists. The sinuous divide between the Atlantic and Pacific follows lateral scars of ice lobes connecting eastward to the LGM terminal moraine. Note that the GCBA (201 m) and the CP (155 m) glacial lakes are outflowing to the Pacific through the Rio Baker outlet. The Rio Baker watershed is draining the Andean Foreland area, crossing the Andes. The Rio Baker system is antecedent drainage with respect to the Andes uplift.

White color shows elevation from 1800 to 4000 m. Thick dash-line–Andean morphotectonic frontline; medium dash-line–Atlantic-Pacific divide; thin dash-line Argentina-Chile boundary. CB—Cosmelli basin; H–Hudson volcano; MCC–Meseta de Chile Chico; LGM–Last Glacial Maximum; MLBA–Meseta del Lago Buenos Aires; MSL–Mt San Lorenzo; MZ–Mt Zeballos; NPI–North Patagonia icefield; SPI–South Patagonia icefield. Location of Fig. 3 is shown. Color refers to the online version.

Figure 3. Main morphotectonic elements. Note the deep glacial lobe trenches bounding the Mt Zeballos Ridge (MZR). MZR lies astride the Andean fold and thrust belt frontline, which follows the Rio Ghio/Rio Zeballos depression (divide at the Zeballos pass). The highest point of the MZR is the Mt Zeballos volcano (2700 m) located E of the Andes frontline. CPGL–Cochrane Pueyrredon Glacial Lake; GCBAGL–General Carrera Buenos Aires Glacial Lake. Locations for Figs. 5, 9, 11, 12, 14, 16, 17, 19, 20, 21, 22 are shown.

Figure 4. Stratigraphic and age constraints for the past 24 Ma. GCBA—General Carrera-Buenos Aires; GPG—Great Patagonian Glaciation; MMCO—Mid Miocene Climatic Optimum; MZVC—Mt Zeballos Volcanic Complex (1.7-4 Ma). Note that the studied segment was at sea level between 18.1 and 20.3 Ma. The Cosmelli basin located 70-80 km W of the Andean frontline exhibits shallow marine sediment of lower Miocene age that spread westward along major embayment over the Andes. (1) Kay et al. (1993); (2) Flint et al. (1994); (3) Gorring et al. (1997); (4) Brown et al. (2004); (5) Blisniuk et al. (2005); (6)

Espinoza et al. (2005); (7) Guivel et al. (2006); (8) De la Cruz and Suarez (2008); (9) Boutonnet et al. (2010); (10) Cuitiño et al. (2015); (11) Folguera et al. (2018); (12) Dal Molin et al. (1998); (13) De Iuliis et al. (2008); (14) Rivas et al. (2015); (15) Encinas et al. (2019). Pale gray–envelop show estimated sea level range; Grey–volcanic episodes (mainly basalt); blue–shallow marine deposit; yellow and orange–fluvial deposits; the 4 stars show the Mid Pliocene warm period 2.97-3.29 Ma. Color refers to the online version.

Figure 5. Geologic and structural map of the Andean morphotectonic frontline along the Las Posadas, Pueyrredon and Cochrane lakes segment (map location, Fig. 3). This area exposes the two main unconformities MU1 and MU2 (Fig. S1). Along cross-sections BB' and CC' (Fig. 6) the Ibañez, Springhill, and Belgrano Fm dipping 80° to the E is unconformably overlying (MU1) the Paleozoic metamorphic basement. The flat lying Rio Tarde Fm (97-118 Ma) and its sedimentary cover including the El Chacay Fm (18.1-20.3 Ma) are unconformably (MU2) overlying older beds. To the north (cross-section AA' Fig.6), at the Chile-Argentina border, the Jurassic Quemado Fm underthrusts the Paleozoic metamorphic basement along the Main Andean Thrust (MAT). Southward (cross-section BB' and CC' Fig. 6), the western and eastern shores of the Pueyrredon lake expose the Paleozoic metamorphic basement to the W and the Quemado Fm to the E, respectively. The low dipping (5-7°) Quemado Fm projected to the W suggests underthrusting beneath the Paleozoic metamorphic basement. Along the so-called "Rio Furioso thin-skinned structure" (RFTSS, Ronda et al., 2019), the Rio Tarde Fm is unconformably overlying the Quemado Fm on one side (E) and the Paleozoic basement and its Upper Jurassic to Lower Cretaceous sedimentary cover on the other side (W). This allows inferring the Rio Tarde Fm sealing the MAT. The most likely age for MAT is ~120 Ma. Black line–fault; thick line with triangle–thrust fault. Location of cross-sections Fig. 6 and maps of Fig. 7 is shown. Star shows the location of Fig. S6. Point X refers

to Fig. 9. See text for more details. Color refers to the online version.

Figure 6. Cross-sections of the Andean morphotectonic frontline along the Las Posadas, Pueyrredon and Cochrane lakes segment. AA', BB', and CC' lines are located on Fig.5. Note that dip of the Rio Tarde Fm exhibits increasing dip as it approaches the basement rock. The bending of layering originates from draping during volcanic ash flow deposit molding the frontal relief of the Proto Andes. No evidence exists for the Rio Tarde Fm together with its sedimentary cover of Cenozoic age underthrusting the Andes. Color refers to the online version.

Figure 7. Detail map (location Fig. 5) along the so-called "Rio Furioso thin-skinned structure" (RFTSS, Ronda et al., 2019). Volcanic flow and interbedded sediment, including the Ibañez, Springhill, Belgrano, Rio Tarde, El Chacay, and Santa Cruz Fm are dipping eastward. No evidence exists documenting any of these Fm underthrusting beneath the Paleozoic metamorphic basement. Location of Fig. S6 and AA', BB', CC' profiles (Fig. 8) is shown. Note that MU2 is an angular unconformity. Barb along fault is on the side of the downthrow block. Color refers to the online version.

Figure 8. Profiles along the so-called "Rio Furioso thin-skinned structure" (RFTSS, Ronda et al., 2019). The Rio Tarde, El Chacay, and Santa Cruz Fm are dipping eastward. No evidence exists suggesting these formations underthrust beneath the frontal zone of the Andes. On the contrary, projection of bedding to the W strongly suggests that these Formations were covering the Andes before being removed by erosion. Color refers to the online version.

Figure 9. Geologic map of the Paso Roballos area and lower Zeballos Pass corridor E of the upper Chacabuco valley (map location Fig. 3). The Eastern Spur fault is proposed to be a

conjugate fault for the right lateral Valle Chacabuco fault. This assumption allows proposing the σ1 maximum stress trending as shown by the thick black arrow. See Fig. 11 for more details regarding the Valle Chacabuco fault. SP–rocky spur; black line–fault; black line with triangle–thrust fault, upper unit with triangle; X and Y–location of specific points referred in the text. Location of cross-sections at Fig. 10 is shown. See text for more details. Color refers to the online version.

Figure 10. Geologic cross-sections of the area shown at Fig. 9. See text for more details. Color refers to the online version.

Figure 11. Geologic map of the Alto Rio Ghio area S of the Zeballos pass. X refers to Fig. S19; Y refers to Fig. S22. CGS–Central Glacial System; DD'–northern segment of cross-section shown at Fig. 10. ELGS–East Lateral Glacial System; T1 to T4–retreating terminal moraines, bounding hummocky flat areas of the retreating CGS; WGLS–West Lateral Glacial System. See text for more details. References for age of samples (numbers refer to Table S1): 2.42 ± 0.03 Ma (95- Brown et al., 2004), 2.76 ± 0.07 Ma (29- Boutonnet et al., 2010), 2.94 ± 0.10 Ma (26- Boutonnet et al., 2010), 3.03 ± 0.03 Ma (94- Brown et al, 2004), 3.08 ± 0.13 Ma (71- Espinoza et al;, 2006), 3.10 ± 0.08 Ma (32- Boutonnet et al., 2010), 3.18 ± 0.04 Ma (93- Brown et al., 2004), 3.23 ± 0.08 Ma (34- Boutonnet et al., 2010), 3.28 ± 0.10 Ma (72- Espinoza et al., 2006), 3.29 ± 0.22 Ma (92- Brown et al., 2004), 3.65 ±0.10 Ma (69- Espinoza et al., 2007), 4.17 ± 0.16 Ma (45- Boutonnet et al, 2010), 4.32 ± 0.23 Ma (50- Guivel et al., 2006), 4.41 ± 0.54 Ma (31- Boutonnet et al., 2010), 4.48 ± 0.14 Ma (33- Boutonnet et al., 2010), 4.81 ± 0.32 Ma (53- Guivel et al., 2006), 4.98 ± 0.15 Ma (48- Guivel et al., 2006), 6.41 ± 0.22 Ma (46- Boutonnet et al., 2010), 6.85 ± 0.15 Ma (35- Boutonnet et al., 2010), 6.95 ±

0.24 Ma (49- Guivel et al., 2006), 12.24 ± 1.56 Ma (28- Boutonnet el al., 2010), 14.48 ± 0.17 Ma (27- Boutonnet et al., 2010). Color refers to the online version.

Figure 12. Geological map of the area north Zeballos Pass corridor (location on Fig. 3). The Chile-Argentina border follows the Rio Jeinimeni (NW of map). On the Chilean side (to the N) is the Meseta de Chile Chico (MCC). ABC, DD', EE', FF' show the location of cross-sections Fig. 13. Location of Fig. 14A is shown (box). Numbers in brackets following ages refer to Table S2; age south of MCC 41.6 ± 1.4 Ma from De La Cruz and Suarez (2008); age along Rio Jeinimeni 46 ± 3 Ma from Kay et al. (1993). X and Y refer to specific points described in text. CRLF–Cerro Risco del Leon fault; JF–Jeinimeni fault; MCC–Meseta de Chile Chico; PF–Pedregoso fault; RLF–Rio Lincoln fault; RZFS–Rio Zeballos fault system. See text for more details. Color refers to the online version.

Figure 13. Cross-sections showing the tectonic relationship along the Andean morphotectonic frontline north of the Zeballos Pass corridor (cross-sections ABC, DD', EE', FF' located on Fig. 12). Note that the Rio Lincoln fault shows no extension to the north along the Rio de Las Nieves (cross-section EE'). See text for more details. Color refers to the online version.

Figure 14. Rio Lincoln cross-section showing Lower Miocene Foreland sediment unconformably overlying the Andean morphotectonic frontline. A- Geological map along the Rio Lincoln. west of map, black basalt of the Ibañez Fm dips 45 to 75° to the E exhibits its sedimentary cover of Lower Cretaceous age dipping 75 to 85° to the E. East of map, the Foreland sediment of the lower Miocene Zeballos Fm exhibits sub-horizontal sandstone beds. Frame shows the location of Fig. 14B. B- Detailed map of the contact zone between the Lower Cretaceous (the Andes) and lower Miocene (Foreland) sediment. C- Cross-section AA'

shown at Fig. 14B. The lower Miocene Foreland sediment is dipping 2 to 4° to the E. Lower Cretaceous and lower Miocene sediment exhibits low internal tectonic deformation. Dip of Cretaceous beds is related to the main contractional event at ~120 Ma. At this site the lower Miocene is inferred sealing the tectonic front of the Andes. C- Cross-section, location at Fig. 14B. AKT Gr–Apeleg, Katterfeld, Toqui Fm of Lower Cretaceous age (Ki); Z–Zeballos Pass Fm of lower Miocene. Thick dash-line–Rio Lincoln fault inferred at depth. Location at Fig. 3. See text for more details. Color refers to the online version.

Figure 15. Geological map of the Meseta de Chile Chico area (modified from De la Cruz and Suarez, 2008). AA' to EE' show locations of cross-sections in Fig. 16. Note that the Jeinimeni and the Chile Chico faults show no prolongation to the N and to the S, respectively. AMR–Arroyo Marques ramp; CCF–Chile Chico fault; JF–Jeinimeni fault; LNFW–Rio de Las Nieves fault West; LNFE–Rio de Las Nieves fault East; PF–Pedregoso fault. Ages reported in the MCC are from De la Cruz and Suarez (2008). The 16.1-16.8 Ma age for the Zeballos Pass-Rio Jeinimeni Fm is from Folguera et al. (2018). Note that MAT is bounding the so-called Upper Tectonic Unit (Ibañez Fm and Lower Cretaceous sedimentary cover) from the Lower Tectonic Unit (Quemado Fm). Ages of intrusive bodies (3.6 ± 0.3 and 9.6 ± 0.6 Ma) document that the Pico Sur volcanic complex (3.6-5.7 Ma) and Upper Basalt (7-16 Ma) were covering the MCC more to the East. Map location at Fig. 3. Color refers to the online version.

Figure 16. Cross-sections along the Andean morphotectonic frontline west of MCC. Location of cross-sections at Fig. 15. AMR–Arroyo Marques ramp; βζ–Pico Sur volcanic complex; CCF–Chile Chico fault; JF–Jeinimeni fault; Kd–Divisadero Fm; Ki–Lower Cretaceous sediment; Lb–Lower Basalt Fm; LNFW–Rio de Las Nieves fault West; LNFE–Rio de Las Nieves fault East; MAT ~120 Ma–Main Andean Thrust at ~120 Ma; MU2–Main

Unconformity 2 at ~120 Ma; PF–Pedregoso fault; ωε–Upper basalt; Z-RJ–Zeballos Pass and Rio Jeinimeni Fm. See text for details. Color refers to the online version.

Figure 17. Geological map located NW of Chile Chico (location at Fig. 3). The thick volcanic flows of the Quemado Fm are dipping few degrees to the east flattening towards the east. This tectonic style documents the tectonic contrast between the two units on either side of the Main Andean Thrust. The Ibañez Fm (Upper tectonic unit) exhibits N-S trending folds and faults (Fig. 15 and 16). Main faults of the Quemado Fm (Lower tectonic unit) are trending N 60-70°E and do not extend into the Upper Tectonic Unit. Along the shoreline of the GCBA glacial lake vertical tectonic lenses document a right lateral tectonic displacement along the Chile Chico fault. See text for more details

Figure 18. The Andean morphotectonic frontline along the Jeinimeni fault zone (MCC eastern edge, Arroyo Quebrada Honda area, location on Fig. 3). A- Geological map. To the west, a complex zone of sub-vertical faults is cutting across the volcanic flows of the Ibañez Fm dipping eastward. The fault zone is 250 to 300 m wide at the Arroyo Hondo riverbed. B- Cross-section XX', the fault zone consists of a succession of vertical tectonic sheets mainly involving the Ibañez Fm to the west. To the east tectonic lenses exhibits deformed sediments including the shallow marine El Chacay Fm. These sediments show an almost-penetrative planar fabric at tectonic lens boundaries. East of the fault zone the Zeballos Pass Fm exhibits an upward bending along the fault zone (Fig. S26). The lower hanging wall is unfaulted documenting two main phases in the tectonic evolution of the Jeinimeni fault zone. A main first phase is associated with the evolution of the tectonic zone involving the El Chacay Fm; the second phase is more localized involving the Zeballos Pass Fm. The Zeballos Pass Fm has accumulated after the first tectonic phase. No evidence exists for any of the lower Miocene

Fm underthrusting the MCC. The El Chacay Fm occurs at high elevation on the MCC Fig. 15, and DD' Fig. 16) has been uplifted by several hundreds of meters. See text for more details. Color refers to the online version.

Figure 19. The Arroyo Marques ramp is a fault zone connecting the Chile Chico and the Jeinimeni right lateral transtensional faults, which show no south and north prolongation, respectively. The ramp zone evolved in two tectonic phases: the first one is a detachment fault zone exhibiting penetrative tectonic stretching features dipping 40-50° towards the N130°E (Fig. S28B); the second one is associated with the sub-vertical El Manzano fault. A- Geological map of the ramp area. B- Cross-section, location Fig. 19A. Thick black line with triangle–Main Andean Thrust at ~120 Ma; black dash-line with blue arrows–detachment fault (first tectonic step). Kd—Divisadero Fm; LB—Lower Basalt Fm; LGM—Last Glacial Maximum; Z-RJ—Zeballos Pass and Rio Jeinimeni Fm. X and Y refer to specific descriptions in the text. Location on Fig. 3. Color refers to the online version.

Figure 20. Rio Baker and Rio Simpson watersheds. Thick brown dash line–Rio Baker watershed; thin brown dash line–Rio Simpson watershed; C–Cay volcano, 2090 m; CB–Cosmelli basin; CP–Cochrane-Pueyrredon glacial lake; CTG–Caleta Tortel gap; GCBA–General Carrera-Buenos Aires glacial lake; H–Hudson volcano, 1905 m; L—Lautaro volcano; M–Mentola volcano; OHSM–O'Higgins-San Martin glacial lake. 1–blue line, water drained towards the Pacific during interglacial periods; 2–pink line, water drained towards the Atlantic mainly during glacial periods; 3–purple dash line, abandoned drainage. Dotted patch–Patagonian batholith (Middle Jurassic to Miocene); grey patches show location studied by Thomson et al. (2001); elevation in meters; yellow patch shows outcrop distribution of the

shallow marine El Chacay and Guadal Fms. See text for more details. Color refers to the online version.

Figure 21. Deep-seated structures at the Patagonia Slab Window area. A–Yellow thick line (A, B, C, and D) shows location of the CCP stacking profiles from Rodriguez and Russo (2020). Thick brown line shows location of boundaries where Moho sharply shallows from 35 to 30 km. White and green thick dashed lines show the edge of the PSW at 50 and 100 km depth from Russo et al. (2010 a and b). Thick orange dashed line shows the South Chile Ridge (SCR 0 and SCR -1) location at depth (Bourgois et al., 2016a). Thick black lines show projection of subducted Fracture Zone, delimiting SCR0 and SCR-1 (northern boundary). B–Cross-section from the Chile Trench (west) to the Foreland area (east), location on Fig. 21A. No vertical exaggeration. ANT ASTH–Antarctic Plate asthenosphere; CB–Cosmelli Basin; CPGL–Cochrane-Pueyrredon Glacial Lake Trench; GCBAGL–General Carrera-Buenos Aires Glacial Lake Trench; CTJ–Chile Triple Junction; HV–Hudson volcano; LC–Lower crust; LOFS–Liquine-Ofqui fault system; MCC–Midcrustal Converters; MSV–Mt San Valentin; MZR–Mt Zeballos Ridge; NAZ ASTH–Nazca Plate asthenosphere; NPI–North Patagonia Icefield; SAM ASTH–South America Plate Asthenosphere; SCR-1–South Chile Ridge segment -1; Sub–subsidence; UC–Upper crust; VE–vertical exaggeration, VE : 5 for topography. Red arrow–uplift and subsidence; green arrow–upward volcanic flow at MZR hinge arch. See text for more details. Color refers to the online version.

Figure 22. The Marques-Zeballos Pass ramp system (MZPRS) and main structural elements. Yellow color shows the lower Miocene Fms including the Rio Jeinimeni and Zeballos Pass Fms overlying the shallow marine El Chacay Fm. All of these formations show no evidence for underthrusting the Andes at the Andean morphotectonic frontline. Minimum extension of

the lower Miocene Fm beneath the MLBA is shown. The zigzag edge of the Andean morphotectonic frontline is controlled by the transtensional MZPRS evolving in two tectonic phases. The first main orogenic pulse (800-1200 m uplift at the MCC) has resulted in the Proto-Andes building and regression of the shallow marine El Chacay Fm. The subsequent fluvial Rio Jeinimeni and Zeballos Pass Fms accumulated outward the morphotectonic frontline of the Proto-Andes. The upper part of Zeballos Pass Fm seals the ramp system. The second tectonic phase is associated with fault systems that follows both in space and time the phase 1 fault network. White stars–site providing shallow marine fauna; white rectangle–elevation of El Chacay Fm; grey rectangle–elevation of Rio Jeinimeni and Zeballos Pass Fms. ACBFS–Argentina-Chile Border fault system; AMR–Arroyo Marques ramp; CP lake–Cochrane-Puerreydon lake; CB–Cosmelli Basin; CPGL–Cochrane-Pueyrredon Glacial Lake; GCBAGL–General Carrera-Buenos Aires Glacial Lake; green rectangle–Main unconformity at ~118-120 Ma; pink line with triangle–Main Andean Thrust (MAT) at ~120 Ma; MZPRS–Marques-Zeballos Pass Ramp System, RJR–Rio Jeinimeni Ramp. Color refers to the online version.

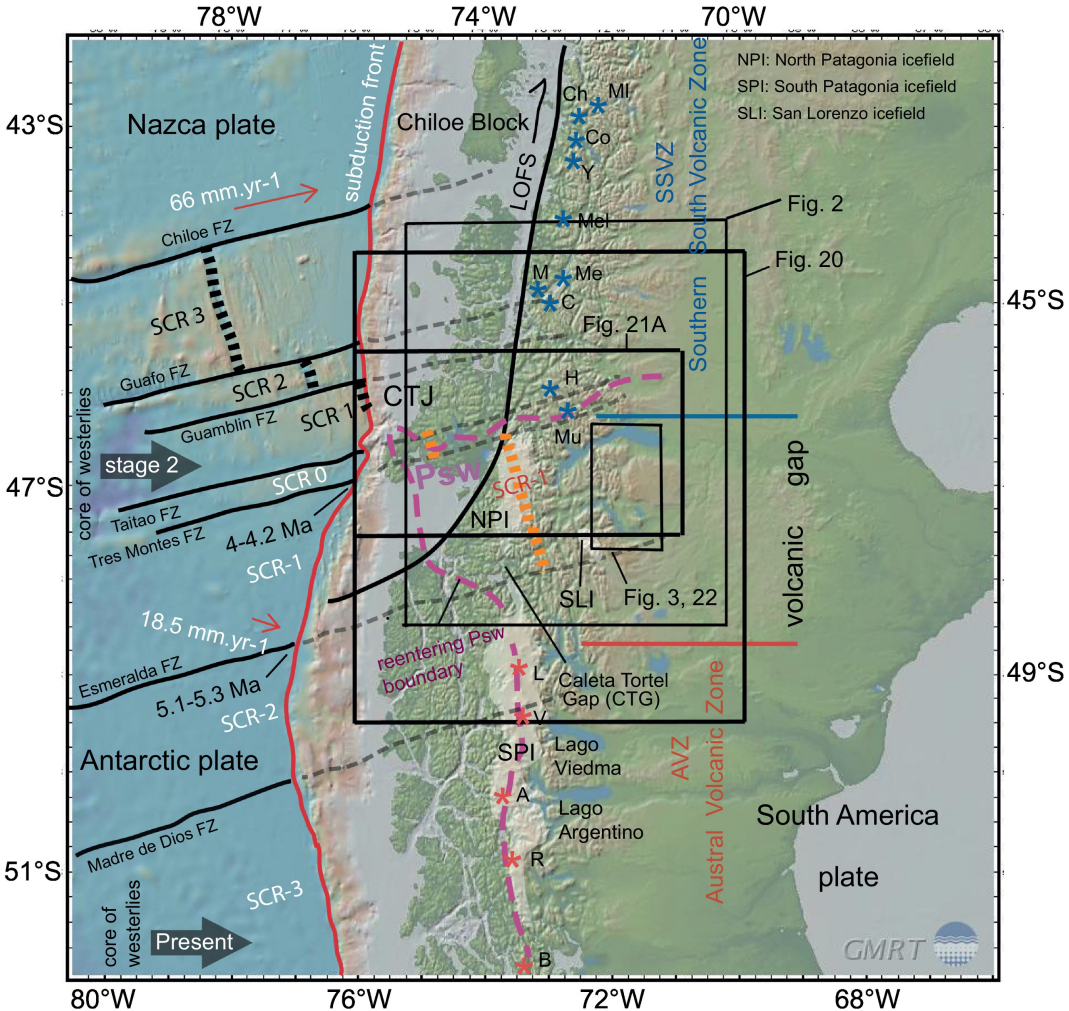
78°W
74°W
70°W
43°S
45°S
47°S
49°S
51°S
80°W
76°W
72°W
68°W
NPI: North Patagonia icefield
SPI: South Patagonia icefield
SLI: San Lorenzo icefield
Nazca plate
Antarctic plate
South America plate
subduction front
Chiloe Block
LOFS
SSVZ
South Volcanic Zone
Southern volcanic gap
AVZ
Austral Volcanic Zone
66 mm.yr-1
18.5 mm.yr-1
Chiloe FZ
Guafo FZ
Guamblin FZ
Taitao FZ
Tres Montes FZ
Esmeralda FZ
Madre de Dios FZ
SCR 3
SCR 2
SCR 1
SCR 0
SCR-1
SCR-2
SCR-3
4-4.2 Ma
5.1-5.3 Ma
core of westerlies
stage 2
Present
CTJ
Psw
reentering Psw boundary
NPI
SLI
SPI
Caleta Tortel Gap (CTG)
Lago Viedma
Lago Argentino
Ch
Ml
Co
Y
Mel
M
Me
C
H
Mu
L
V
A
R
B
Fig. 2
Fig. 20
Fig. 21A
Fig. 3, 22
GMRT

Figure 1

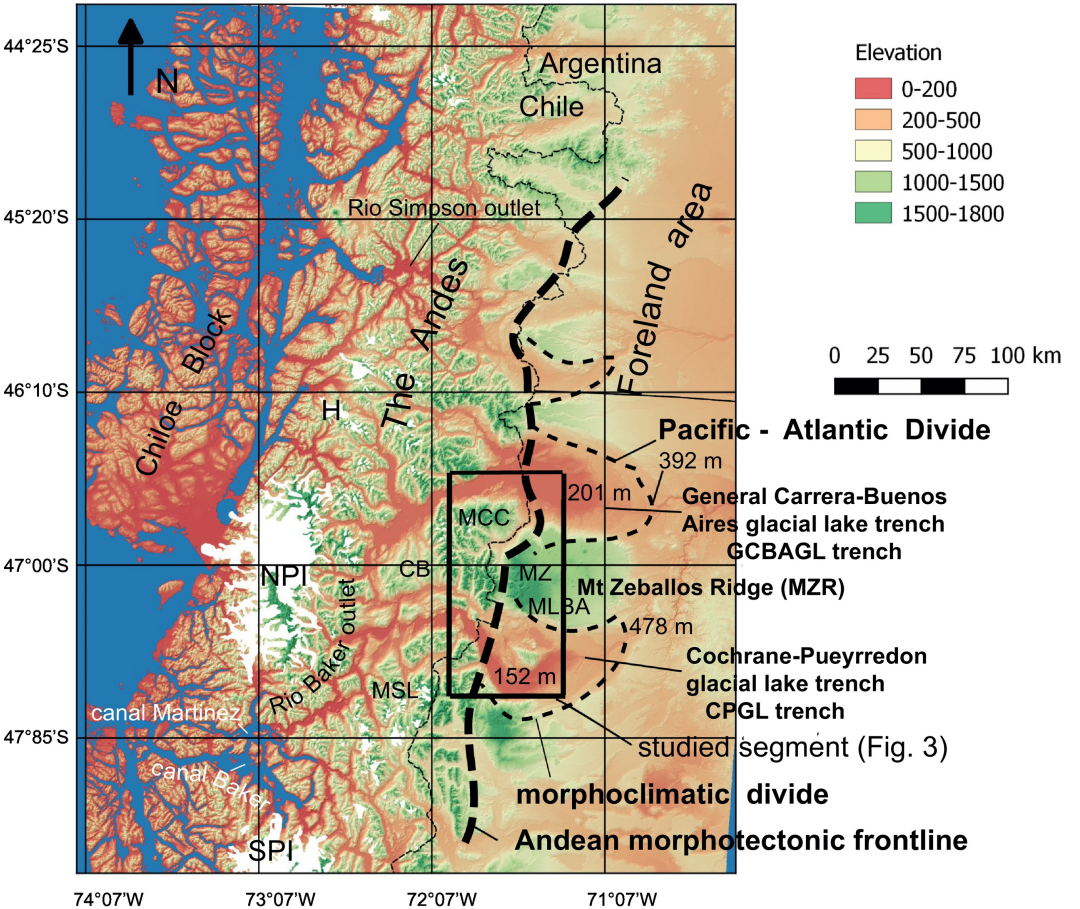
44°25'S
45°20'S
46°10'S
47°00'S
47°85'S
74°07'W
73°07'W
72°07'W
71°07'W
N
Argentina
Chile
Rio Simpson outlet
The Andes
Foreland area
Chiloe Block
H
NPI
SPI
CB
MCC
MZ
MLBA
MSL
Rio Baker outlet
canal Martinez
canal Baker
Elevation
0-200
200-500
500-1000
1000-1500
1500-1800
0 25 50 75 100 km
Pacific - Atlantic Divide
392 m
201 m
General Carrera-Buenos Aires glacial lake trench
GCBAGL trench
Mt Zeballos Ridge (MZR)
478 m
Cochrane-Pueyrredon glacial lake trench
CPGL trench
152 m
studied segment (Fig. 3)
morphoclimatic divide
Andean morphotectonic frontline

Figure 2

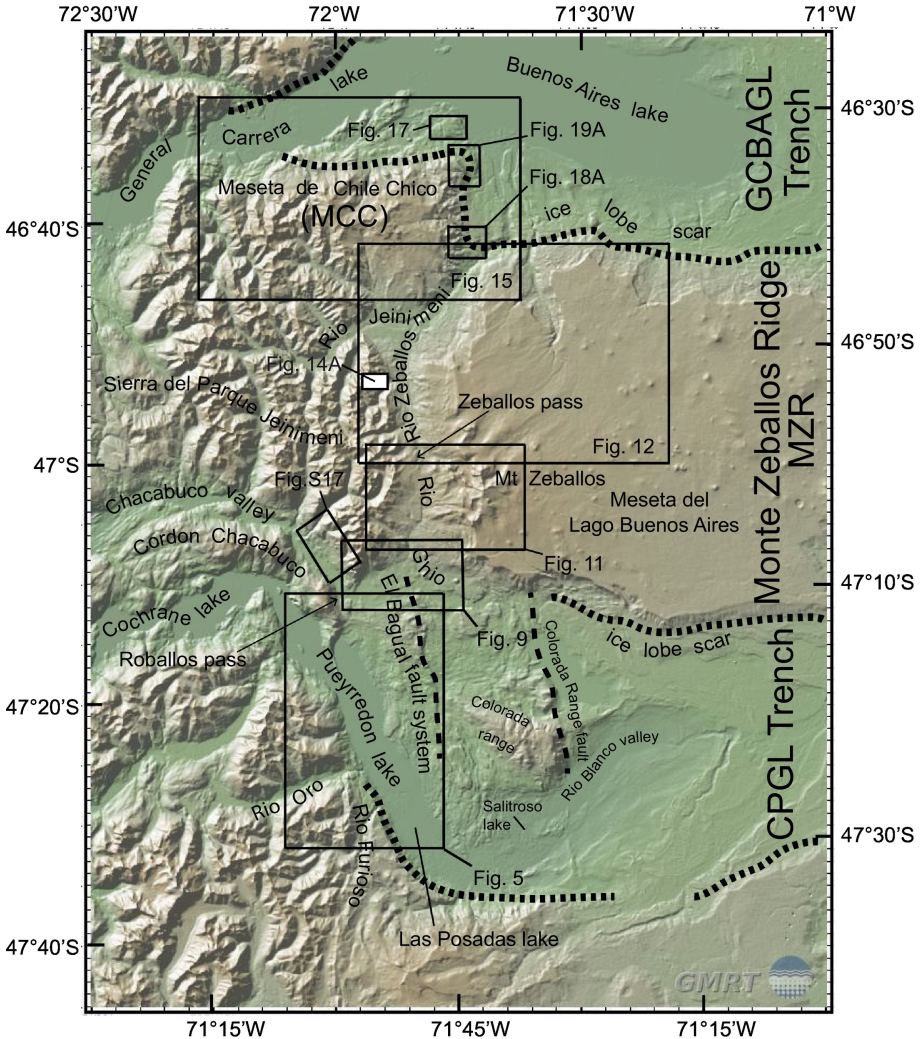
72°30'W
72°W
71°30'W
71°W
46°30'S
46°40'S
46°50'S
47°S
47°10'S
47°20'S
47°30'S
47°40'S
71°15'W
71°45'W
71°15'W
Buenos Aires lake
General Carrera lake
Meseta de Chile Chico (MCC)
Fig. 17
Fig. 19A
Fig. 18A
Fig. 15
Fig. 14A
Fig. 12
Fig. 11
Fig. 9
Fig. 5
Fig. S17
ice lobe scar
GCBAGL Trench
Monte Zeballos Ridge MZR
CPGL Trench
Rio Jeinimeni
Sierra del Parque Jeinimeni
Rio Zeballos
Zeballos pass
Mt Zeballos
Meseta del Lago Buenos Aires
Chacabuco valley
Cordon Chacabuco
Rio Ghio
El Bagual fault system
Cochrane lake
Roballos pass
Pueyrredon lake
Colorada range
Colorada Range fault
Rio Blanco valley
Salitroso lake
Rio Oro
Rio Furioso
Las Posadas lake
GMRT

Figure 3

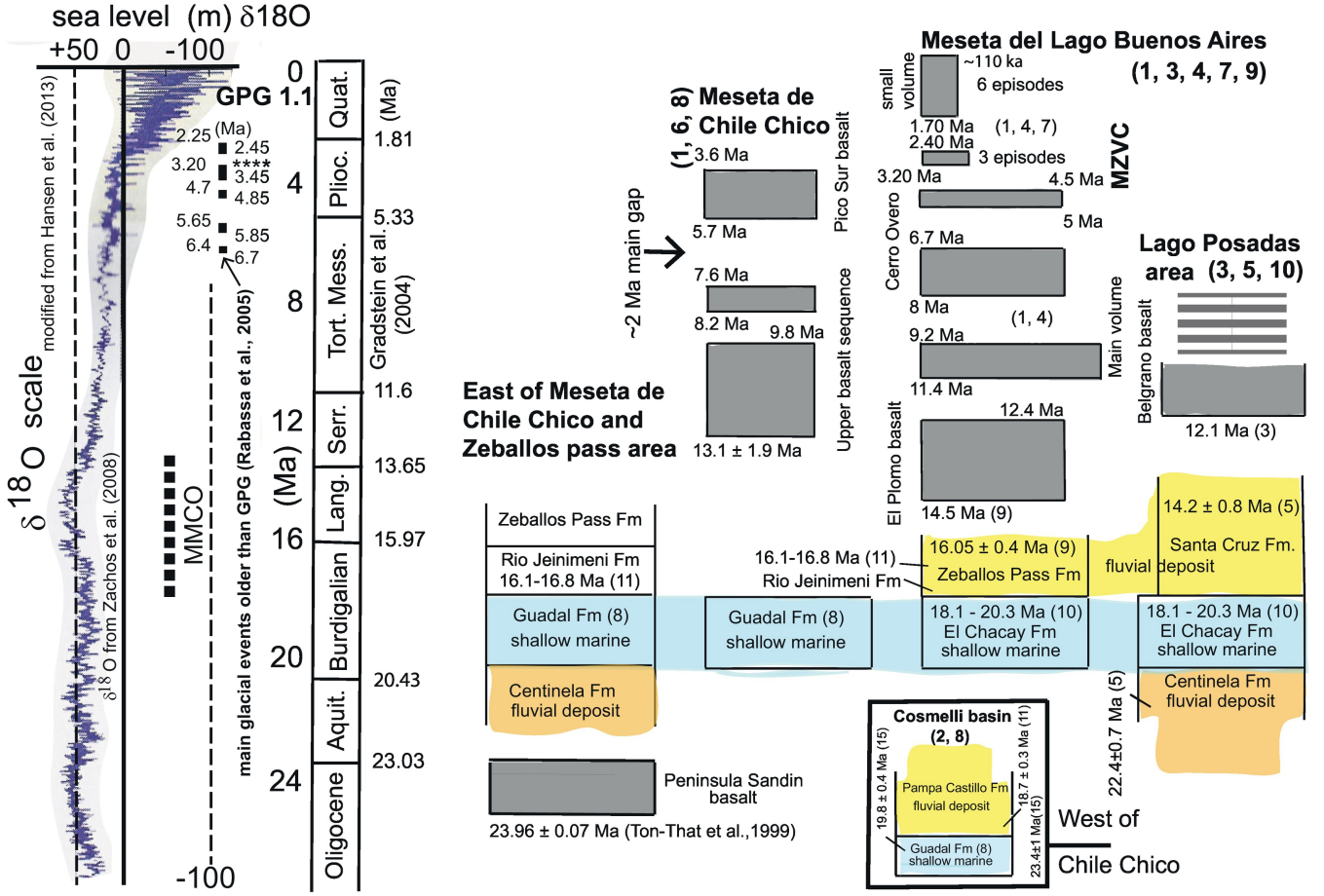
sea level (m) δ18O
+50 0 -100
GPG 1.1
2.25 (Ma)
2.45
3.20
3.45
4.7
4.85
5.65
5.85
6.4
6.7
δ18O scale
modified from Hansen et al. (2013)
δ18O from Zachos et al. (2008)
MMCO
main glacial events older than GPG (Rabassa et al., 2005)
-100
0
4
8
12
16
20
24
(Ma)
Quat.
Plioc.
Tort. Mess.
Serr.
Lang.
Burdigalian
Aquit.
Oligocene
(Ma)
1.81
5.33
11.6
13.65
15.97
20.43
23.03
Gradstein et al. (2004)
Meseta del Lago Buenos Aires
(1, 3, 4, 7, 9)
small volume
~110 ka
6 episodes
1.70 Ma
(1, 4, 7)
2.40 Ma
3 episodes
3.20 Ma
4.5 Ma
5 Ma
MZVC
Cerro Overo
6.7 Ma
8 Ma
(1, 4)
9.2 Ma
11.4 Ma
Main volume
12.4 Ma
El Plomo basalt
14.5 Ma (9)
Meseta de Chile Chico
(1, 6, 8)
3.6 Ma
5.7 Ma
Pico Sur basalt
~2 Ma main gap
7.6 Ma
8.2 Ma
9.8 Ma
Upper basalt sequence
13.1 ± 1.9 Ma
East of Meseta de Chile Chico and Zeballos pass area
Lago Posadas area (3, 5, 10)
Belgrano basalt
12.1 Ma (3)
Zeballos Pass Fm
Rio Jeinimeni Fm
16.1-16.8 Ma (11)
Guadal Fm (8)
shallow marine
Centinela Fm
fluvial deposit
Peninsula Sandin basalt
23.96 ± 0.07 Ma (Ton-That et al.,1999)
16.1-16.8 Ma (11)
Rio Jeinimeni Fm
16.05 ± 0.4 Ma (9)
Zeballos Pass Fm
Guadal Fm (8)
shallow marine
18.1 - 20.3 Ma (10)
El Chacay Fm
shallow marine
14.2 ± 0.8 Ma (5)
Santa Cruz Fm.
fluvial deposit
18.1 - 20.3 Ma (10)
El Chacay Fm
shallow marine
Centinela Fm
fluvial deposit
22.4±0.7 Ma (5)
Cosmelli basin
(2, 8)
19.8 ± 0.4 Ma (15)
Pampa Castillo Fm
fluvial deposit
18.7 ± 0.3 Ma (11)
23.4±1 Ma(15)
Guadal Fm (8)
shallow marine
West of
Chile Chico

Figure 4

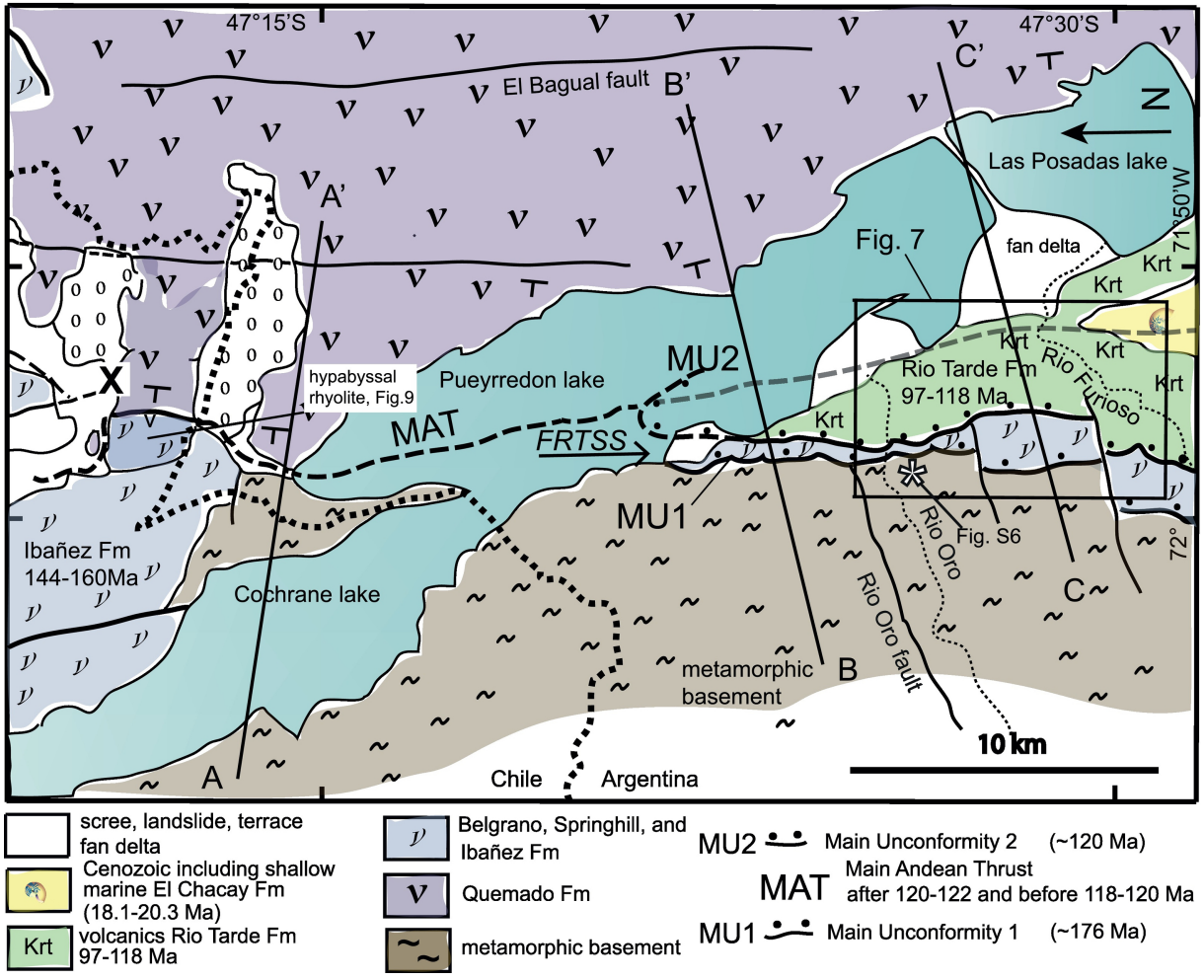
47°15'S
47°30'S
El Bagual fault
A
A'
B
B'
C
C'
N
Las Posadas lake
71°50'W
Fig. 7
fan delta
Krt
Rio Furioso
Rio Tarde Fm
97-118 Ma
hypabyssal
rhyolite, Fig.9
Pueyrredon lake
MU2
MAT
FRTSS
MU1
Fig. S6
Rio Oro
Rio Oro fault
Ibañez Fm
144-160Ma
Cochrane lake
metamorphic
basement
10 km
72°
Chile
Argentina
scree, landslide, terrace
fan delta
Cenozoic including shallow
marine El Chacay Fm
(18.1-20.3 Ma)
volcanics Rio Tarde Fm
97-118 Ma
Belgrano, Springhill, and
Ibañez Fm
Quemado Fm
metamorphic basement
Main Unconformity 2 (~120 Ma)
Main Andean Thrust
after 120-122 and before 118-120 Ma
Main Unconformity 1 (~176 Ma)

Figure 5

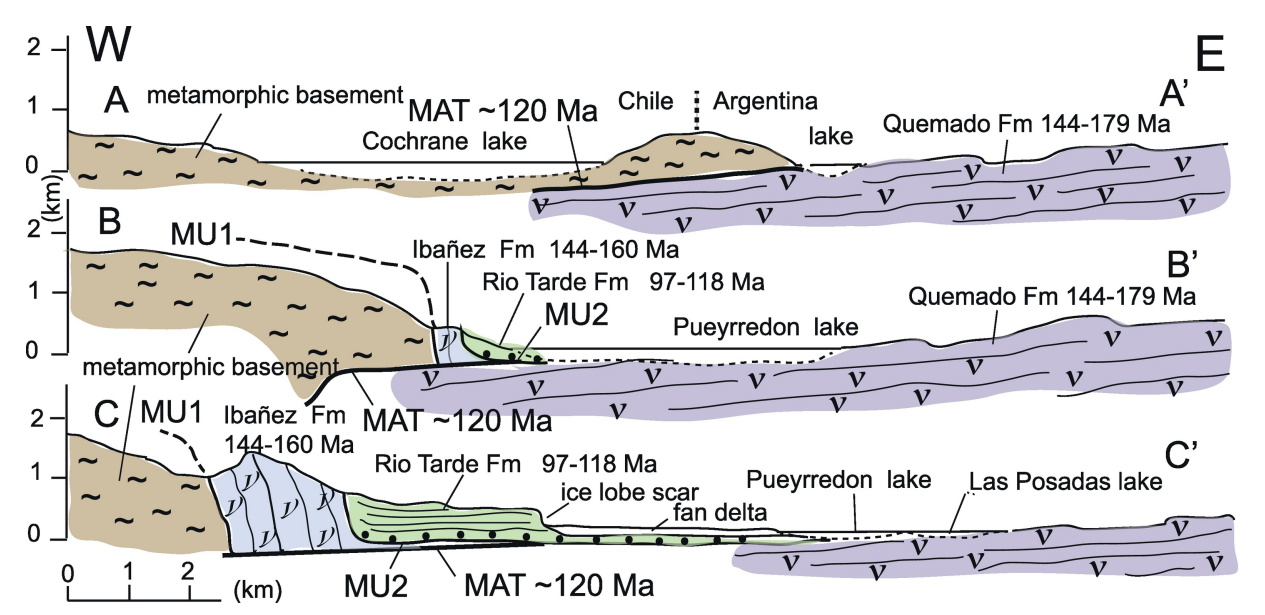
W
E
A
A'
metamorphic basement
MAT ~120 Ma
Chile
Argentina
Cochrane lake
lake
Quemado Fm 144-179 Ma
(km)
B
B'
MU1
Ibañez Fm 144-160 Ma
Rio Tarde Fm 97-118 Ma
MU2
Pueyrredon lake
Quemado Fm 144-179 Ma
metamorphic basement
C
C'
MU1
Ibañez Fm
144-160 Ma
MAT ~120 Ma
Rio Tarde Fm 97-118 Ma
ice lobe scar
fan delta
Pueyrredon lake
Las Posadas lake
MU2
MAT ~120 Ma
(km)

Figure 6

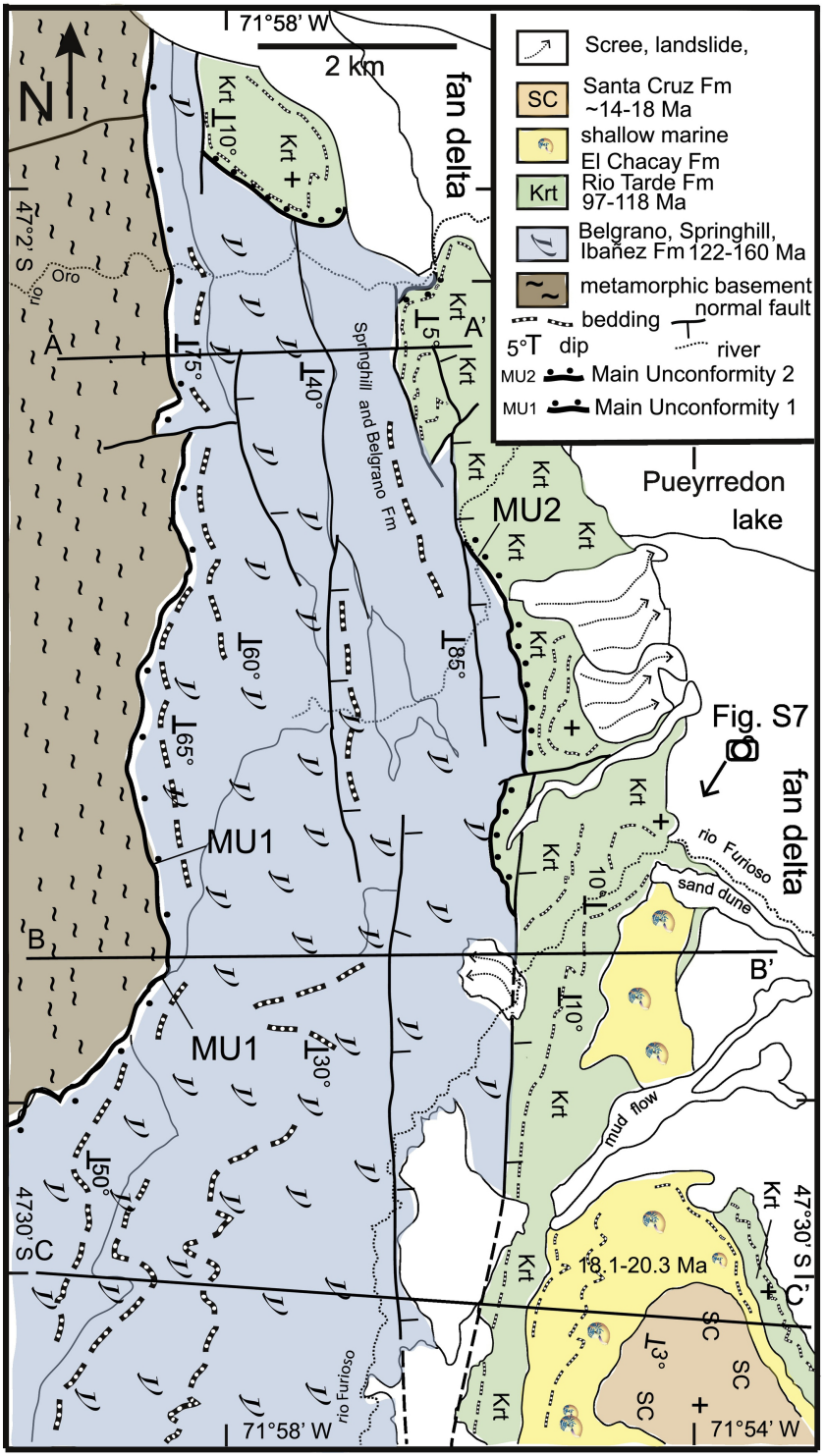
71°58' W
2 km
N
Scree, landslide,
SC
Santa Cruz Fm
~14-18 Ma
shallow marine
El Chacay Fm
Krt
Rio Tarde Fm
97-118 Ma
Belgrano, Springhill,
Ibañez Fm 122-160 Ma
metamorphic basement
normal fault
bedding
5°T dip
river
MU2 Main Unconformity 2
MU1 Main Unconformity 1
fan delta
Pueyrredon
lake
MU2
MU1
Fig. S7
fan delta
rio Furioso
sand dune
mud flow
18.1-20.3 Ma
Springhill and Belgrano Fm
Oro
47°2' S
47°30' S
A
A'
B
B'
C
C'
71°58' W
71°54' W
rio Furioso

Figure 7

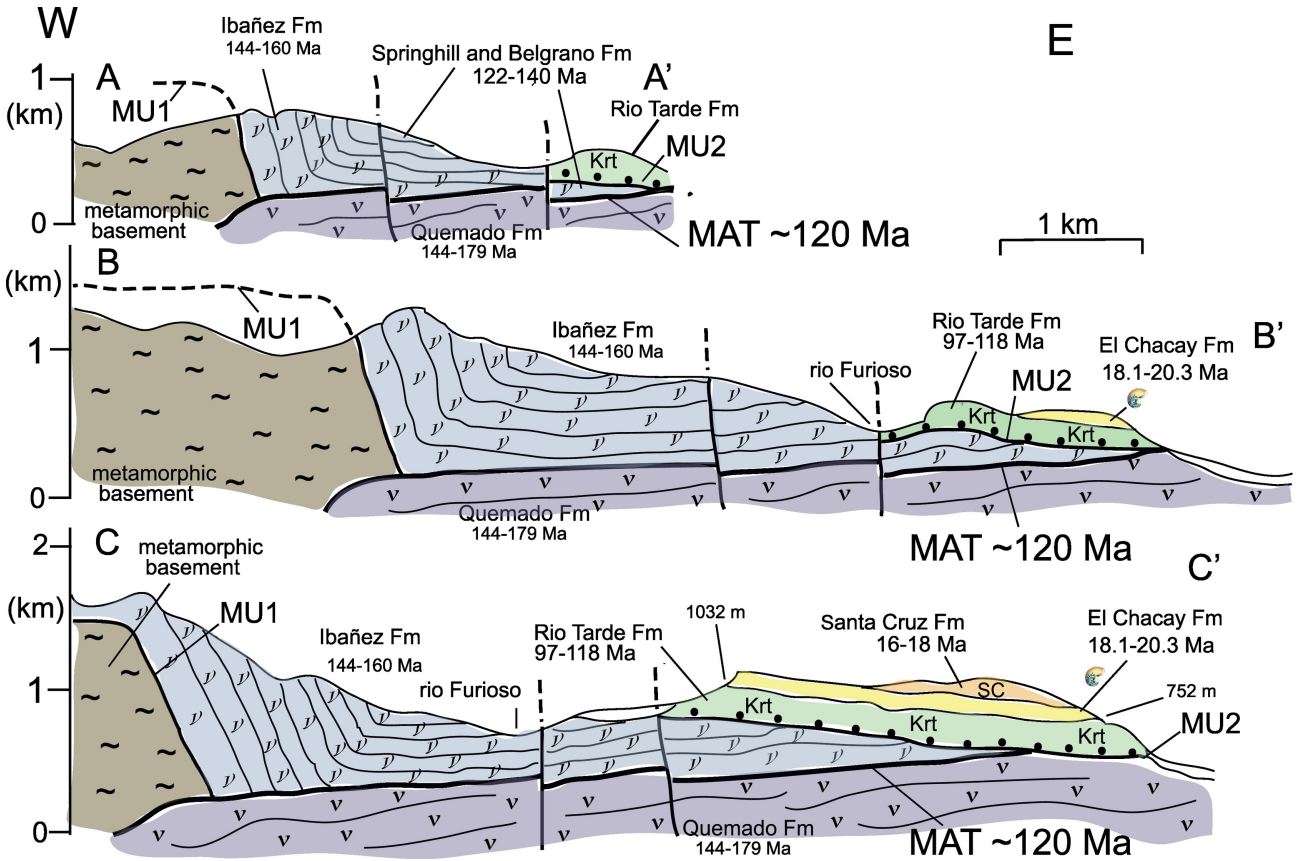
W
E
A
A'
1
(km)
0
MU1
Ibañez Fm
144-160 Ma
Springhill and Belgrano Fm
122-140 Ma
Rio Tarde Fm
MU2
Krt
metamorphic
basement
Quemado Fm
144-179 Ma
MAT ~120 Ma
1 km
B
B'
(km)
1
0
MU1
Ibañez Fm
144-160 Ma
Rio Tarde Fm
97-118 Ma
El Chacay Fm
18.1-20.3 Ma
rio Furioso
MU2
Krt
Krt
metamorphic
basement
Quemado Fm
144-179 Ma
MAT ~120 Ma
C
C'
2
(km)
1
0
metamorphic
basement
MU1
Ibañez Fm
144-160 Ma
rio Furioso
Rio Tarde Fm
97-118 Ma
1032 m
Santa Cruz Fm
16-18 Ma
SC
El Chacay Fm
18.1-20.3 Ma
752 m
MU2
Krt
Krt
Krt
Quemado Fm
144-179 Ma
MAT ~120 Ma

Figure 8

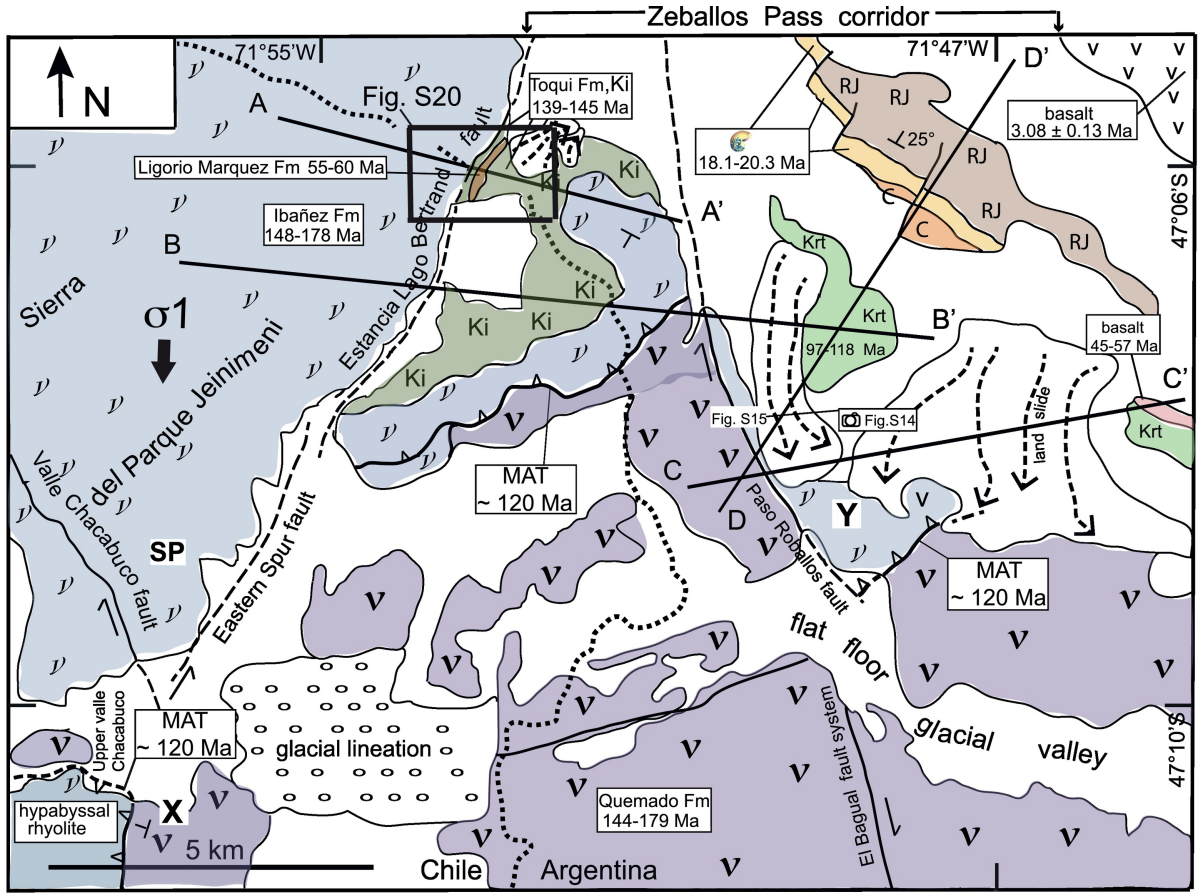
Zeballos Pass corridor
71°55'W
71°47'W
N
Fig. S20
A
A'
B
B'
C
C'
D
D'
Toqui Fm,Ki
139-145 Ma
Ligorio Marquez Fm 55-60 Ma
Ibañez Fm
148-178 Ma
Estancia Lago Bertrand fault
18.1-20.3 Ma
basalt
3.08 ± 0.13 Ma
25°
basalt
45-57 Ma
97-118 Ma
47°09'S
47°10'S
Sierra
del Parque Jeinimeni
σ1
Valle Chacabuco fault
Eastern Spur fault
SP
MAT
~ 120 Ma
Fig. S15
Fig.S14
land slide
Paso Robles fault
Y
flat floor
glacial valley
Upper valle Chacabuco
glacial lineation
hypabyssal rhyolite
X
5 km
Chile
Argentina
Quemado Fm
144-179 Ma
El Bagual fault system
scree, landslide, terrace,
Mt Zeballos volcanic complex
fluvial deposit Rio Jeinimeni Fm
Shallow marine El Chacay Fm
fluvial deposit Centinela Fm
Eocene basalt 45-57 Ma
volcanics Rio Tarde and Divisadero Fm, 97-118 Ma
Shallow marine Toqui Fm, 139-145 Ma
volcanics Ibañez Fm
volcanics Quemado Fm
Main Andean Thrust
Main Unconformity 2 ~120 Ma

Figure 9

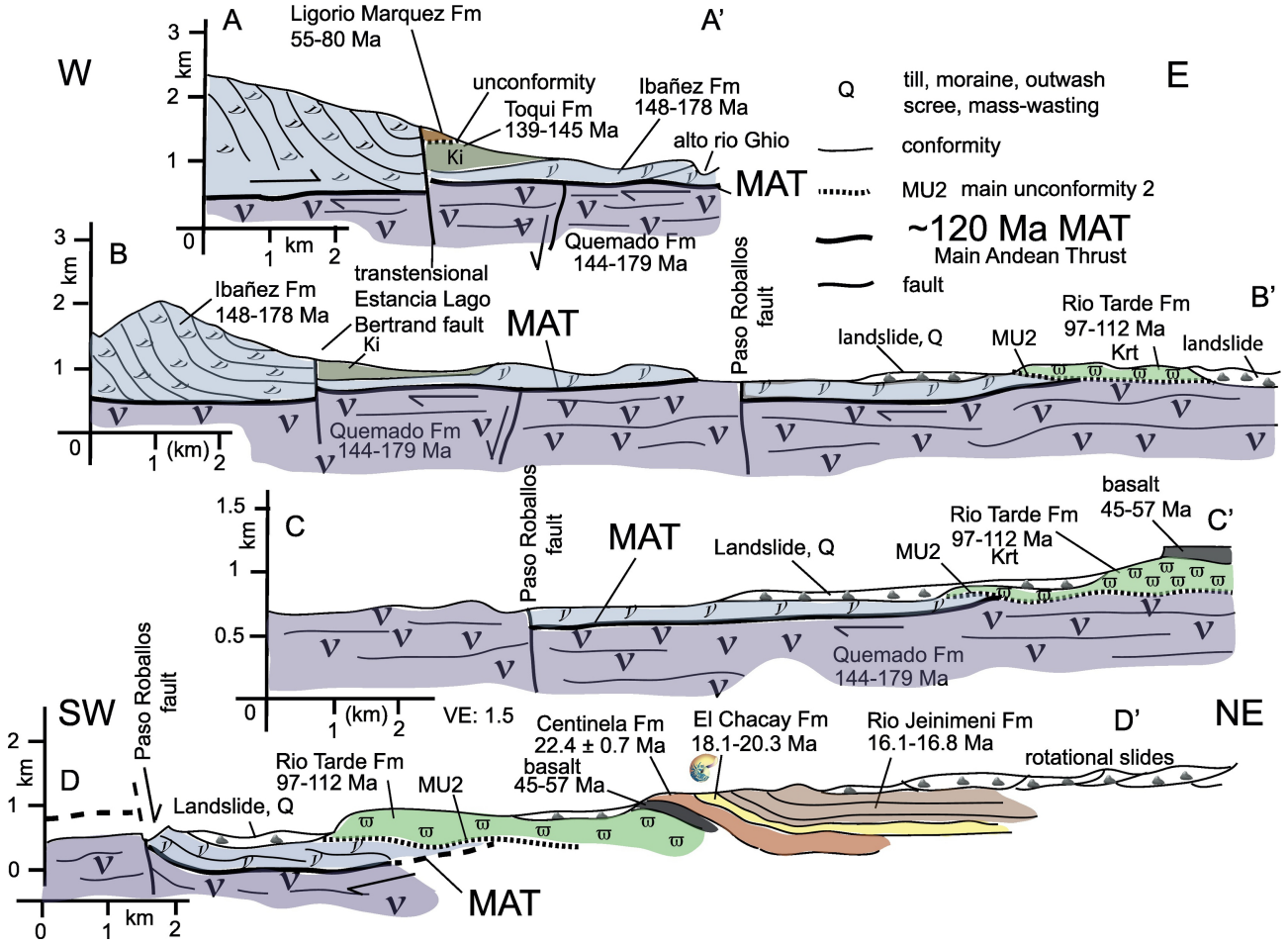
A
A'
W
E
Ligorio Marquez Fm
55-80 Ma
unconformity
Toqui Fm
139-145 Ma
Ibañez Fm
148-178 Ma
alto rio Ghio
Ki
MAT
Quemado Fm
144-179 Ma
transtensional
Estancia Lago
Bertrand fault
Paso Roballos
fault
B
B'
Ibañez Fm
148-178 Ma
Ki
MAT
Quemado Fm
144-179 Ma
landslide, Q
MU2
Rio Tarde Fm
97-112 Ma
Krt
landslide
C
C'
Paso Roballos
fault
MAT
Landslide, Q
MU2
Rio Tarde Fm
97-112 Ma
Krt
basalt
45-57 Ma
Quemado Fm
144-179 Ma
VE: 1.5
SW
NE
D
D'
Paso Roballos
fault
Rio Tarde Fm
97-112 Ma
MU2
Landslide, Q
MAT
Centinela Fm
22.4 ± 0.7 Ma
basalt
45-57 Ma
El Chacay Fm
18.1-20.3 Ma
Rio Jeinimeni Fm
16.1-16.8 Ma
rotational slides
Q
till, moraine, outwash
scree, mass-wasting
conformity
MU2 main unconformity 2
~120 Ma MAT
Main Andean Thrust
fault
km
(km)

Figure 10

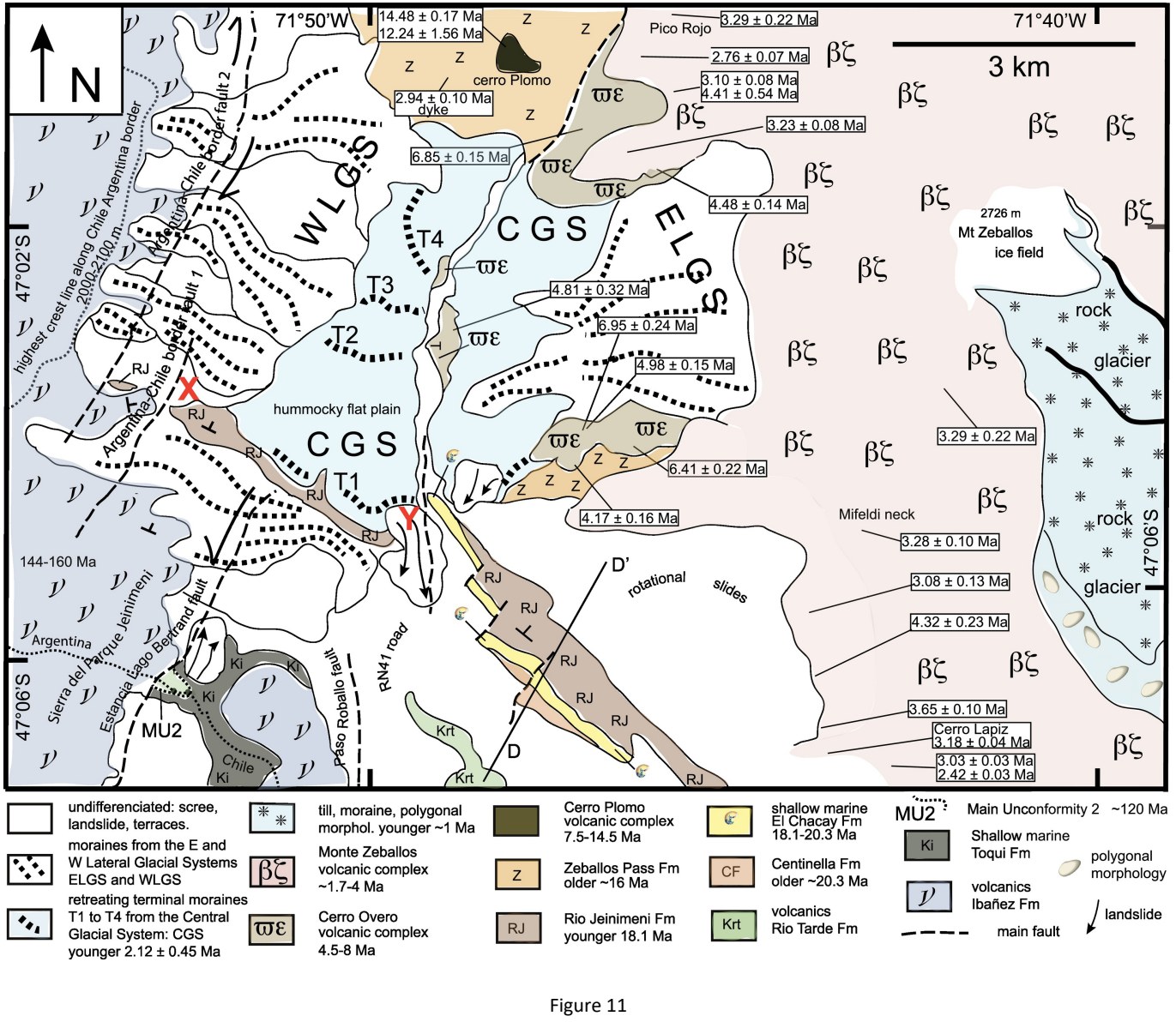

undifferenciated: scree, landslide, terraces.

moraines from the E and W Lateral Glacial Systems ELGS and WLGS

retreating terminal moraines T1 to T4 from the Central Glacial System: CGS younger 2.12 ± 0.45 Ma

till, moraine, polygonal morphol. younger ~1 Ma

Monte Zeballos volcanic complex ~1.7-4 Ma

Cerro Overo volcanic complex 4.5-8 Ma

Cerro Plomo volcanic complex 7.5-14.5 Ma

Zeballos Pass Fm older ~16 Ma

Rio Jeinimeni Fm younger 18.1 Ma

shallow marine El Chacay Fm 18.1-20.3 Ma

Centinella Fm older ~20.3 Ma

volcanics Rio Tarde Fm

MU2 Main Unconformity 2 ~120 Ma

Ki Shallow marine Toqui Fm

volcanics Ibañez Fm

polygonal morphology

landslide

main fault

Figure 11

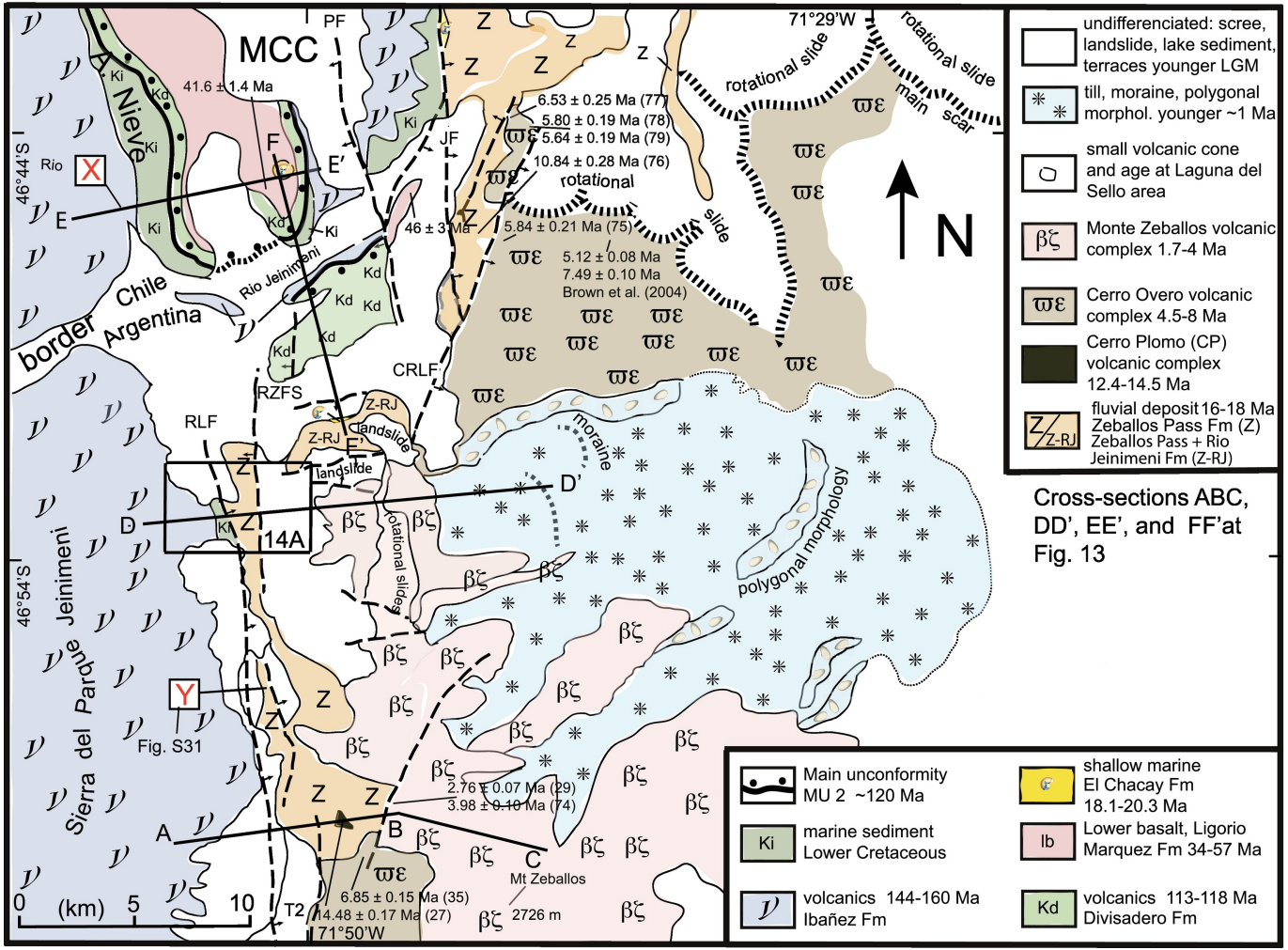
MCC
PF
A. Nieve
41.6 ±1.4 Ma
Ki
Kd
F
E'
E
X
Rio
46°44'S
Rio Jeinimeni
Chile
Argentina
border
46 ± 3 Ma
JF
Z
6.53 ± 0.25 Ma (77)
5.80 ± 0.19 Ma (78)
5.64 ± 0.19 Ma (79)
10.84 ± 0.28 Ma (76)
rotational
5.84 ± 0.21 Ma (75)
5.12 ± 0.08 Ma
7.49 ± 0.10 Ma
Brown et al. (2004)
71°29'W
rotational slide
main scar
slide
ωε
N
CRLF
RZFS
RLF
Z-RJ
landslide
moraine
D'
D
14A
rotational slides
polygonal morphology
βζ
46°54'S
Sierra del Parque Jeinimeni
Y
Fig. S31
2.76 ± 0.07 Ma (29)
3.98 ± 0.10 Ma (74)
A
B
C
Mt Zeballos
2726 m
6.85 ± 0.15 Ma (35)
14.48 ± 0.17 Ma (27)
T2
71°50'W
0
(km)
5
10
Cross-sections ABC, DD', EE', and FF'at Fig. 13
undifferenciated: scree, landslide, lake sediment, terraces younger LGM
till, moraine, polygonal morphol. younger ~1 Ma
small volcanic cone and age at Laguna del Sello area
Monte Zeballos volcanic complex 1.7-4 Ma
Cerro Overo volcanic complex 4.5-8 Ma
Cerro Plomo (CP) volcanic complex 12.4-14.5 Ma
fluvial deposit 16-18 Ma Zeballos Pass Fm (Z) Zeballos Pass + Rio Jeinimeni Fm (Z-RJ)
Main unconformity MU 2 ~120 Ma
marine sediment Lower Cretaceous
volcanics 144-160 Ma Ibañez Fm
shallow marine El Chacay Fm 18.1-20.3 Ma
Lower basalt, Ligorio Marquez Fm 34-57 Ma
volcanics 113-118 Ma Divisadero Fm

Figure 12

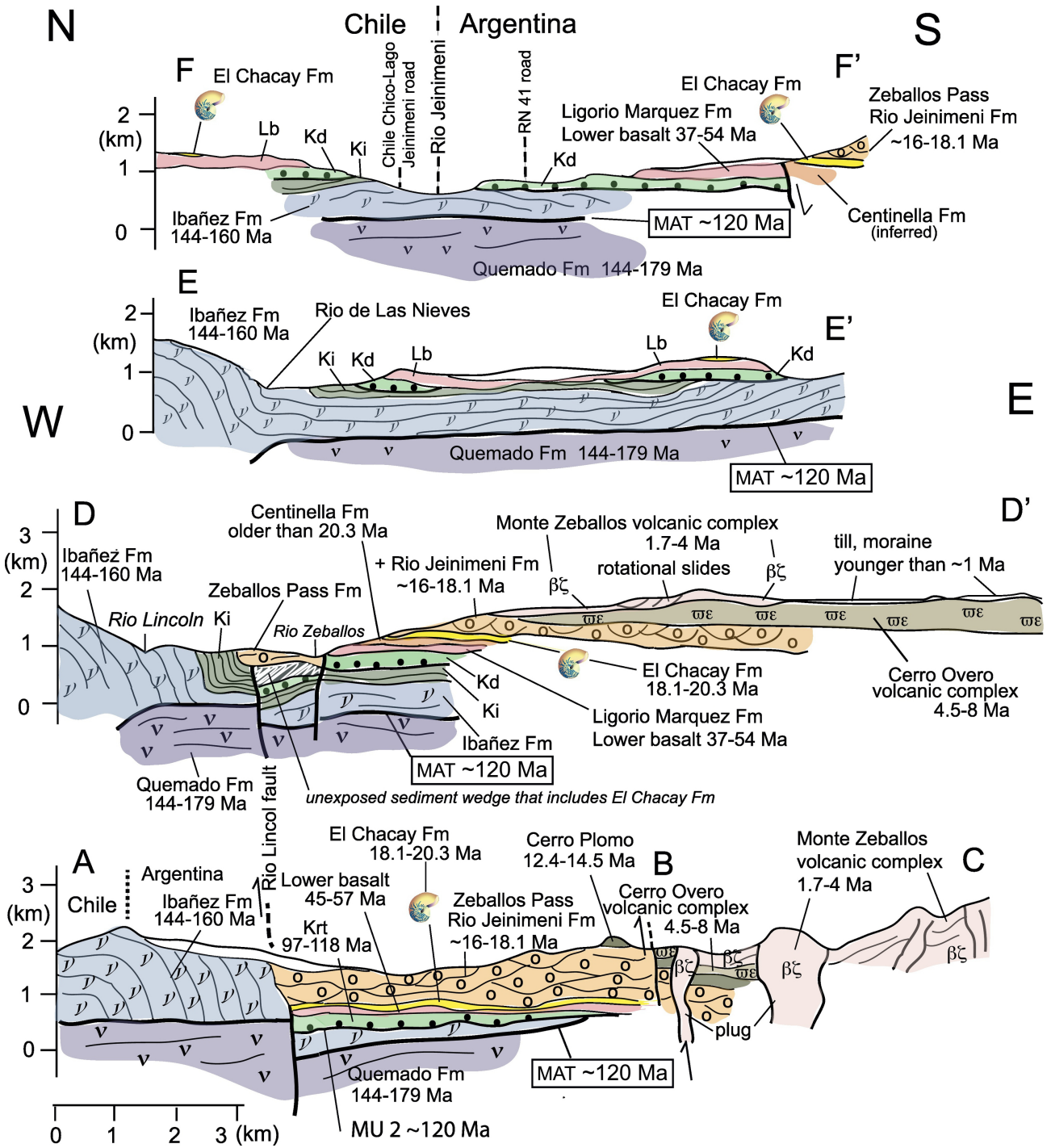
N
Chile
Argentina
S
F
El Chacay Fm
Chile Chico-Lago Jeinimeni road
Rio Jeinimeni
RN 41 road
F'
El Chacay Fm
Zeballos Pass
Rio Jeinimeni Fm
~16-18.1 Ma
Ligorio Marquez Fm
Lower basalt 37-54 Ma
2
(km)
1
0
Lb
Kd
Ki
Kd
Ibañez Fm
144-160 Ma
MAT ~120 Ma
Centinella Fm
(inferred)
Quemado Fm 144-179 Ma
E
Ibañez Fm
144-160 Ma
Rio de Las Nieves
El Chacay Fm
E'
Ki
Kd
Lb
Lb
Kd
W
E
Quemado Fm 144-179 Ma
MAT ~120 Ma
D
D'
3
(km)
2
1
0
Ibañez Fm
144-160 Ma
Centinella Fm
older than 20.3 Ma
Monte Zeballos volcanic complex
1.7-4 Ma
+ Rio Jeinimeni Fm
~16-18.1 Ma
rotational slides
till, moraine
younger than ~1 Ma
Zeballos Pass Fm
Rio Lincoln
Ki
Rio Zeballos
El Chacay Fm
18.1-20.3 Ma
Cerro Overo
volcanic complex
4.5-8 Ma
Kd
Ki
Ligorio Marquez Fm
Lower basalt 37-54 Ma
Ibañez Fm
MAT ~120 Ma
Quemado Fm
144-179 Ma
unexposed sediment wedge that includes El Chacay Fm
Rio Lincol fault
A
B
C
3
(km)
2
1
0
Argentina
Chile
Ibañez Fm
144-160 Ma
El Chacay Fm
18.1-20.3 Ma
Cerro Plomo
12.4-14.5 Ma
Monte Zeballos
volcanic complex
1.7-4 Ma
Lower basalt
45-57 Ma
Krt
97-118 Ma
Zeballos Pass
Rio Jeinimeni Fm
~16-18.1 Ma
Cerro Overo
volcanic complex
4.5-8 Ma
plug
MAT ~120 Ma
Quemado Fm
144-179 Ma
MU 2 ~120 Ma
0
1
2
3 (km)

Figure 13

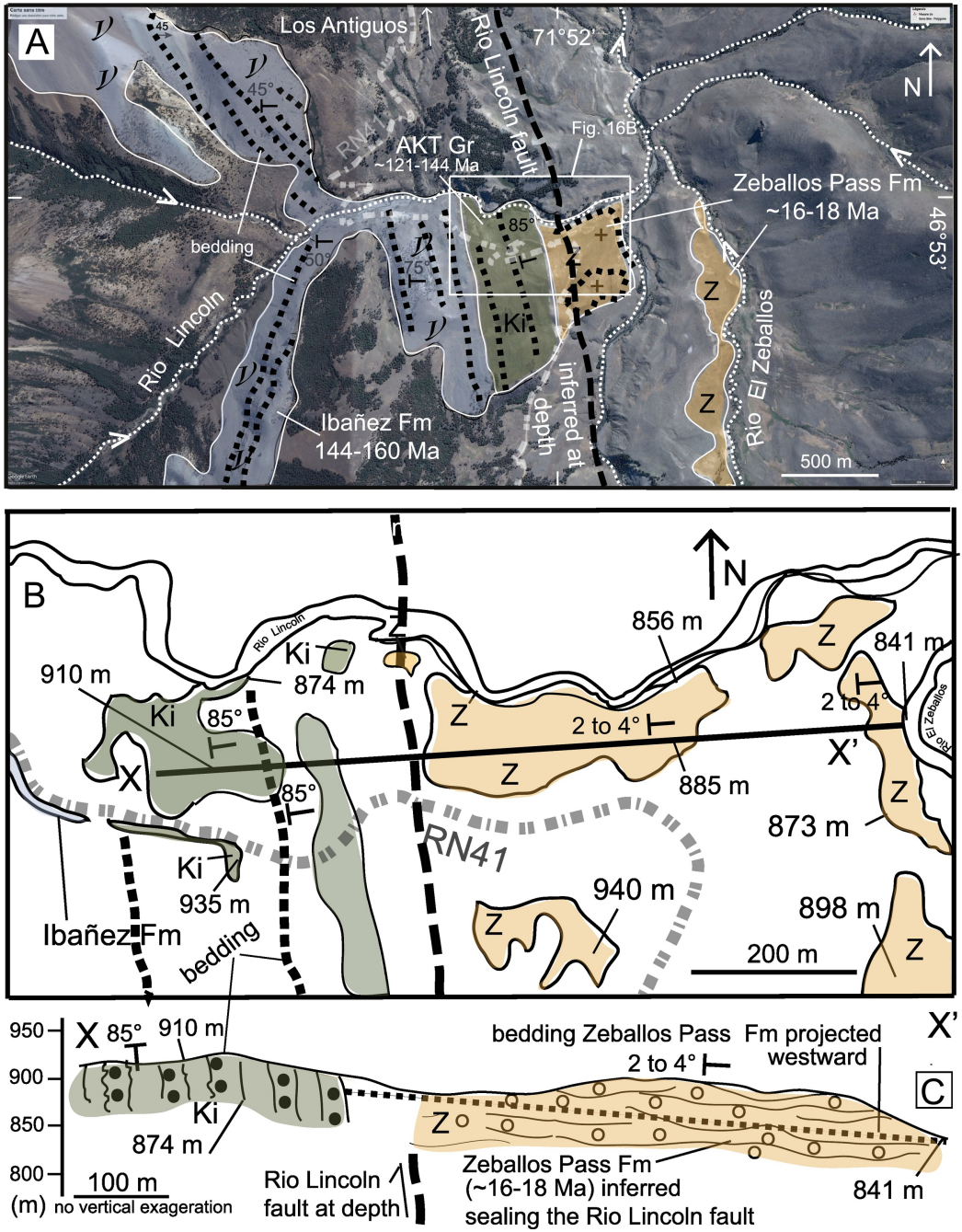
A
Los Antiguos
Rio Lincoln fault
71°52'
N
45°
RN41
AKT Gr
~121-144 Ma
Fig. 16B
Zeballos Pass Fm
~16-18 Ma
46°53'
bedding
50°
75°
85°
Ki
Z
Rio Lincoln
Rio El Zeballos
inferred at depth
Ibañez Fm
144-160 Ma
500 m
B
Rio Lincoln
Ki
874 m
910 m
856 m
841 m
2 to 4°
885 m
873 m
935 m
940 m
898 m
200 m
X
X'
RN41
Ibañez Fm
bedding
C
950
900
850
800
(m)
910 m
bedding Zeballos Pass Fm projected westward
100 m
no vertical exageration
Rio Lincoln fault at depth
Zeballos Pass Fm (~16-18 Ma) inferred sealing the Rio Lincoln fault

Figure 14

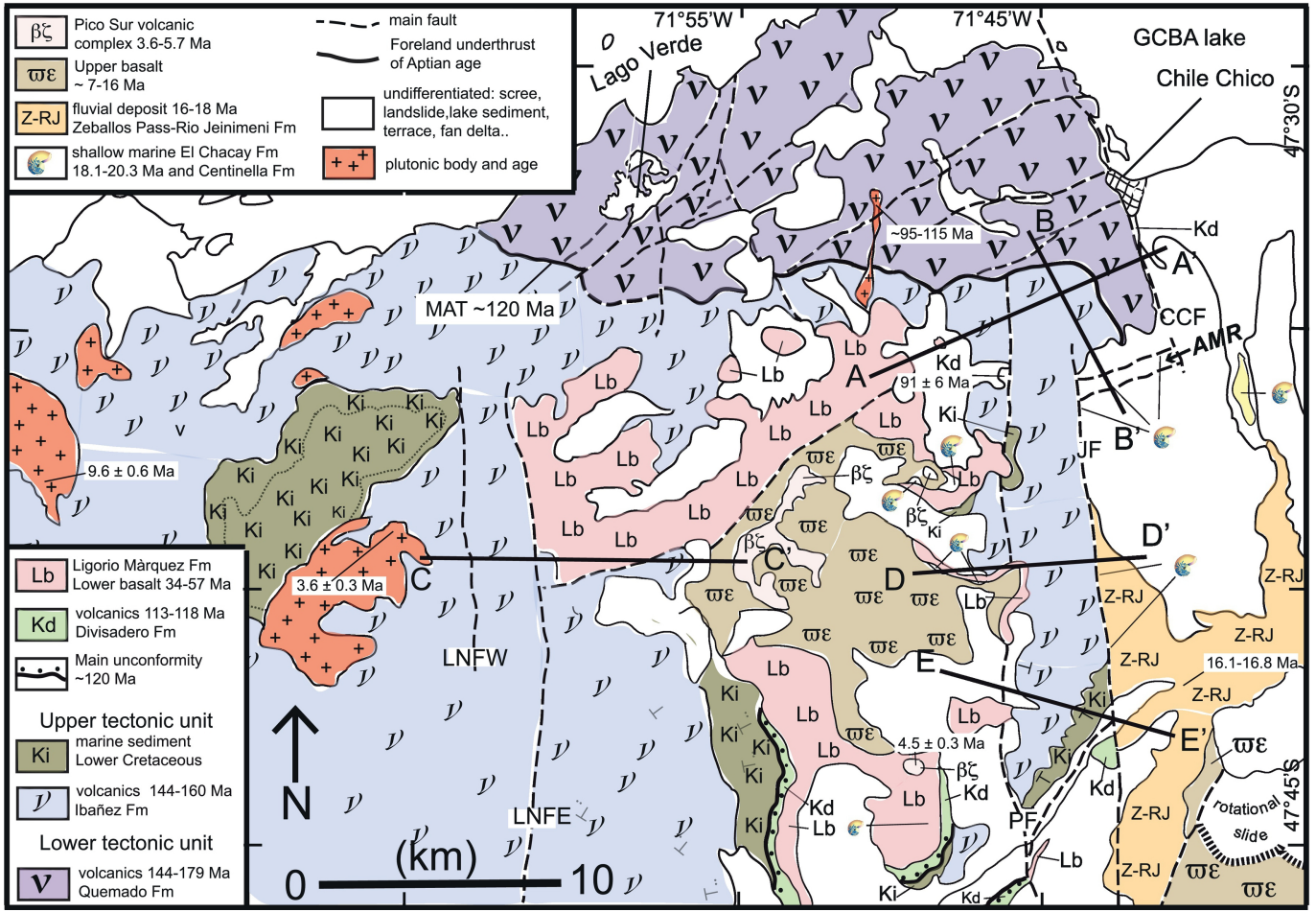
βζ Pico Sur volcanic complex 3.6-5.7 Ma
ωε Upper basalt ~ 7-16 Ma
Z-RJ fluvial deposit 16-18 Ma Zeballos Pass-Rio Jeinimeni Fm
shallow marine El Chacay Fm 18.1-20.3 Ma and Centinella Fm
main fault
Foreland underthrust of Aptian age
undifferentiated: scree, landslide,lake sediment, terrace, fan delta..
plutonic body and age
Lb Ligorio Màrquez Fm Lower basalt 34-57 Ma
Kd volcanics 113-118 Ma Divisadero Fm
Main unconformity ~120 Ma
Upper tectonic unit
Ki marine sediment Lower Cretaceous
volcanics 144-160 Ma Ibañez Fm
Lower tectonic unit
v volcanics 144-179 Ma Quemado Fm
71°55'W
71°45'W
47°30'S
47°45'S
Lago Verde
GCBA lake
Chile Chico
~95-115 Ma
MAT ~120 Ma
91 ± 6 Ma
9.6 ± 0.6 Ma
3.6 ± 0.3 Ma
4.5 ± 0.3 Ma
16.1-16.8 Ma
CCF
AMR
JF
PF
LNFW
LNFE
rotational slide
A
A'
B
B'
C
C'
D
D'
E
E'
N
0
10
(km)

Figure 15

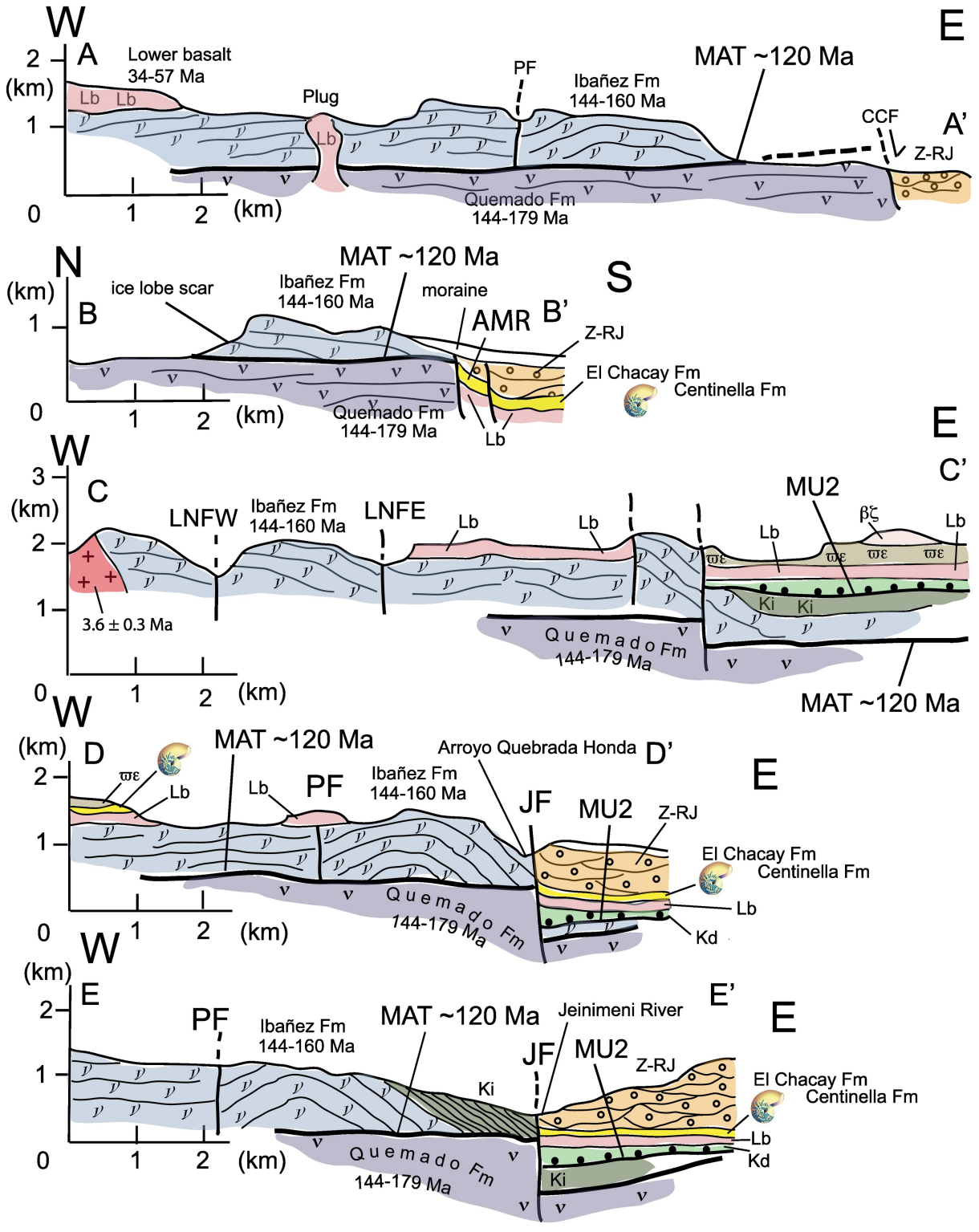
W
E
A
A'
Lower basalt
34-57 Ma
Lb
Plug
PF
Ibañez Fm
144-160 Ma
MAT ~120 Ma
CCF
Z-RJ
Quemado Fm
144-179 Ma
(km)
N
S
B
B'
ice lobe scar
moraine
AMR
El Chacay Fm
Centinella Fm
C
C'
LNFW
LNFE
MU2
3.6 ± 0.3 Ma
D
D'
Arroyo Quebrada Honda
JF
Kd
E
E'
Jeinimeni River
Ki

Figure 16

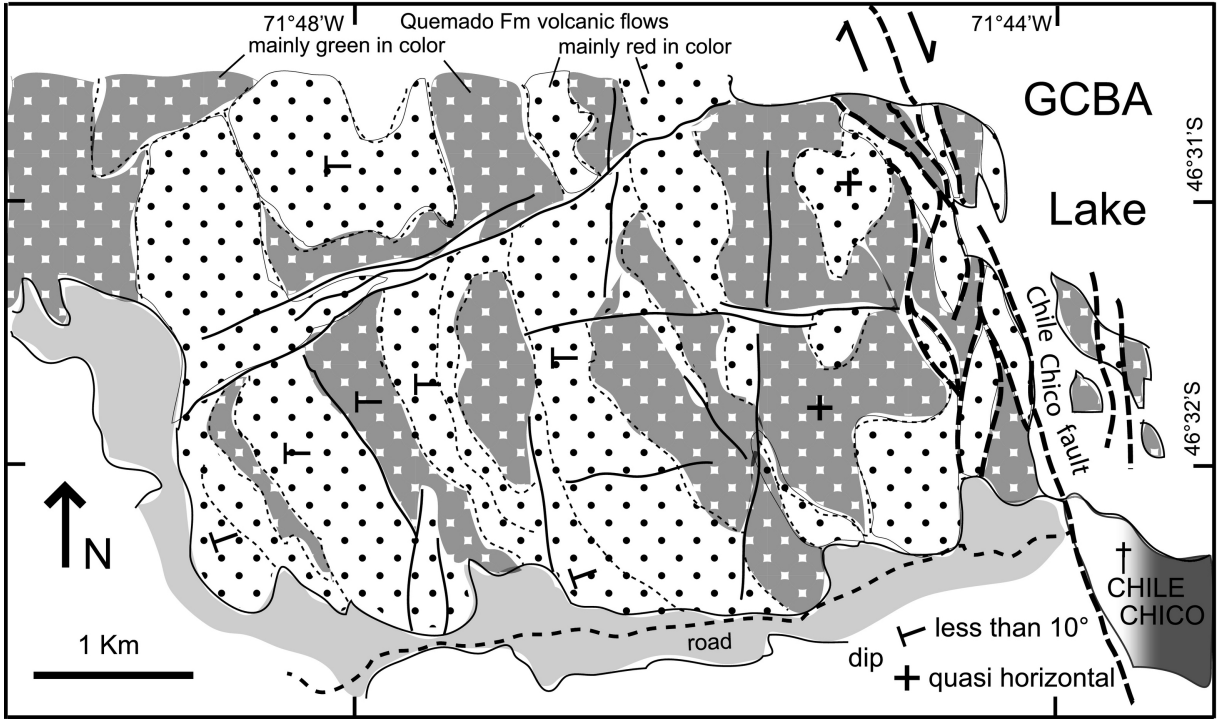
71°48'W
Quemado Fm volcanic flows
mainly green in color
mainly red in color
71°44'W
GCBA
Lake
46°31'S
46°32'S
Chile Chico fault
N
1 Km
road
CHILE
CHICO
less than 10°
dip
quasi horizontal

Figure 17

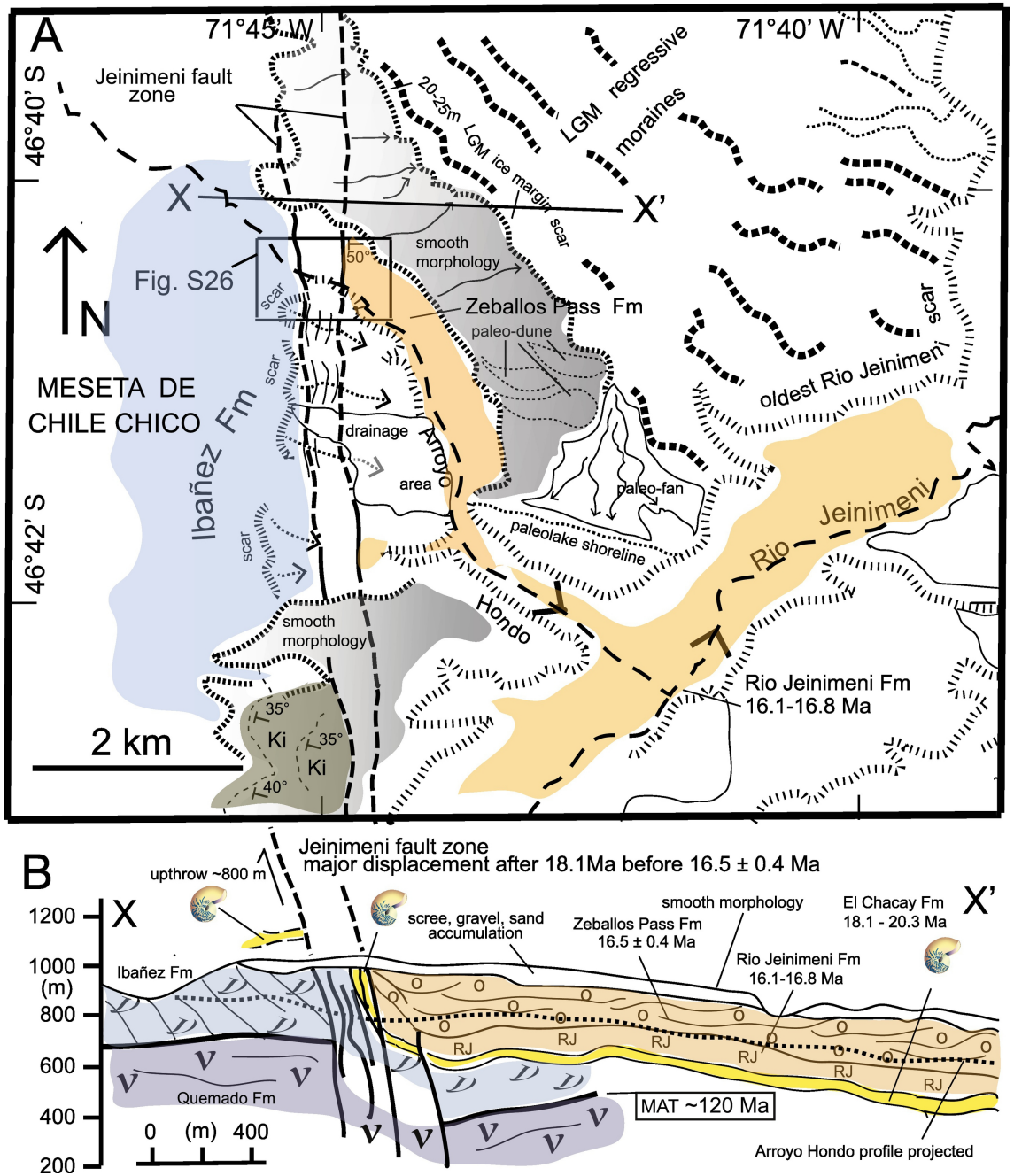
A
71°45' W
71°40' W
46°40' S
46°42' S
Jeinimeni fault zone
20-25m LGM ice margin
LGM regressive moraines
X
X'
Fig. S26
N
scar
smooth morphology
50°
Zeballos Pass Fm
paleo-dune
oldest Rio Jeinimeni
MESETA DE CHILE CHICO
Ibañez Fm
drainage area
Arroyo Hondo
paleo-fan
paleolake shoreline
Rio Jeinimeni
Rio Jeinimeni Fm
16.1-16.8 Ma
35°
Ki
40°
2 km
B
Jeinimeni fault zone
major displacement after 18.1Ma before 16.5 ± 0.4 Ma
upthrow ~800 m
scree, gravel, sand accumulation
Zeballos Pass Fm
16.5 ± 0.4 Ma
smooth morphology
El Chacay Fm
18.1 - 20.3 Ma
Rio Jeinimeni Fm
16.1-16.8 Ma
1200
1000
(m)
800
600
400
200
Ibañez Fm
Quemado Fm
RJ
MAT ~120 Ma
0 (m) 400
Arroyo Hondo profile projected

Figure 18

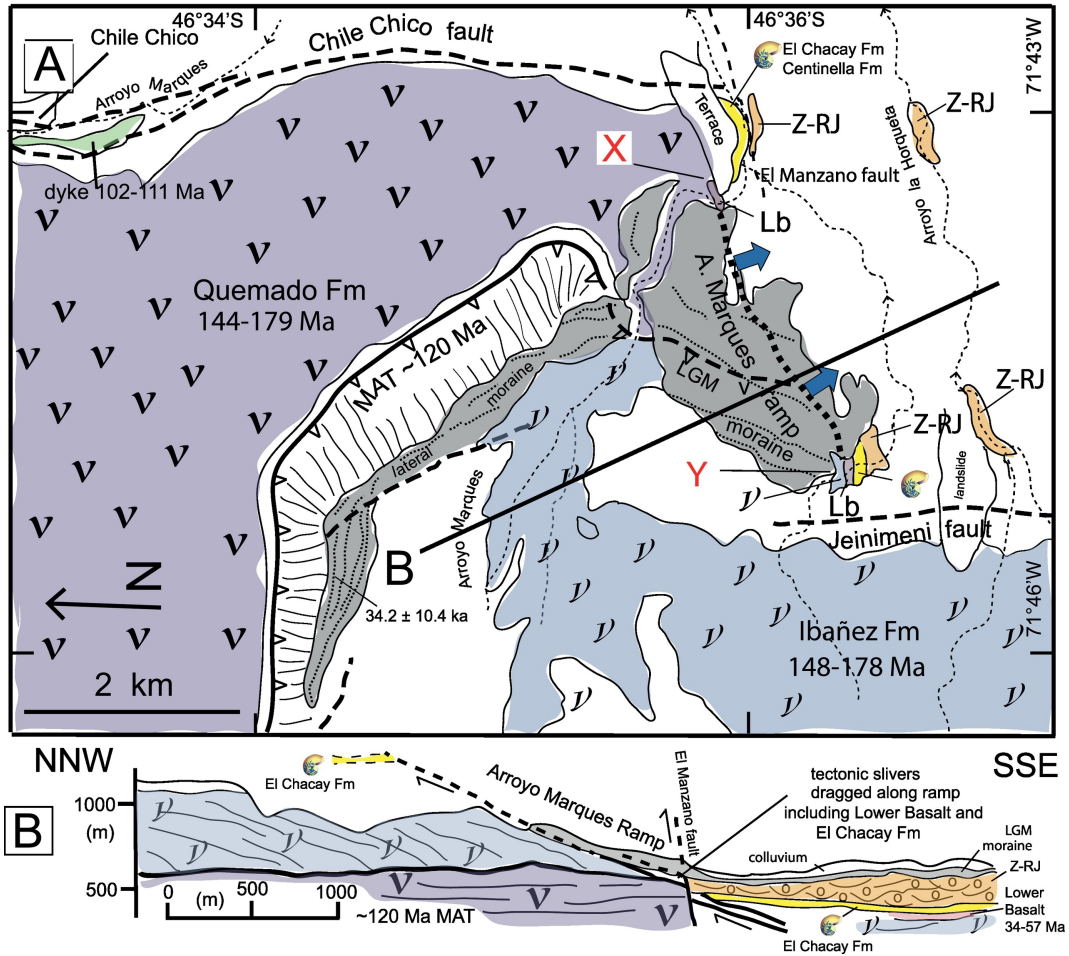
A
Chile Chico
46°34'S
Chile Chico fault
Arroyo Marques
dyke 102-111 Ma
Quemado Fm
144-179 Ma
MAT ~120 Ma
moraine
lateral
34.2 ± 10.4 ka
X
Y
B
Arroyo Marques
A. Marques ramp
LGM
moraine
Lb
El Manzano fault
46°36'S
El Chacay Fm
Centinella Fm
Terrace
Z-RJ
Arroyo la Hondada
71°43'W
landslide
Jeinimeni fault
Ibañez Fm
148-178 Ma
71°46'W
N
2 km
NNW
SSE
1000
(m)
500
0
(m)
500
1000
El Chacay Fm
Arroyo Marques Ramp
El Manzano fault
~120 Ma MAT
tectonic slivers
dragged along ramp
including Lower Basalt and
El Chacay Fm
colluvium
LGM
moraine
Z-RJ
Lower
Basalt
34-57 Ma
El Chacay Fm

Figure 19

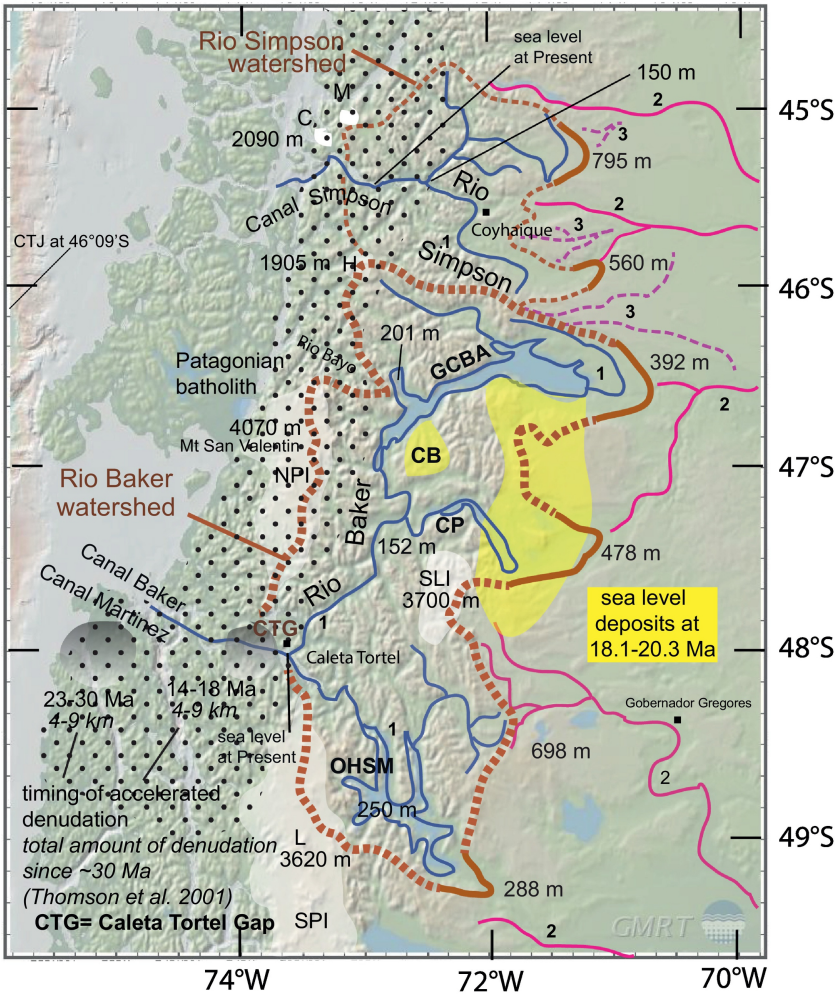
Rio Simpson watershed
sea level at Present
150 m
2
45°S
M
C
2090 m
3
795 m
Rio
Canal Simpson
2
Coyhaique
3
CTJ at 46°09'S
1
Simpson
1905 m H
560 m
46°S
3
201 m
Rio Bayo
GCBA
Patagonian batholith
1
392 m
2
4070 m
Mt San Valentin
CB
NPI
47°S
Rio Baker watershed
Baker
CP
152 m
478 m
Canal Baker
Canal Martinez
Rio
SLI
3700 m
sea level deposits at 18.1-20.3 Ma
1
CTG
48°S
Caleta Tortel
23-30 Ma
4-9 km
14-18 Ma
4-9 km
sea level at Present
Gobernador Gregores
1
698 m
OHSM
2
timing of accelerated denudation
250 m
total amount of denudation since ~30 Ma
(Thomson et al. 2001)
L
3620 m
49°S
288 m
CTG= Caleta Tortel Gap
SPI
2
GMRT
74°W
72°W
70°W

Figure 20

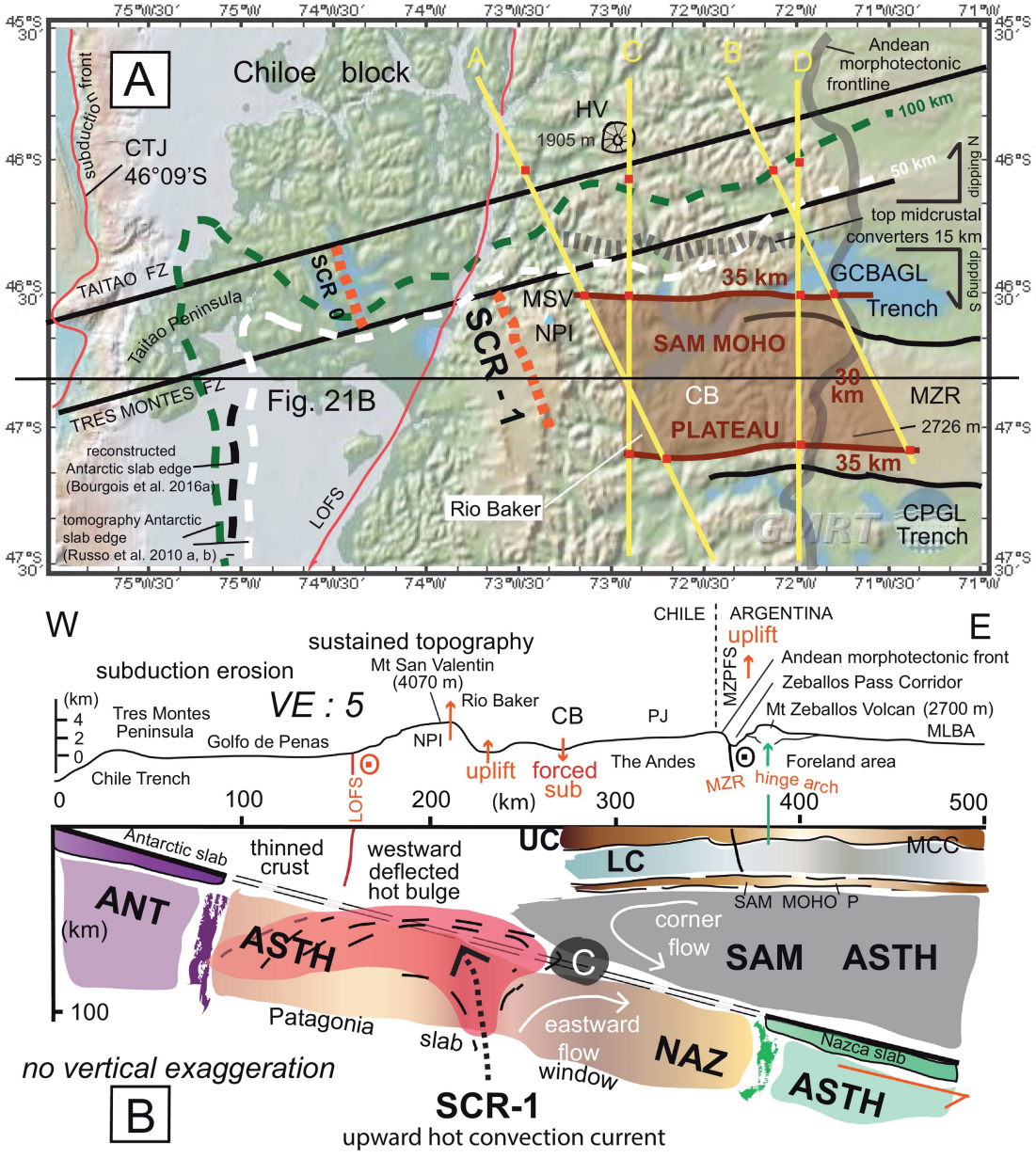
A
Chiloe block
subduction front
CTJ
46°09'S
HV
1905 m
Andean
morphotectonic
frontline
100 km
50 km
dipping N
top midcrustal
converters 15 km
dipping S
TAITAO FZ
Taitao Peninsula
SCR 0
SCR -1
MSV
NPI
35 km
GCBAGL
Trench
SAM MOHO
TRES MONTES FZ
Fig. 21B
CB
PLATEAU
30
km
MZR
2726 m
35 km
reconstructed
Antarctic slab edge
(Bourgois et al. 2016a)
tomography Antarctic
slab edge
(Russo et al. 2010 a, b)
LOFS
Rio Baker
CPGL
Trench
A
B
C
D
W
E
CHILE
ARGENTINA
uplift
subduction erosion
sustained topography
Mt San Valentin
(4070 m)
Rio Baker
MZPFS
Andean morphotectonic front
Zeballos Pass Corridor
Mt Zeballos Volcan (2700 m)
MLBA
(km)
4
2
0
Tres Montes
Peninsula
VE : 5
Golfo de Penas
NPI
CB
PJ
Chile Trench
LOFS
uplift
forced
sub
The Andes
MZR
hinge arch
Foreland area
0
100
200
(km)
300
400
500
Antarctic slab
thinned
crust
westward
deflected
hot bulge
UC
LC
MCC
SAM MOHO P
ANT
(km)
ASTH
corner
flow
SAM
ASTH
100
Patagonia
slab
eastward
flow
window
NAZ
Nazca slab
ASTH
no vertical exaggeration
B
SCR-1
upward hot convection current

Figure 21

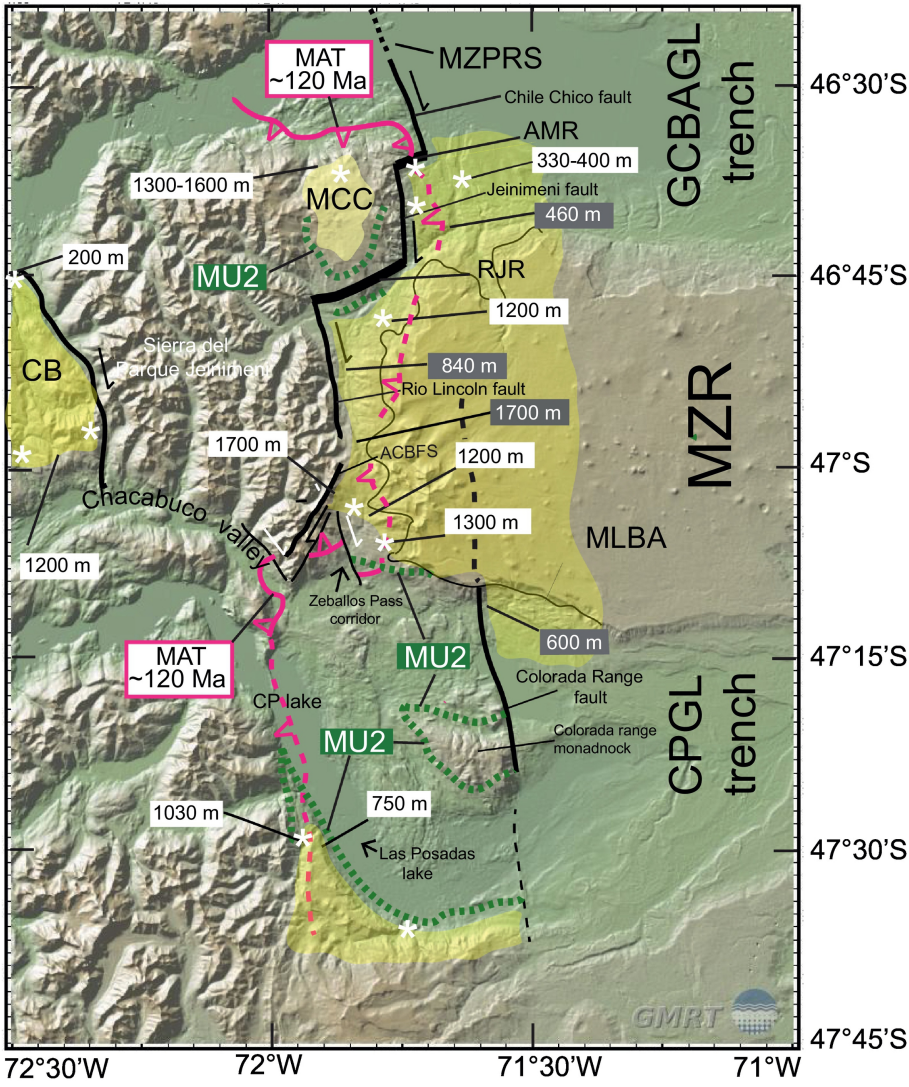
MAT
~120 Ma
MZPRS
Chile Chico fault
AMR
330-400 m
1300-1600 m
MCC
Jeinimeni fault
460 m
GCBAGL
trench
200 m
MU2
RJR
1200 m
Sierra del
Parque Jeinimeni
CB
840 m
Rio Lincoln fault
1700 m
MZR
1700 m
ACBFS
1200 m
Chacabuco valley
1300 m
MLBA
1200 m
Zeballos Pass
corridor
600 m
MAT
~120 Ma
MU2
Colorada Range
fault
CP lake
MU2
Colorada range
monadnock
CPGL
trench
1030 m
750 m
Las Posadas
lake
GMRT
46°30'S
46°45'S
47°S
47°15'S
47°30'S
47°45'S
72°30'W
72°W
71°30'W
71°W

Figure 22

SUPPLEMENTARY DATA FOR :

Journal Pre-proof EARTH-SCIENCE REVIEWS (2021)

The internal versus external dynamics in building the Andes (46°-30′–47°-30′ S) at the Patagonia slab window, with special references to the lower Miocene morphotectonic frontline: a review

Jacques Bourgois, Jose Frutos, Maria Eugenia Cisternas

PII: S0012-8252(21)00323-8
DOI: https://doi.org/10.1016/j.earscirev.2021.103822
Reference: EARTH 103822

To appear in: Earth-Science Reviews
Received date: 9 July 2020
Revised date: 7 September 2021
Accepted date: 26 September 2021

Please cite this article as: J. Bourgois, J. Frutos and M.E. Cisternas, The internal versus external dynamics in building the Andes (46Åã30′–47Åã30′ S) at the Patagonia slab window, with special references to the lower Miocene morphotectonic frontline: A review, Earth-Science Reviews (2021), https://doi.org/10.1016/j.earscirev.2021.103822

File S1. Geologic framework: Basic papers and geologic mapping such as those by Ecosteguy et al. (2003), De la Cruz and Suarez (2008), Fosdick et al. (2011), Navarrete et al. (2015), Ghiglione et al. (2015, 2016, 2019), Folguera et al. (2018), Ronda et al. (2019) and references therein provide basic descriptions, successions, and ages (Fig. S1). The extensional stress that has controlled the evolution of Western Gondwana during Lower Jurassic to Cretaceous times was described and interpreted in term of pre-, syn-, and post-rift stages (Dalziel, 1981; Kay et al., 1989; Macdonald et al., 2003; Navarrete et al., 2015; Gianni et al., 2015; Paton et al., 2017) in relation with the South Atlantic rifting (Channell et al., 1995; Granot and Dyment, 2015; Lovecchio et al., 2020). The ignimbrite and pyroclastic fall deposits of the El Quemado (Argentina) and Ibañez (Chile) Fms with ages ranging from 144 to 179 Ma together form one of the largest silicic igneous provinces on Earth (Pankhurst et al.,

1998, 2000; Feraud et al., 1999). This volcanic material unconformably (MU1) overlies a Paleozoic metamorphic basement, which contains Liassic marine sediment preserved in half-grabens (i.e. pre-rift structures).

Upsection of the volcanics, marine sediment accumulated during Lower Cretaceous time (Berriasian to Lower Aptian). From base to top, it includes the Toqui, Katterfeld and Apeleg Fms (Chile), which are components of the Coyhaique Group (De la Cruz et al., 2003). These marine formations are considered to be the northward prolongation of the Rocas Verdes Basin that exhibits the marine accumulation of the Springhill, Rio Mayer and Rio Belgrano formations (Argentina) from base to top. Marine incursion during the Lower Cretaceous (~120-145 Ma) is a pervasive signature of the studied area. The Rocas Verdes Basin closure during the Early Cretaceous (Bruhn and Dalziel, 1977; Hervé et al., 2007) is coeval with the main shortening tectonic event at ~120 Ma documented in the study area. Volcanic material of Cretaceous age unconformably overlies (Main unconformity 2 = MU2) the marine sediment of the Rocas Verdes/Austral Magallanes Basin (Biddle et al., 1986; Ramos, 1989; Stern and de Wit, 2003; Fildani and Hessler, 2005; Fosdick et al., 2011; Varela et al., 2012; Malkowski et al., 2015; Ghiglione et al., 2015). This MU2 unconformity (Fig. S2) is well exposed along the southern bank of the Jeinimeni river (46°47'43"S-71°49'40"W, Argentina). North of 46°30'S the volcanic accumulations consist of pyroclastic material of the Divisadero Group (113 to 118 Ma, Chile). South of 47°S (Fig. S3) the pyroclastic material of the Upper Rio Tarde Fm (97 ± 4 Ma to 112 ± 2 Ma, Argentina) is significantly younger than the Divisadero Group. The continental red beds of the Lower Rio Tarde Fm are equivalent in age to the Divisadero Group.

A continental environment characterizes the time period extending from the late Upper Cretaceous (82 Ma) to Oligocene (~24 Ma). South of 46° 30'S, fluvial deposits include the Ligorio Marquez Fm of Upper Paleocene age and the San Jose Fm of Lower Eocene age

(Flint et al., 1994; Suarez and De la Cruz, 2000; Folguera et al., 2018; Encinas et al., 2019). Upsection, the Lower Basalt Fm (Chile, 34-57 Ma) and Posadas basalt (Argentina, 45-57 Ma, Fig. S3) overlie the continental deposits where they are present.

The Austral Basin of Burdigalian age is a wide depression (Fig. S4) forming a gulf closing to the North in the studied area (Raigemborn et al., 2015). Trending NNW-SSE, it extends between the Deseado Massif to the east and the Andes to the west. At ~ 46°-47°S shallow marine sediment spreads 70-80 km westward into the Andes (Meseta de Chile Chico, MCC) and Cosmelli Basin (CB); Fig. 2). The Austral Basin has experienced various episodes of transgression and regression leaving marine and continental deposits. Along the Atlantic coastal area, a marine transgression has occurred during Oligocene to lower Miocene time. Recently, Trayler et al. (2019) have dated the base of the Santa Cruz Fm (overlying the marine Monte Leon Fm, i.e. the El Chacay Fm) along the Atlantic coastal area at 18.27 ± 0.6 Ma. Afterwards, the Austral Basin exhibits only continental accumulations from the Atlantic coastal area to the Andes foothills.

File S2. **Patagonia Slab Window:** The westward South Chile Ridge (SCR) jumps resulted in formation of the Chonos (Bourgois et al., 2000) and Cabo Elena ephemeral microplates (Bourgois et al., 2016a) that existed between 4.9 to 5.7 and 0.6 Ma to present time, respectively. This process (DeLong and Fox, 1977; DeLong et al., 1978; DeLong et al., 1979; Luhr et al., 1985; Rohr and Furlong, 1995) intimately connected to the SCR subduction induces the along-strike fragmentation of the incoming-slab in small pieces. The closely spaced transforms together with the across-strike partition of SCR into sub-segments increased the slab fragmentation process and major subduction-erosion (Bourgois et al., 1996). The resulting slab puzzle makes it difficult to infer a potential relationship between the Patagonia volcanism and any projected structure at depth.

File S3. Paleoclimatic background: The development of Southern Hemisphere ice sheet on Antarctica began at ~34 Ma (Shackleton et al., 1995; Zachos et al., 2008). A warm Antarctica event at 15.7 Ma (Warny et al., 2009) occurred between 13-14 and 17-18 Ma during the Mid Miocene Climatic Optimum (MMCO, Böhme, 2003; Ji et al., 2018). Hansen et al. (2013) have calculated from δ18O data that sea level at that time was ~50 m higher than at Present. Major growth of the Antarctica ice sheet following the Mid Miocene Climatic Optimum (MMCO) has driven a steady recession of the mean sea level until recent time (Fig. 4). However, during the Mid Pliocene Warm Period (2.97 to 3.29 Ma) the mean sea level has reached a similar elevation than in recent time (Haywood et al., 2010). At ~7 Ma ago, large areas of the continents experienced major drying (Herbert et al., 2016; Rabassa et al., 2005). The proximity of the Antarctica makes the Patagonia Andes prone to climatic variations in phase with Antarctic ice development since the appearance of the Southern Hemisphere ice sheet.

The Patagonian Andes have been repeatedly glaciated during the Late Cenozoic (Mercer, 1976). Piedmont glacier lobes in the Eastern Andes are key sites that record successive advances and chronology of successive glacial events that occurred over the Late Tertiary and Quaternary periods (Caldenius, 1932; Feruglio, 1944, 1950; Sinito, 1980; Mercer, 1983; Berger and Loutre, 1991; Ton-That et al., 1999; Singer et al., 2004; Kaplan et al., 2005, 2007; Clague et al., 2020). Mercer (1969, 1976) first established that the Patagonian glaciations extend not only throughout the Plio-Quaternary but also back to the late Miocene (~5-7 Ma) and the early Pliocene. Subsequently, Mercer and Sutter (1982); Rabassa and Claperton (1990), Shellmann (1999), Ton That et al. (1999), Wenzens (1999, 2000), Singer et al. (2004), Kaplan et al. (2004), Rabassa et al. (2005) have documented in detail the pioneer Mercer's framework. Several glacial events occurring between 1 and 3 Ma have left geomorphic

imprints (Sylwan, 1989; Wenzens, 2000; Clague et al., 2020). Since the middle Late Pliocene (OIS 82), 22 to 24 glacial events have been identified (Rabassa et al., 2005).

Along the study area, the 2 to 4 km high Patagonian Andes form a prominent topographic barrier to the atmospheric circulation of the Western winds in the Southern Hemisphere, and cause one of the most pronounced orographic rain shadows on Earth. Between 46° and 49°S rainfall along the Pacific western slopes is >3000 mm.yr-1, ~10 times higher than along the eastern side of the Argentina Andes and foreland (Hoffman, 1975). The Pacific Ocean to the west together with the Andean peaks raising above 3000 m control the dry climate of Patagonian steppes of Argentina. The cool temperate belt extends South of 42°S (Miller, 1976) while the Westerlies and precipitation reach a maximum at around 50°S where the mean annual precipitation may exceed 5000 mm.yr-1 at sea level. Precipitation totals decrease sharply northward from 2000 mm at 40°S to <150 mm at 30°S. Numerical modeling (Hulton et al., 1994) aiming to reconstruct the climate of Patagonia during the Last Glacial Maximum (LGM) shows a 5° southward migration of maximum precipitation since that time (Fig. 1). This is associated with a relative increase of the annual precipitation totals at 50°S, with the Westerlies now reaching a minimum at 47°S. It is anticipated that the Andes topographic barrier is controlling the atmospheric circulation similarly through time during both colder and warmer periods.

File S4. Active tectonics in the Upper Chacabuco valley: The Chacabuco Valley (Fig. 3) is a major glacial depression located north of the Cochrane-Pueyrredon glacial lake. The crescent-shaped Cordon Chacabuco separates these two main glacial depressions. At point X (Fig. 9) the upper Chacabuco Valley exhibits beds of the Quemado Fm dipping 20-25° westward beneath a hypabyssal rhyolite stock (SW corner of Fig. 9 and north of Fig. 5). De la Cruz et al. (2004) have proposed the rhyolite stock to be an equivalent in age (144-160 Ma) to

the Ibañez Fm. The thrust fault juxtaposing the rhyolite stock over the Quemado Fm is the northward extension of the ~120 Ma MAT identified along Pueyrredon Lake (Fig. 5). Entering the Chacabuco valley from E to W, the thrust fault trace follows the topographic contour line documenting a low-angle dip for the MAT.

The north-south trending cliff bounding the Sierra del Parque de Jeinimeni and the deep Chacabuco valley exhibits two main scarps (Fig. S16, and S17). The more elevated one, which exhibits very steep scree slopes covering the cliff foot is ~1000 m high. The strong active erosion shaping the cliff side dates back to the last ice retreat. The lower one is 100-150 m high. It has evolved during a post LGM warmer period. It forms a boundary between the Chacabuco Valley floor and a wide, irregular flat rocky morphology extending up to the main scarp. The flat rocky morphology exhibits beheaded stream valleys that abruptly terminate against the main scarp suggesting tectonic activity at its foot (Fig. S17). The Estero El Calera and Estero El Cono are streams crossing the active tectonic zone at Present time. The abandoned valleys of the beheaded streams associated with the Estero El Cono stream are displaced several hundreds of meters in a right-lateral sense. The total cumulative displacement is about 2170 m. This major right-lateral displacement suggests that activity along the Valle Chacabuco fault occurred over a protracted interval of time. The offset intervals between beheaded stream B1 to B5 —410, 660, 720, 250, and 230 m from the younger to the older, respectively— must originate from a long period recurring events. It is suggested that beheaded-stream morphological records are the signatures of inter-glacial warm periods allowing strong runoff erosion. Accordingly, the morphology acquired during warm period should be considered as protected from erosion underneath the ice cap during cold events. If these assumptions were correct, the beheaded-stream B5 would date back to at least Marine Isotope Stage 11 (~400 ka), suggesting a maximum displacement rate in the order of 5 mm.yr-1.

The southern wedge of the Sierra del Parque Jeinimeni is a north-south trending rocky spur (SP, Fig. 9) exhibiting two 1000 m high cliffs bounding the Chacabuco Valley to the west and the Zeballos Pass corridor to the East (Fig. 3). Both cliffs exhibit the same morphological signature showing a steep lower slope of the glacial valley covered by its own scree. The high-dipping scree slope angle exposed talus with size sorting blocks, with smaller, more angular material found at the top of the slope and larger blocks at the bottom. The scree material, which accumulated during ice retreat thereby allowing a high slope angle, is preserved. It is inferred that both cliffs evolved similarly resulting in a similar morphological signature. The two cliffs bounding the SP intersect each other at an angle of ~65°. We speculate that their evolution was controlled by conjugate faults: the Valle Chacabuco and the Eastern Spur faults trending N30°W and N35°E, respectively. Accepting this assumption allows us to propose a σ1 maximum stress trending N-S, at least for the past 400 ka.

The lateral displacement along the Valle-Chacabuco fault makes it challenging to establish geological correlations between the two sides of the upper Chacabuco Valley. Despite this, we are considering the MAT identified along the Pueyrredon Lake (Fig. 5) extending to the lower part of the Zeballos Pass corridor.

Post-glacial faulting and glacially induced seismic activity have been identified in eastern Canada (e.g. Adams, 1989; Wu and Hasegawa, 1996; Wu and Johnston, 2000; Brooks and Adams, 2020) and northern Europe (e.g. Brandes et al., 2018). The low seismic activity south of CTJ (Bourgois et al., 1993) is one of the main reasons that few seismological investigations have been carried out in the studied area. Except for glacial rebound analyses (Ivins and James, 1999; Dietrich et al., 2010; Bourgois et al., 2016b), description of tectonic features potentially induced by Patagonian glaciations remains anecdotal in term of inducing faults and folds. This work documents structures that have developed during the past ~400 kyr while this area has been repeatedly covered of ice.

The Valle-Chacabuco fault (Fig. S17) is a strike-slip fault that has recorded 2170 m of right-lateral displacement during the past ~400 ka. We contemplate a tectonic evolution through 10-12 cold events and major glaciations separated by many warm interglacial events. Also, the Valle-Chacabuco fault is considered as a conjugate fault for the Estancia Lago Bertrand fault both controlling the topography of a 1000 m-high rocky spur bounding the Chacabuco Valley and Zeballos Pass corridors (Fig. 9), two major glacial valleys. We therefore infer a possible climate control on the tectonic evolution of these faults.

File S5. Glacial deposits: The Alto Rio Ghio valley (Fig. 11, and S21) exhibits a morphology arranged into three wide strips trending N-S. These strips are 2-3 km wide. It consists in an ablation till plain along the flat valley floor (Central Glacial System, CGS hereafter) edged on either side by steep rock-glacier tongues. Eastward, the East Lateral Glacial System (ELGS hereafter) includes two major glacier lobes originating from the high cirques excavating the Mt Zeballos Volcano (1.7-4 Ma) constructed above the older MLBA basalt flows. Westward, the West Lateral Glacial System (WLGS hereafter) consists in E-W trending glacier tongues originating from four cirques located along the highest crest line at the Argentina-Chile border. These glaciers and associated lateral moraines obscure the fault system at the Andean morphotectonic frontline. The ELGS and WLGS overlie the recessional moraine system covering the flat valley floor (CGS) documenting a younger age for the two lateral glacial systems of the Alto Rio Ghio.

The oldest T1 frontal moraine of the CGS (Fig. 11) has mainly accumulated volcanic material originating from volcanic complexes of the MLBA (foreland area, 1.7 to 14.5 Ma). Also, scarce blocks of metamorphic Paleozoic basement document that ice flows originating from the W (i.e. the Andes) have provided glacial material to the T1 moraine. The Alto Rio Ghio cuts the T1 moraine at point Y (Fig. 11). At this site a scar along the alto Rio Ghio

Valley (Fig. S22) exhibits a well-exposed relationship between glacial sediment and lava flow. A 2 to 3 m-thick basalt flow covers an older glacial till. An exomorphic zone (metamorphic aureole) characterizes the underside of the lava flow. Upsection the T1 moraine covers the lava flow. The scar also shows a vertical dyke cutting the T1 moraine. Lagabrielle et al. (2007) have reported a 4.32 ± 0.23 Ma age for this dyke. Because this sample was first reported by Guivel et al. (2006) as being located 10-15 km to the east of this locality, the age constraint should be used with caution. If correct this age constrains that of the morphological depression of the Zeballos Pass corridor (Alto Rio Ghio valley). However, available ages from local volcanic flows originating from the MLBA western cliff (Fig. 11, Table S1) suggest an age older than 4-6 Ma for the depression.

The CGS extends ~5 km along trend exhibiting a hummocky flat zone (Fig. S23) from point Y (Fig. 11) northward to the Cerro Plomo (Fig. S23). This flat zone shows four retreating moraines (T1 to T4) all reworking massively volcanic material. The ice flowed from NNE to S along the Alto Rio Ghio Valley. Mapping of the glacial CGS and WLGS (Fig. 11, and S21) shows the CGS unconformably overlying a swarm of mafic dykes intruding into the Zeballos Pass Fm. One of these dykes is 2.12 ± 0.45 Ma constraining a maximum possible age for the CGS at this site. If this age is correct it constrains the age of the morphological depression of the Zeballos Pass corridor as post 2.12 ± 0.45 Ma.

File S6. Volcanism during glaciations at Andean frontline: The Mt Zeballos volcano (2726 m), located just east of the Andean morphotectonic frontline, is a major cone (1.7-4 Ma) resting on a surface previously eroded down to the lower Miocene section in the Zeballos Pass area. Volcanic flows from the Mt Zeballos volcano cover the gently eastward-dipping volcanic flows of the MLBA with ages ranging from 4.5 to 14.5 Ma, including the Cerro Plomo and the Cerro Overo volcanic complexes. All of these older volcanic flows have

mainly originated from the Zeballos Pass corridor, which follows the tectonically weakened MZPRS zone at 16-18 Ma. In other words, evidence exists documenting tectonic disruptions of the MLBA basalt flows older than or coeval from the onset outpouring of the Zeballos volcano beginning at 4 Ma. It has been documented that the polygonal morphologies characterizing the flat surface of the MLBA east of Mt Zeballos (Fig. 12) are younger than ~1 Ma. The polygonal morphologies are likely related to ice lobes originating from Mt Zeballos volcano in a similar way of what exists at Present.

The Alto Rio Ghio area provides evidence constraining the minimum age for the morphological depression following the Zeballos Pass corridor southward. Volcanic flows at the riverbed originating from the eastern flank of the corridor have provided ages as old as 5 to 7 Ma, documenting that the depression existed at that time. Accepting the age reported on Fig. S22 to be correct, the frontal moraine of the CGS would be older than 4.32 ± 0.23 Ma documenting that a glacier was flowing southward along the Zeballos Pass corridor at that time. These data suggest that the Alto Rio Ghio depression had existed by the end of the Miocene.

It has been proposed that glacial morphologies located on the flat MLBA surface originated from relief located west of the Andean morphotectonic frontline (Lagabrielle et al., 2007). It must be noted that the Jeinimeni valley (Fig. 3) is the only one existing channel able to drain an ice lobe toward the MLBA area. Also ashes and volcanic flows (1.7-4 Ma) originating from the Mt Zeballos volcano cover the eastern edge of the Rio Zeballos valley (Fig. 12, and DD' Fig. 13). It is proposed that the Mt Zeballos cone was likely obstructing access not only to the upper Rio Zeballos valley but also to the MLBA in general. The major cone of the Mt Zeballos volcano was thus likely producing ice lobes not only toward the Rio Zeballos and Jeinimeni valleys but also to the east covering the MLBA. This

morphostructural situation is still active at Present. A major cirque at the Mt Zeballos is producing a rock glacier lobe flowing eastward onto the MLBA.

REFERENCE FOR SUPPLEMENTARY DATA

Ackert, Jr.R.P., Singer, B.S., Guillou, H., Kaplan, M.R., and Kurz, M.D., 2003. Long-term cosmogenic ^{3}He production rates from ^{40}Ar/^{39}Ar and K-Ar dated Patagonian lava flows at 47°S. Earth and Planetary Science Letters 210, 119-136.

Adams, J., 1989, Postglacial faulting in eastern Canada: nature, origin and seismic hazard implications: Tectonophysics, v. 163, p. 323-331.

Baker, P.E., Rea, W.J., Skarmeta, J., Caminos, R., Rex, D.C., 1981. Igneous history of the Andean Cordillera and Patagonian Plateau around latitude 46°S. Philos. Trans. R. Soc. Lond., A 303, 105–149.

Barberon, V., Ronda, G., Leal, P.R., Sue, C., and Ghiglione, M.C., 2015, Lower Cretaceous provenance in the northern Austral basin of Patagonia from sedimentary petrography: Journal of American Earth Sciences, v. 64, p. 498-510. doi.org/10.1016j.jsames.2015.08.014

Berger, A.L., and Loutre, M.F., 1991, Insolation values for the climate of the last 10 Millions years: Quaternary Science Reviews, v. 10, p. 297-318.

Biddle, K.T., Uliana, M.A., Mitchum jr., R.M., Fitzgerald, M.G., and Wright, R.C., 1986, The stratigraphic and structural evolution of the central and eastern Magallanes basin, Southern South America: foreland Basins, Book editors P.A. Allen, P. Homewood, p. 41-61, Wiley Online Library, https://doi.org/10.1002/9781444303810.ch2

Blisniuk, P.M., Stern, L.A., Chamberlain, P., Idleman, B., and Zeitler, P.K., 2005, Climatic and ecologic changes during Miocene surface uplift in the southern Patagonian Andes: Earth Planet. Sc. Lett., v. 230, p. 125-142.

Böhme, M., 2003, The Miocene Climate Optimum: evidence from ectothermic vertebrates of central Europe: Pal. Pal. Pal., v. 195, p. 389-401.

Bourgois, J**.,** Cisternas, M.E., Braucher, R., Bourles, D., and Frutos, J., 2016b, Geomorphic records along the General Carrera (Chile)-Buenos Aires (Argentina) glacial lake (46-48°S), climate inferences and glacial rebound for the past 7-9 ka: *The Journal of Geology, v*. 124, p. 27-53, DOI: 10.1086/684252.

Bourgois, J**.,** Lagabrielle, Y., Martin, H., Dyment, J., Frutos, J., and Cisternas, M.E., 2016a, A review on forearc ophiolite obduction, adakite-like generation, and slab window development at the Chile Triple Junction area: uniformitarian framework for spreading-ridge subduction: *Pure and Applied Geophysics: v. 173, p. 3217-3246,* DOI: 10.1007/s00024-016-1317-9.

Bourgois, J., Guivel, C., Lagabrielle, Y., Calmus, T., Boulègue, J., and Daux, V., 2000, Glacial interglacial trench supply variation, spreading-ridge subduction, and feedback controls on the Andean margin development at the Chile triple junction area (45-48°S): J. of Geophys. Res., v. 105, p. 8355-8386.

Bourgois, J., Martin, H., Lagabrielle, Y., Le Moigne, J., and Frutos, J., 1996, Subduction-erosion related to spreading-ridge subduction: Taitao peninsula (Chile margin triple junction area): Geology, v. 24, p. 723-726.

Bourgois, J., Lagabrielle, Y., Le Moigne, J., Urbina, O., Janin, M.-Ch., and Beuzard, P., 1993, Preliminary results of a field study of the Taitao ophiolite (southern Chile): implications for the evolution of the Chile triple junction: Ofioliti, v. 18, p. 113-129.

Boutonnet, E., Arnaud, N., Guivel, C., Lagabrielle, Y., Scalabrino, B., and Espinoza, F., 2010, Subduction of the South Chile active spreading ridge: a 17 Ma to 3 Ma magmatic record in central Patagonia (western edge of Meseta del Lago Buenos Aires, Argentina): J. of Volcanology and Geothermal Res., v. 189, N° 3-4, p. 319-339. doi: 10.1016/j.jvolgeores.2009.11.022

Brandes, C., Steffen, H., Sandersen, P.B.E., Wu, P., and Winsemann, J., 2018, Glacially induced faulting along the NW segment of the Sorgenfrei-Tornquist zone, northern Denmark: implications for neotectoniocs and Late glacial fault-bound basin formation: Quat. Sc. Reviews, v. 189, p. 149-168.

Brooks, G.R., and Adams, J., 2020, A review of evidence of glacially-induced faulting and seismic shaking in eastern Canada: Quat. Sc. Reviews, v. 228, 106070, https://doi.org/10.1016/j.quascirev.2019.106070.

Brown, L.L., Singer, B.S., and Gorring, M.L., 2004, Paleomagnetism and 40Ar/39Ar chronology of lavas from Meseta del Lago Buenos Aires, Patagonia: Geochem. Geophys. Geosyst., v. 5 (1), Q01H04, doi:10.1029/2003GC000526.

Bruhn, R.L., and Dalziel, I.W.D., 1977, Destruction of the Early Cretaceous marginal basin in the Andes of Tierra del Fuego, in Talwani, M., and Pitman, W.C., III, eds., Island Arcs, Deep Sea Trenches, and Back-Arc Basins: American Geophysical Union, Maurice Ewing Series 1, p. 395–405.

Caldenius, C., 1932, Las glaciaciones cuaternarias en Patagonia y Tierra del Fuego: Anales, Direccion General de Geologia y Mineria, Buenos Aires, v. 95, 150 p.

Channell, J.E.T., Erba, E., Nakanishi, N., and Tamaki, K., 1995, Late Jurassic-Early Cretaceous time scales and oceanic magnetic anomaly block models. In Berggren, W.A., Kent, D.V., Aubry, M-P., Hardenbol, J. (Eds.): Geochronology, Time scales and global stratigraphic correlation. SEPM Spec. Publ., p. 51-64.

Clague, J.J., Barendregt, R.W., Menounos, B., Roberts, N.J., Rabassa, J., Martinez, O., Ercolano, B., Corbella, H., and Hemming, S.R., 2020, Pliocene and Early Pleistocene glaciation and landscape evolution on the Patagonian Steppe, Santa Cruz Province, Argentina: Quat. Sci. Rev., v. 227, doi.org/10.1016/j.quascirev.2019.105992.

Cuitiño, J.I., Ventura Santos, R., Muruaga, P.J.A., and Scasso, R.A., 2015, Sr-stratigraphy and sedimentary evolution of early Miocene marine foreland deposits in the northern Austral (Magallanes) Basin, Argentina: Andean Geology, v. 42, N°3, doi: 10.5027/andgeoV42n3-a05

Dalziel, I.W., 1981, Back-arc extension in the Southern Andes: a review and critical reappraisal: Phil. Trans. R. Soc. Lond. A 300, p. 319-335.

De la Cruz, R., and Suarez, M., 2006, Geologia del area Puerto Guadal-Puerto Sanchez, Region Aisen del General Carlos Ibañez del Campo, Servicio Nacional de Geología y Minería, Carta Geológica de Chile, Serie Geología Básica, N° 95 ; 58 p., 1 mapa escala 1:100,000, Santiago.

De la Cruz, R., and Suarez, M., 2008, Geologia del area Chile Chico-Rio de las Nieves, Region del General Carlos Ibañez del Campo, Servicio Nacional de Geología y Minería, Carta Geológica de Chile, Serie Geología Básica, N° 112, 67 p., 1 mapa escala 1:100, 000, Santiago.

De la Cruz, R., Welkner, D., Suárez, M., and Quiroz, D., 2004, Geología del Área Oriental de las Hojas Cochrane y Villa O'Higgins, Región Aisén del General Carlos Ibáñez del Campo. Servicio Nacional de Geología y Minería, Carta Geológica de Chile, Serie Geología Básica, No. 85, 57 p., 1 mapa escala 1:250 000, Santiago.

De la Cruz, R., Suarez, M., Belmar, M., Quiroz, D., and Bell, M., 2003, Area Coihaique-Balmaceda, Region Aisen del General Carlos Ibañez del Campo: Servicio Nacional de Geologia y Mineria, Carta geologica de Chile, Serie Geologia Basica, N° 80, 40 p., 1

mapa, escala 1:100 000, Santiago.

DeLong, S.E., and Fox, P.J., 1977, Geological consequences of ridge subduction, In Island arc, deep sea trenches, and back-arc basins, Maurice Ewing Ser., v. 1 (ed. Talwani, M. and Pitman III, W.C.) (AGU Washington D.C.), p. 221–228.

DeLong, S.E., Fox, P.J., and MacDowell, F.W., 1978, Subduction of the Kula Ridge at the Aleutian Trench: Geol. Soc. of Am. Bull., v. 89, p. 83-95.

DeLong, S.E., Schwarz, W.M., and Anderson, R.N., 1979, Thermal effects of ridge subduction, Earth Planet. Sc. Lett., v. 44, p. 239–246.

Dietrich, R., Ivins, E. R., Casassa,G., Lange, H.,Wendt, J., and Fritsche, M., 2010, Rapid crustal uplift in Patagonia due to enhanced ice loss: Earth Planet. Sci. Lett., v. 289, p. 22–29.

Douglass, D. C., Singer, B. S., Kaplan, M. R., Mickelson, D. M., and Caffee, M. W., 2006, Cosmogenic nuclide surface exposure dating of boulders on last-glacial and late-glacial moraines, lago Buenos Aires, Argentina: interpretative strategies and paleoclimate implications: Quat. Geochronol., v. 1, p. 43–58.

Ecosteguy, L., Dal Molín, C., Franchi, M., Geuna, S., and Lapido, O., 2003, Hoja Geológica 4772-II Lago Buenos Aires, Provincia de Santa Cruz, Programa Nacional de cartas geologicas de la Republica Argentina 1:250 000, Boletin N°339, Buenos Aires, 80 p.

Encinas, A., Folguera, A., Riffo, R., Molina, P., Fernandez Paz, L., Litvak, V.D., Colwyn, D.A., Valencia, V.A., and Carrasco, M., 2019, Cenozoic basin evolution of the Central Patagonia Andes: Evidence from geochronology, stratigraphy, and geochemistry: Geoscience Frontiers, v. 10, p. 1139-1165, https://doi.org/10.1016/j.gsf.2018.07.004.

Espinoza, F., Morata, D., Polve, M., Lagabrielle, Y., Maury, R.C., Guivel, C., Cotten, J., Bellon, H., and Suarez, M., 2007, Bimodal back-arc alkaline magmatism after ridge subduction, Pliocene felsic rocks from Central Patagonia (47.S): Lithos, v. 101, p. 191-

217.

Espinoza, F., Morata, D., Polvé, M., Maury, R., Cotten, J., Bellon, H., Guivel, C., Lagabrielle, Y., Suarez, M., and Rossello, E., 2006, Mio-Pliocene magmatic variability in the central Patagonia back-arc region (47°5′S), paper presented at Backbone of the Americas, Patagonia to Alaska. Geol. Soc. of Am., Mem., Mendoza, Argentina.

Espinoza, F., Morata, D., Pelleter, E., Maury, R.C., Suarez, M., Lagabrielle, Y., Polvé, M., Bellon, H., Cotten, J., De la Cruz, R., and Guivel, C., 2005, Petrogenesis of the Eocene and Mio-Pliocene alkaline basaltic magmatism in Meseta Chile Chico, Southern Patagonia, Chile: evidence for the participation of two slab windows: Lithos, v. 82, p. 83-96, doi:10.1016/j.lithos.2004.09.024.

Feraud, G., Alric, V., Fornari, M., Bertrand, H., and Haller, M., 1999, ^{40}Ar/^{39}Ar dating of the Mesozoic silicic volcanic Province of Patagonia and its relationship to Gondwana breakup and subduction: Earth Planet. Sc. Lett., v. 172, p. 83-96.

Feruglio, E., 1944, Estudios geologicos y glaciologicos en la region del Lago Argentino (Patagonia): Bol. Acad. Nac. Ciencias Cordoba, v. 37, p. 1-208.

Feruglio, E., 1950, Descripcion geologica de la Patagonia. Tomo 3, YPF, Buenos Aires.

Fildani, A., and Hessler, A.M., 2005, Stratigraphic record across a retro-arc basin inversion: Rocas Verdes Magallanes basin, Patagonian Andes, Chile: Bull. Geol. Soc. Am., v. 117, p. 1596-1614, Doi.org/10.1130/B25708.1.

Flint, S.S., Prior, D.J., Agar, S.M., and Turner, P., 1994, Stratigraphic and structural evolution of the Tertiary Cosmelli basin and its relationship to the Chile triple junction: Journal of the Geological Society of London, v. 151, p. 251-268.

Folguera, A., Encinas, A., Echaurren, A., Gianni, G., Orts, D., Valencia, V., and Carrasco, G., 2018, Constraints on the Neogene growth of the central Patagonian Andes at the latitude of the Chile Triple Junction (45-47°S) using U/Pb geochronology in synorogenic strata:

Tectonophysics, v. 744, p. 134-154.

Fosdick, J.C., Romans, B.W., Fildani, A., Bernhardt, A., Calderon, M., and Stephan, A.G., 2011, Kinematic evolution of the Patagonian retroarc fold-andthrust belt and Magallanes foreland basin, Chile and Argentina, 51°30'S: Geol. Soc. Am. Bull., v. 123, p. 1679-1698, doi : 10.1130/B30242.1.

Ghiglione, M.C., Ronda, G., Rodrigo J. Suárez, J.R., Aramendía, I., Barberón, V., Ramos, M.E., Tobal, J., García Morabito, E., Matrinod, J., and Christian Sue, C., 2019, Structure and tectonic evolution of the South Patagonian fold and thrust belt : coupling between subduction dynamics, climate and tectonic deformation: Andean Tectonics, Elsevier, Chapter 4, p. 675-698. https://doi.org/10.1016/B978-0-12-816009-1.00024-1

Ghiglione, M.C., Naipauer, M., Sue, C., Barberon, V., Valencia V., Aguirre-Urreta, B., and Ramos, V.A., 2015, U-Pb zircon ages from the northern Austral basin and their correlation with the Early Cretaceous exhumation and volcanism of Patagonia: Cretac. Res., v. 55, p. 116–128. Doi.org/10.1016j.cretres.2015.02.006.

Ghiglione, M.C., Ramos, V.A., Cuitiño, J., and Barberon, V., 2016, Growth of the Southern Patagonian Andes (46-53°S) and their relation to subduction processes, A. Folguera et al. (eds.) Growth of the Southern Andes: Springer Earth System Sciences, p. 201-240, DOI 10.1007/978-3-319-23060-3_10.

Gianni, G., Navarrete, C., Orts, D., Tobal, J., Folguera, A., and Gimenez, M., 2015, Patagonian broken foreland and related synorogenic rifting: the origin of the Chubut Group Basin: Tectonophysics, v. 649, p. 81–99.

Gorring, M.L., Kay, S.M., Zeitler, P.K., Ramos, V.A., Rubiolo, D., Fernandez, M.I., and Panza, J.L., 1997, Neogene Patagonian plateau lavas: continental magmas associated with ridge collision at the Chile triple junction: Tectonics, v. 16, p. 1-17.

Granot, R., and Dyment, J., 2015, The Cretaceous opening of the South Atlantic Ocean: Earth

Planet. Sc. Lett., v. 414, p. 156-163, http://dx.doi.org/10.1016/j.epsl.2015.01.015

Guivel, C., Morata, D., Pelleter, E., Espinoza, F., Maury, R., Polvé, M., Bellon, H., Cotton, J., Benoit, M., Suarez, M., and De la Cruz, R., 2006, Miocene to Late Quaternary Patagonian basalts (46-47° S): Geochronometric and geochemical evidence for slab tearing due to active spreading ridge subduction: J. of Volcan. Geotherm Research, v. 149, p. 346–370.

Hansen, J., Sato, M., Russell, G., and Kharecha, P., 2013, Climate sensitivity, sea level and atmospheric carbon dioxide: Phil. Trans.R. Soc. A371, 20120294, http://dx.doi.org/10.1098/rsta.2012.0294.

Haywood AM, Dowsett HJ, Otto-Bliesner B, Chandler MA, Dolan AM, Hill DJ, Lunt DJ, Robinson MM, Rosenbloom N, and Salzmann U., 2010, Pliocene Model Intercomparison Project (PlioMIP): experimental design and boundary conditions (Experiment 1). Geoscientific Model Development, 3(1), p. 227-242, doi:10.5194/gmd-3-227-2010

Herbert, T.D., Lawrence, K.T., Tzanova, A., Cleaveland Peterson, L., Caballero-Gill, R., and Kelly, C.S., 2016, Late Miocene global cooling and the rise of modern ecosystems: Nature Geoscience, v. 9, p. 843–847, DOI: 10.1038/NGEO2813.

Hervé, F., Pankhurst, R.J., Fanning, C.M., Calderón, M., and Yaxley, G.M., 2007, The South Patagonian Batholith: 150 my of granite magmatism on a plate margin: Lithos, v. 97, p. 373–394, doi: 10.1016/j.lithos.2007.01.007.

Hoffman, J.A.J., 1975, Atlas Climatico de America del Sur. WMO, Unesco, Geneva.

Hulton, N.D., Sugden, D., Payne, A., and Clapperton, C., 1994, Glacier modeling and climate of Patagonia during the last glacial maximum: Quaternary Research, v. 42, p. 1–19.

Ivins, E. R., and James, T. S. 1999, Simple models for late Holocene and present-day Patagonian glacier fluctuations and predictions of a geodetically detectable isostatic

response: Geophys. J. Int., v. 138, p. 601–624.

Ji, S., Nie, J., Lechler, A., Huntington, .W., Heitmann, E.O., and Breecker, D.O., 2018, A symmetrical CO2 peak and asymmetrical climate change during the Middle Miocene: Earth Planet. Sc. Lett., v. 499, p. 134-144, doi.org/10.1016/j.epsl.2018.07.011.

Kaplan, M.R., Hulton, N.R.J., Coronato, A., Rabassa, J.O., Stone, J.O., Kubik, P.W., and Freeman, S., 2007, Cosmogenic nuclide measurements in Southernmost South America and implications for landscape change: Geomorphology, v. 87, p. 284-301.

Kaplan, M.R., Douglass, D.C., Singer, B.S., Ackert, R.P., and Cafee, M.W., 2005, Cosmogenic nuclide chronology of pre-Last Glacial Maximum moraines at Lago Buenos Aires, 46°S, Argentina: Quaternary Research, v. 63, p. 301-315.

Kaplan, M.R., Ackert, Jr., Singer, B.S., Douglass, D.C., and Kurz, M.D., 2004, Cosmogenic nuclide chronology of millenial-scale glacial advances during O-isotope stage 2 in Patagonia: Geol. Soc. Amer. Bull., v. 116, p. 321-384.

Kay, M.S., Ramos, V.A., Mpodozis, C., and Sruoga, P., 1989, Late Paleozoic to Jurassic silisic magmatism at the Gondwanaland margin: analog to the Middle Proterozoic in North America?: Geology, v. 17, p. 324–328.

Lagabrielle, Y., Suarez, M., Malavieille, J., Morata, D., Espinoza, F., Maury, R., Scalabrino, B., Barbero, L., De la Cruz, R., Rossello, E., and Bellon, H., 2007, Pliocene extensional tectonics in the Eastern Central Patagonian cordillera: geochronological constraints and new field evidences: Terra Nova, v. 19, p. 413–424, doi/10.1111/j.1365-3121.2007.00766.x.

Luhr, J.F., Nelson, S., Allan, J.F., and Carmichael, I.S.E., 1985, Active rifting in South-western Mexico: manifestations of an incipient eastward spreading-ridge jump: Geology, v. 13, p. 54–57.

Macdonald, D., Gomez-Perez, I., Franzese J., Spalletti, L., Lawver, L., Gahagan, L., Dalziel,

I., Thomas, C., Trewin, N., Hole, M., and Paton, D., 2003, Mesozoic break-up of SW Gondwana: implications for regional hydrocarbon potential of the Southern South Atlantic: Marine and Petroleum Geology, v. 20, p. 287–308.

Malkowski, M.A., Grove, M., and Graham, S.A., 2015, Unzipping the Patagonian Andes-long-lived influence of rifting history on foreland basin evolution: Lithosphere, v. 8, p. 23–28, doi:10.1130/L489.1.

Mercer, J.H., 1983, Cenozoic glaciation in the Southern Hemisphere: Annual Review of Earth and Planetary Sciences, v. 11, p. 99–132.

Mercer, J., and Sutter, J., 1982, Late Miocene-earliest Pliocene glaciation in Southern Argentina: implications for global ice-sheet history: Pal. Pal. Pal., v. 38, p. 185–206

Mercer, J., 1976, Glacial history of Southernmost South America, Quaternary Research, v. 6, p. 125–166.

Mercer, J., 1969, Glaciation in Southern Argentina more than 2 million years ago: Science, v. 164, p. 823–825.

Miller, A., 1976, The climate of Chile, in World Survey of Climatology, vol. 12. Climates of Central Chile and South America: edited by W. Schwerdtferger, p. 113-145, Elsevier, Amsterdam-Oxford-New York.

Morata, D., Barbero, L., Sua´rez, M., De la Cruz, R., 2002, Early Pliocene magmatism and high exhumation rates in the Patagonian Cordillera (46°40'S): K–Ar and fission track data. Fifth International Symposium on Andean Geology. ISAG, Toulouse, France, pp. 433–436.

Navarrete, C.R., Gianni, G.M., and Folguera, A., 2015, Tectonic inversion events in the Western San Jorge Gulf Basin from seismic, borehole and field data: J. of South Amer. Earth Sc., v. 64, p. 486–497, Doi.org10.1016j.jsames.2015.09.012.

Pankhurst, R.J., Riley, T.R., Fanning, C.M., and Kelley, S.P., 2000, Episodic silicic volcanism in Patagonia and the Antarctic Peninsula: Chronology of magmatism associated with the break-up of Gondwana: Journal of Geology, v. 41, N°5, p. 605–625.

Pankhurst, R.J., Leat, P.T., Sruoga, P., Rapela, C.W., Marquez, M., Storey, B.C., and Riley, T.R., 1998, The Chon Aike province of Patagonia and related rocks in West Antarctica: a silicic large igneous province: J. Volcanol. Geotherm. Res., v. 81, p. 113–136.

Paton, D.A., Pindell, J., McDermott, K., Bellingham, P., and Horn, B., 2017, Evolution of seaward-dipping reflectors at the onset of oceanic crust formation at volcanic passive margins: insight from the South Atlantic: Geology, v. 45, p. 439–442, doi: 10.1130/G38706.1.

Pelleter, E. 2003, Diversite geochimique et geochronologique des basaltes de la region du lac General Carrera–Buenos Aires: nouvelles contraintes sur la subduction de la dorsale active du Chili. Unpublished DEA thesis, Universite´ de Bretagne Occidentale, Brest, France.

Rabassa, J., and Clapperton, C.M., 1990, Quaternary glaciations of the Southern Andes: Quat. Sc. Reviews., v. 9, p. 153–174.

Rabassa, J., Coronato, A.M., and Salemme, M., 2005, Chronology of the Late Cenozoic Patagonian glaciations and their correlation with biostratigraphic units of the Pampean region (Argentina): J. South Amer. Earth Sc., v. 20, p. 81–103, doi:10.1016/j.jsames.2005.07.004.

Raigemborn, S.M., Matheos, S.D., Krapovickas, V., Vizcaino, S.F., Bargo, S.,M., Kay, R.F., Fernicola, J.C., and Zapata, L., 2015, Paleoenvironmental reconstruction of the coastal Monte Léon and Santa Cruz formations (Early Miocene) at Rincon del Buque, Southern Patagonia : a revisited locality: J. South Amer. Earth Sci., v. 60, p. 31–55.

Ramos, V.A., 1989, Andean foothills structure in northern Magallanes basin, Argentina,

Amer. Ass. Petrol. Geologists Bull., v. 73, p. 887-903, DOI: 10.1306/44B4A28A-170A-11D7-8645000102C1865D.

Rodriguez, E.E., and Russo, R.M., 2020, Southern Chile crustal structure from teleseismic receiver functions: responses to ridge subduction and terrane assembly of Patagonia. Geosphere, v. 16 (1), p. 378–391, https://doi.org/10.1130/GEOS016921.1.

Rohr, K.M.M., and Furlong, K.P., 1995, Ephemeral plate tectonics at the Queen Charlotte triple junction: Geology, v. 23, p. 1035-1038.

Ronda, G., Ghiglione, M., Barberon, V., Coutand, I., and Tobal, J., 2019, Mesozoic-Cenozoic evolution of the Southern Patagonian Andes fold and thrust belt (47°–48°S): Influence of the Rocas Verdes basin inversion and onset of Patagonian glaciations: Tectonophysics, v. 765, p. 83–101.

Shackleton, N.J., Crowhurst, S., Hagalberg, T., Pisias, N.G., and Schneider, D.A., 1995, A new late Neogene time scale: application to LEG 138 sites. Proceedings of the Ocean Drilling Program, Scientific Results, v. 138, p. 73–90.

Shellmann, G., 1999, Landscape evolution and glacial history of Southern Patagonia (Argentine) since the Late Miocene -some general aspects: Zentralblatt Geologie und Paläeontologie, Teil 1, v. 7-8, p.1013–1026.

Singer, B., Ackert, Jr. R.P., and Guillou, H., 2004, $^{40}Ar/^{39}Ar$ and K/Ar chronology of Pleistocene glaciations in Patagonia: Geol. Soc. Amer. Bull., v. 116, p. 434–450. doi:10.1130/B25177.1.

Sinito, A.M., 1980, Edades geologicas, radiometricas y magneticas de algunas vulcanitas cenozoicas de las provincias de Santa Cruz y Chubut: Rev. Asoc. Geol. Argent., v. 35, p. 332–339.

Suarez, M., De la Cruz, R., 2000, Tectonics in the Eastern Central Patagonian Cordillera (45°30'– 47°30' S): Journal of the Geological Society 157, 995–1001, London.Sylwan,

C., 1989, Paleomagnetism, Paleoclimate and Chronology of Late Cenozoic deposits in Southern Argentina, 277: Meddelanden Stockholms Universittets Geologiska Inst., Nr, 110 pp.

Ton-That, T., Singer, B., Mörner, N.A., and Rabassa, J., 1999, Datacion por el metodo $^{40}Ar/^{39}Ar$ de lavas basalticas y geologia del Cenozoico superior en la region del Lago Buenos Aires, Provincia de Santa Cruz: Revista de la Asociacion Geologica Argentina (Buenos Aires), v. 54, p. 333–352.

Trayler, R.B., Schmitz, M.D., Cuitiño, J.I., Kohn, M.J., Bargo, M.S., Kay, R.F., Strömberg, A.E., and Vizcaino, S.F., 2019, An improved approach to age-modeling in deep time: implications for the Santa Cruz Formation, Argentina: Geol. Soc. Am. Bull., https://doi.org/10.1130/B35203.1.

Varela, A.N., Poiré, D.G., Martin, T., Gerdes, A., Goin, F.J., Gelfo, J.N., and Hoffmann, S., 2012, U-Pb zircon constraints on the age of the Cretaceous Mata Amarilla Formation, Southern Patagonia, Argentina: its relationship with the evolution of the Austral basin: Andean Geology, v. 39, p. 359–379.

Warny, S., Askin, R.A., Hannah, M.J., Mohr, B.A.R., Raine, J.I., Harwood, D.M., Florindo, F., and SMS Science Team, 2009, Palynomorphs from a sediment core reveal a sudden remarkably warm Antarctica during the middle Miocene: Geology, v. 37, p. 955–958.

Welkner, D., 2000, Geocronologia de los plutons del area del Cerro San Lorenzo, XI Region de Aysen in Congreso Geologico Chileno, N)9, Actes 2, Puerto Varas, p. 269-273.

Wenzens, G., 1999, Fluctuations of outlet and valley glaciers in the Southern Andes (Argentina) during the past 13,000 years: Quaternary Research, v. 51, p. 238-247.

Wenzens, G., 2000, Pliocene piedmont glaciation in the rio Shehuen valley, Southwest Patagonia, Argentina: Arctic, Antarctic and Alpine Research, v. 32, p. 46–54.

Wu, P., and Hasegawa, H.S., 1996, Induced stresses and fault potential in eastern Canada due

to a realistic load: a preliminary analysis : Geophys. J. Int., v. 127, p. 215–229.

Wu, P., and Johnston, P., 2000, Can deglaciation trigger earthquakes in N. America?: Geophys. Res. Lett., v. 27, p. 1323–1326.

Zachos J.C., Dickens G.R., and Zeebe R.E.. 2008, An Early Cenozoic perspective on greenhouse warming and carbon-cycle dynamics: Nature, v. 451, p. 279–283, doi:10.1038/nature06588).

CAPTION OF FIGURES FOR SUPPLEMENTARY DATA

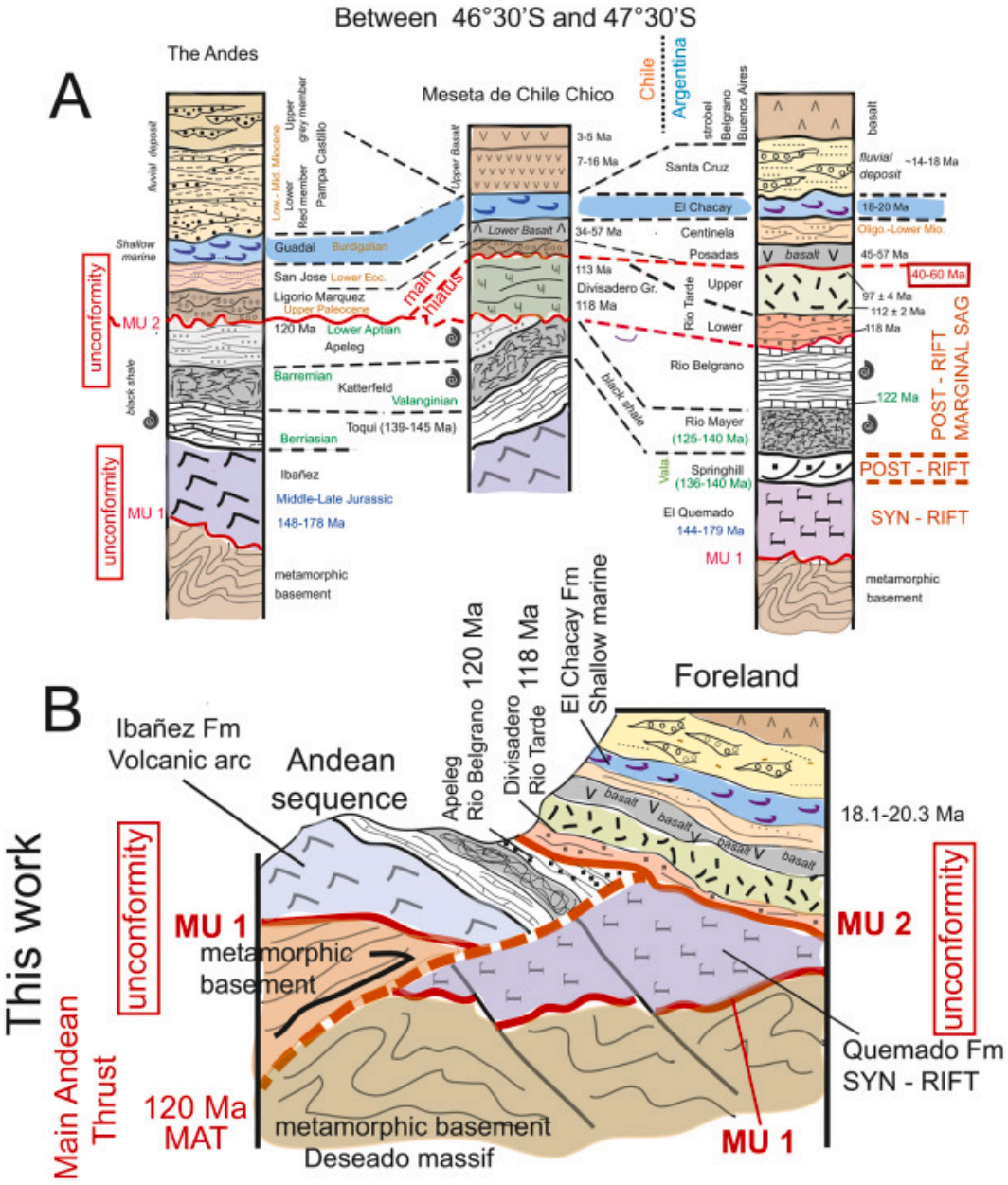

Figure S1. A–Basic stratigraphic data as reported in published works. The column on the left (the Andes) is modified from De la Cruz and Suarez. (2006). The column in the center (Meseta de Chile Chico) is modified from De la Cruz and Suarez (2008). The column on the right (Foreland area) is modified from Fosdick et al. (2011), Barberon et al. (2015). **B**–This work: the Ibañez and the Quemado volcanic flows originated from two different geodynamic environments, volcanic arc and syn-rift, respectively. Major east-verging thrusting event at ~120 Ma resulted in the closure of the Ibañez back-arc basin. The calc-alkaline volcanic product of the Ibañez Fm and its shallow marine sediment cover has been transported

eastward onto the syn-rift Quemado Fm. Volcanic and sediment sequences younger than ~118 Ma seal the ~120 Ma Main Andean Thrust. MAT–Main Andean Thrust; MU1–Main unconformity 1; MU2–Main unconformity 2. See text for more details.

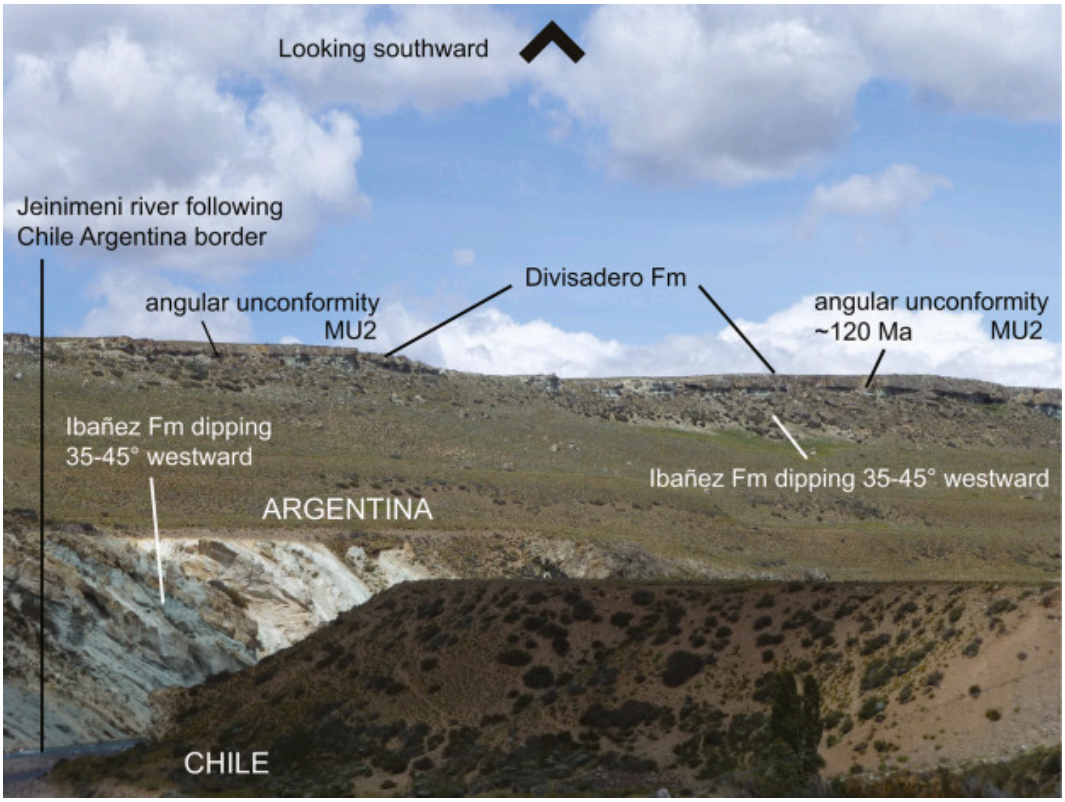

Figure S2. Main angular Unconformity 2 = MU2 well exposed south of the Rio Jeinimeni (Argentina). Sub-horizontal volcanic beds of the Divisadero Fm (= Rio Tarde Fm) unconformably overlies volcanics of the Ibañez Fm dipping 35-45° westward.

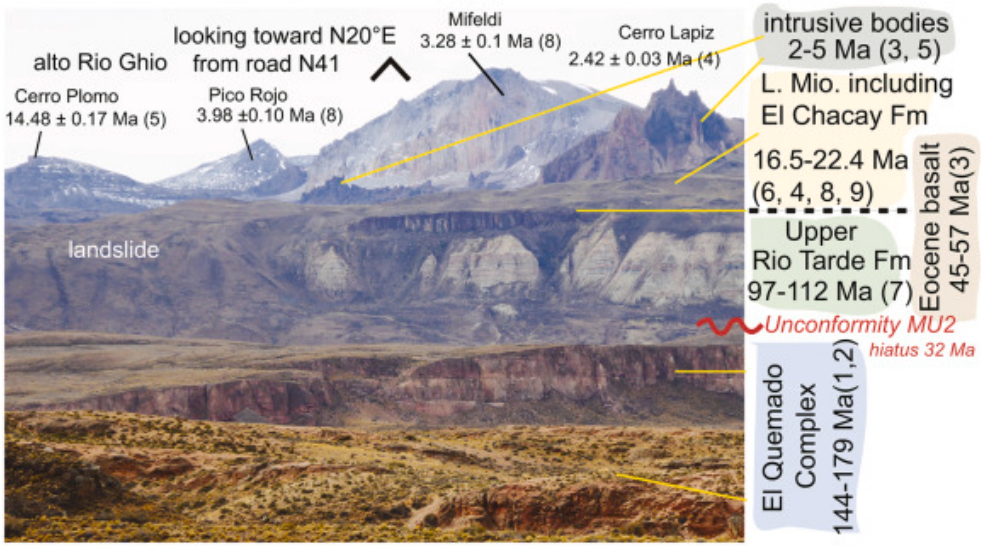

Figure S3. Eastern side of the southern entrance of the Zeballos pass (eastern bank of the Alto Rio Ghio). The southwestern edge of the MLBA exhibits the typical stratigraphical succession of the Foreland area. From base to top are the volcanic flows of the Quemado Fm (foreground), the white tuffs of the Upper Rio Tarde Fm, the black Eocene basalt (i.e. Posadas basalt), and the lower Miocene sediment (including the shallow marine sediment of the El Chacay Fm). Though exhibiting a sub-horizontal layering, this volcano-sedimentary accumulation has recorded several major hiatuses. Most of intrusive bodies (Cerro Lapiz, Pico Rojo, Midelfi) in the background are plugs related to the Mt Zeballos volcanic complex (MZVC). Basalt of the Cerro Plomo overlies the Lower Miocene fluvial sediment of the Zeballos pass Fm.

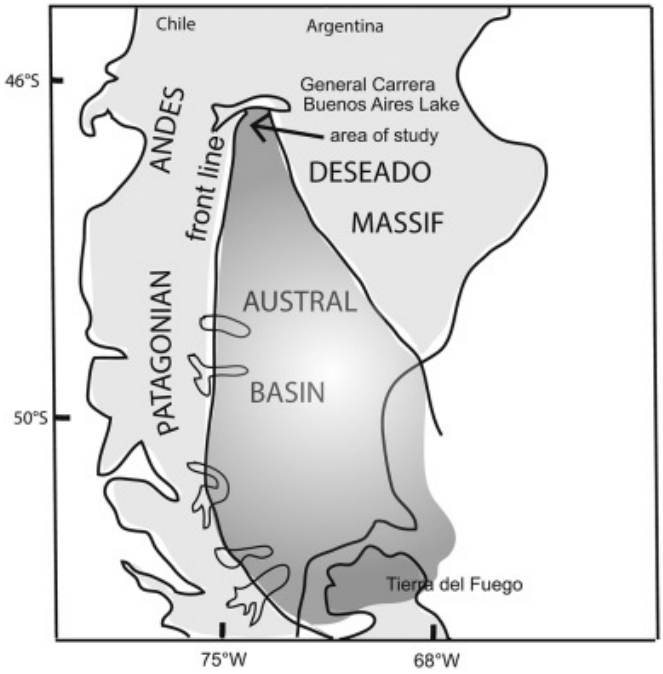

Figure S4. Marine transgression of the Austral basin (after Raigemborn et al., 2015). At 46°30'-47°30'S, deposit of the shallow-marine El Chacay Fm (18.1-20.3 Ma) follows the morphotectonic front line of the Proto Andes.

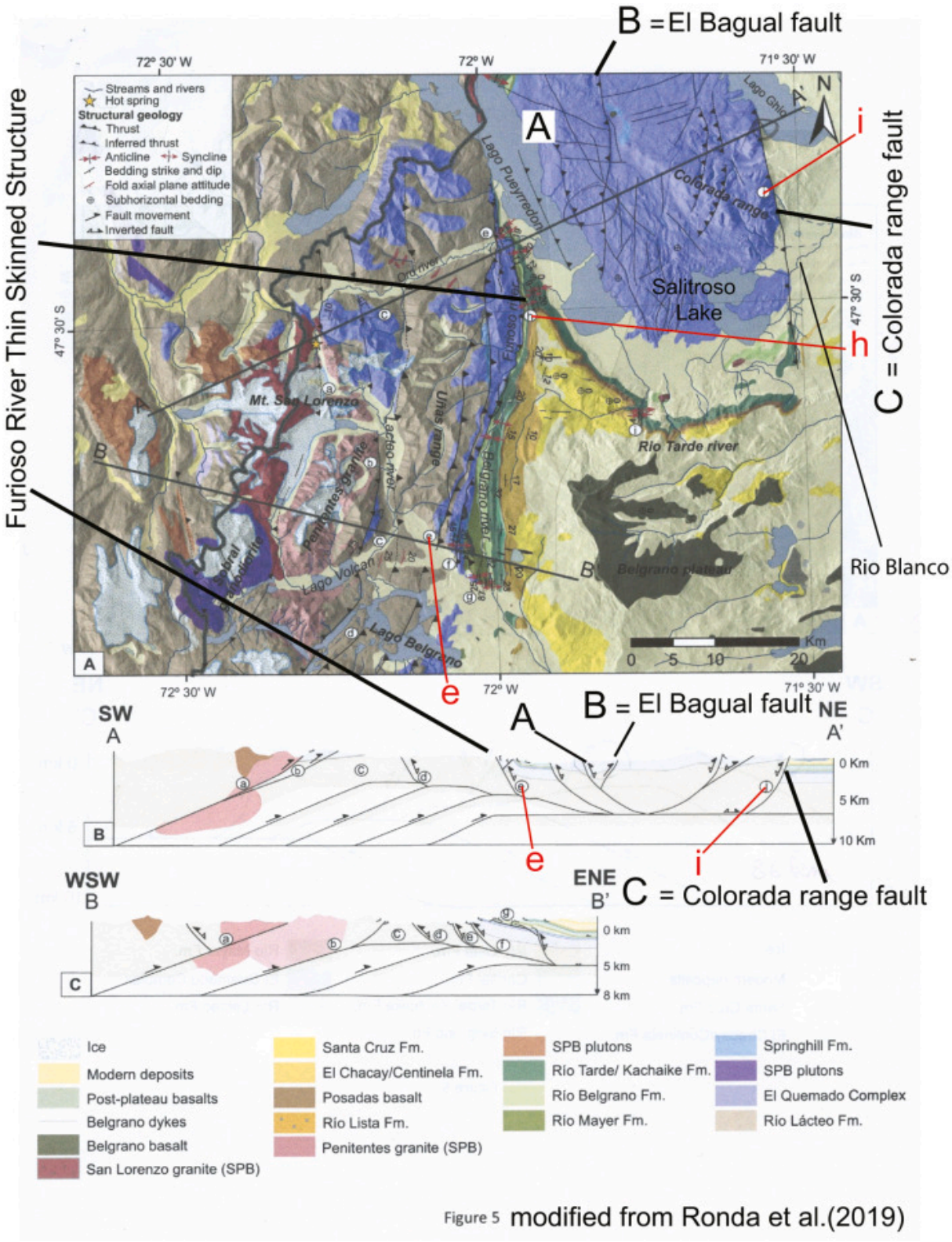

Figure S5. Modified from Ronda et al. (2019). Map shows the location of the Furioso River Thin-Skinned Structure and the Bagual fault (A and B) proposed by Ronda et al. (2019) to be

tectonic elements of the Miocene Andean Fold and Thrust Belt. Red letters refer to specific points in main text. See text for more details.

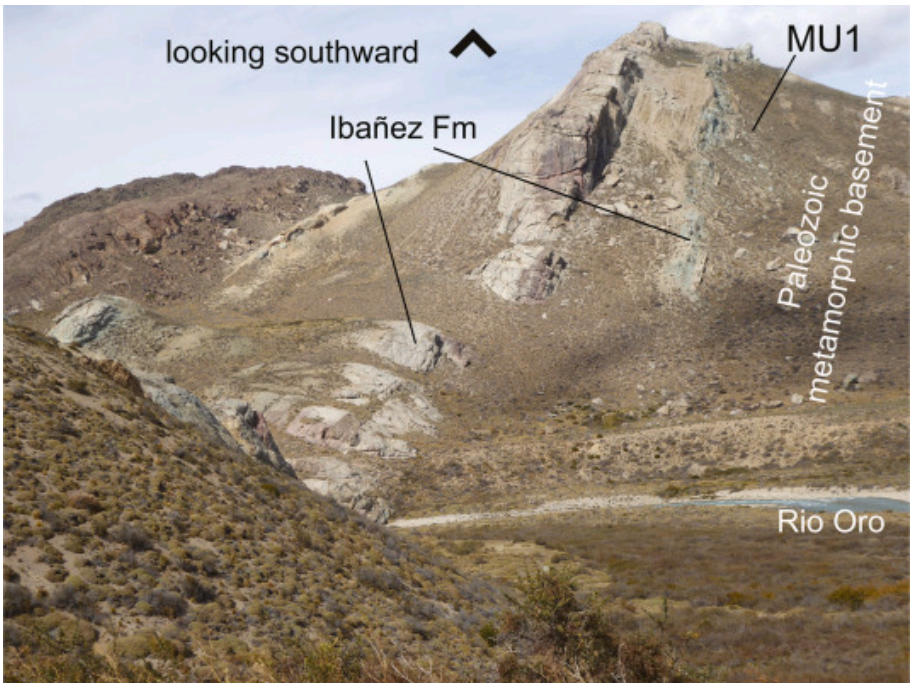

Figure S6. Main Unconformity 1 (MU1). Volcanic beds of the Ibañez Fm is unconformably overlying the Paleozoic metamorphic basement. The Ibañez Fm is at its own correct place. This is in disagreement with the Ronda et al. (2019) interpretation. At this site (black star, Fig. 5), Ronda et al. (2019) have proposed a major fault emerging along the limit between the Paleozoic metamorphic basement and its volcano-sedimentary cover. This limit is the western boundary of the so-called "Rio Furioso thin-skinned structure" proposed by Ronda et al. (2019).

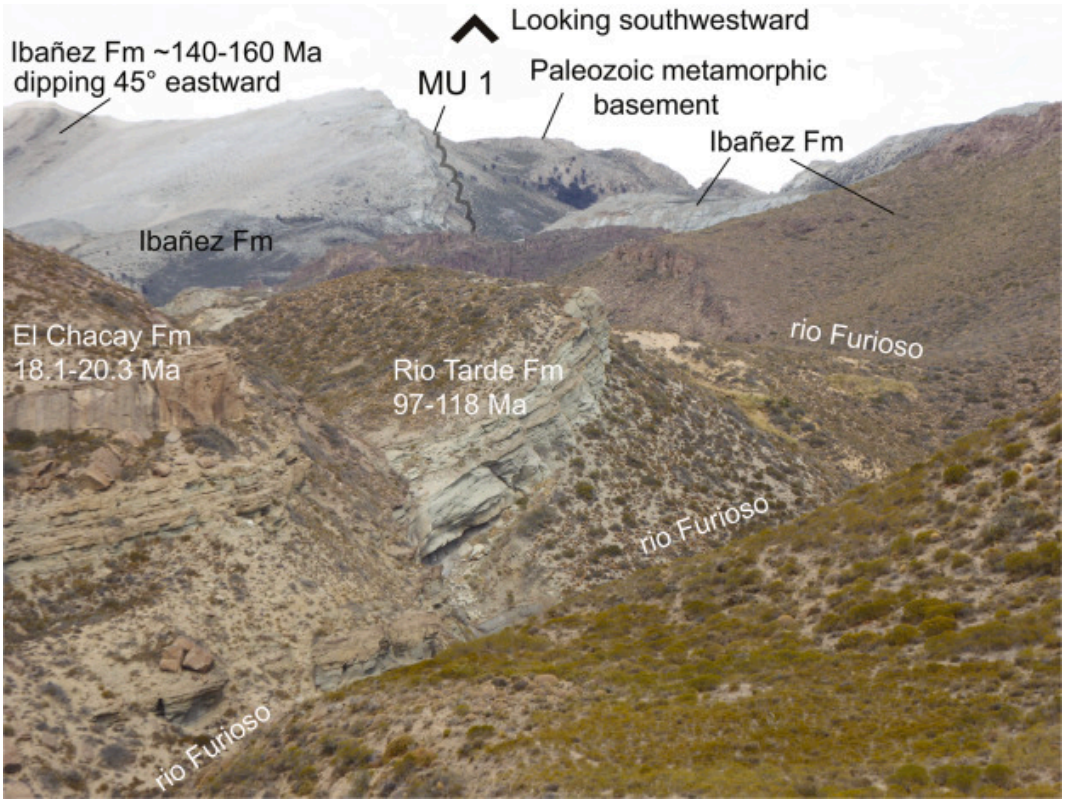

Figure S7. The so-called "Rio Furioso Thin-Skinned Structure" (Ronda et al., 2019), looking southwestward from the Rio Furioso fan delta (location Fig. 7). The Ibanez Fm dipping 45-50° to the East is unconformably overlying the Paleozoic metamorphic basement (this unconformity is in the southern prolongation of that shown at the Fig. S6). In turn, the Ibañez Fm is dipping eastward beneath the Rio Tarde Fm. At this site, no evidence exists for the Rio Tarde Fm (or any other Fm) being underthrusted beneath the Ibañez Fm.

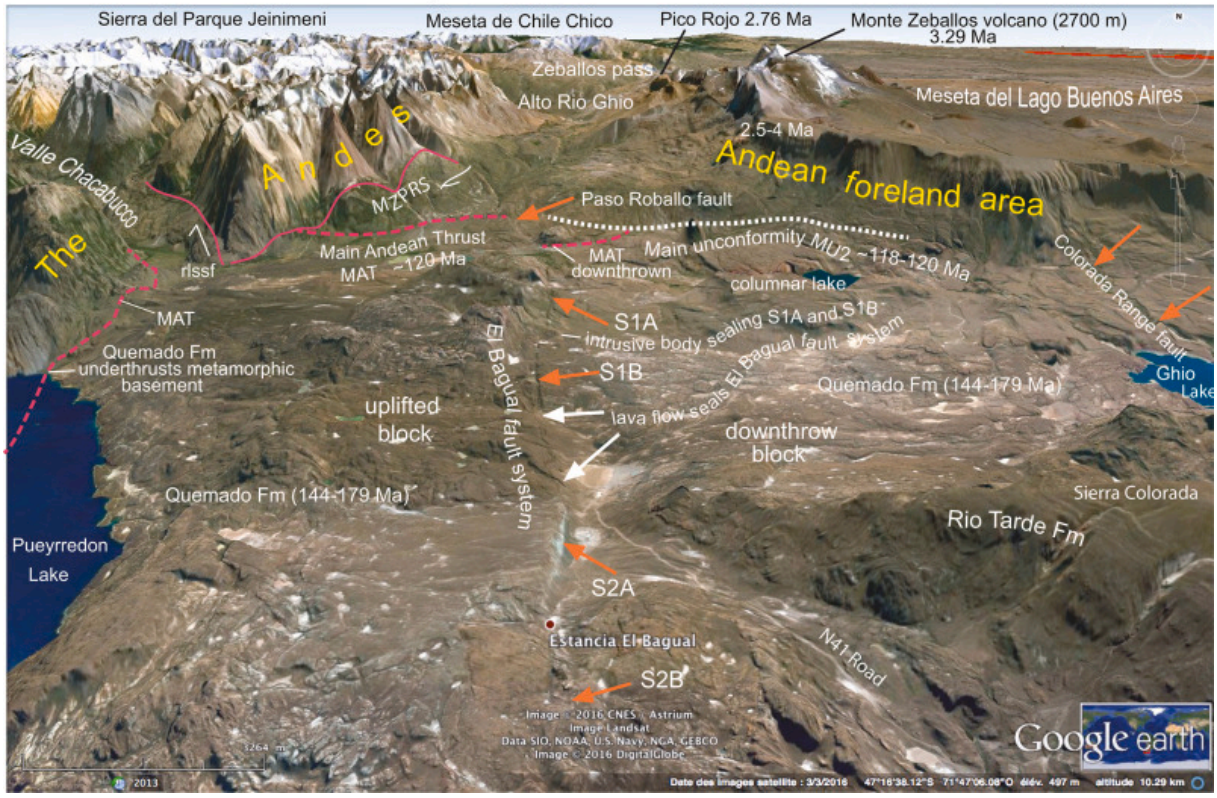

Figure S8. View (looking to the north) of the region south of the Zeballos pass showing the El Bagual fault system exhibiting two segments, S1 and S2. The segment S1 shows two sub-segments, S1A and S1B. Evidence suggests that no major displacement has occurred along this fault system after the Upper Jurassic-Lower Cretaceous (see Fig. S9, S10, and S13).

North of the El Bagual fault system is the Zeballos pass roughly located along the morphotectonic frontline of the Andes. To the east is the Foreland area including the Meseta del Lago Buenos Aires (volcanic flows) with ages younger than ~14 Ma. The Mt Zeballos (2700 m, highest point of the MZR) volcanic complex with ages ranging from 1.7 to 4 Ma is bordering the western limit of the Foreland area. rlssf—right lateral strike slip fault (Valle Chacabuco fault) ; MZPRS—Marques-Zeballos Pass Ramp System.

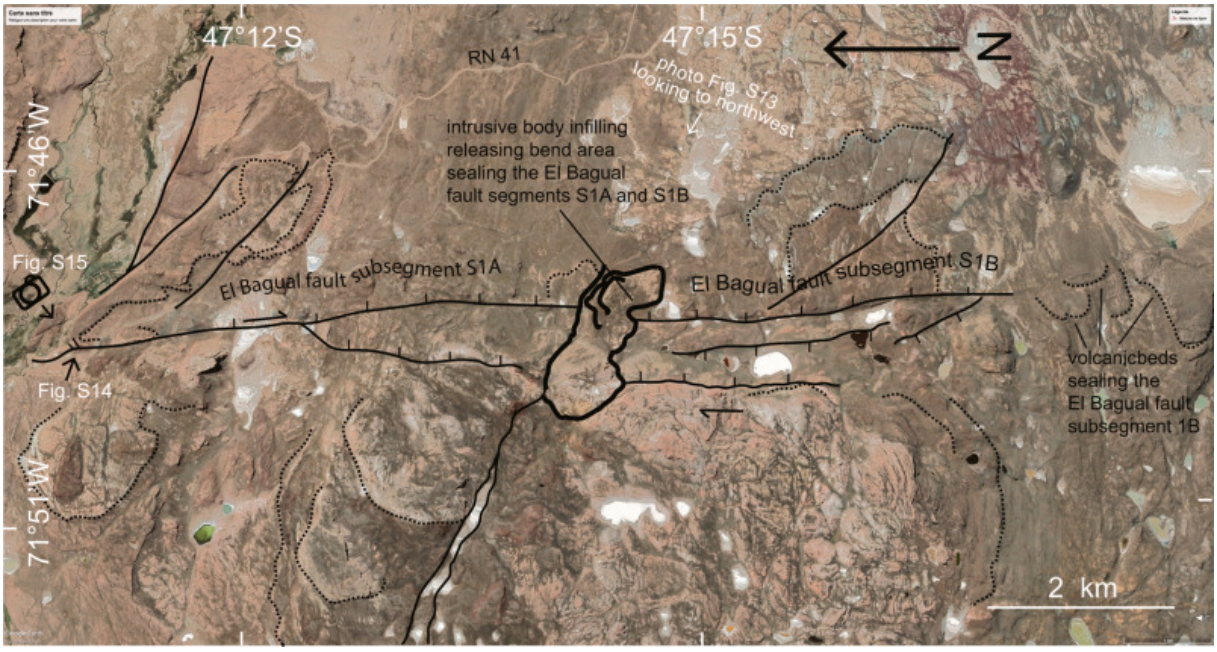

Figure S9. The right-lateral transtensional segment S1 of the El Bagual fault system exhibits two sub-segments S1A and S1B. An intrusive body with an age similar to the Quemado Fm seals these two sub-segments. This intrusive body is interpreted as a volcanic infill of a releasing bend along the right-lateral fault. At the Southern tip of the subsegment S1B thick lava flows dipping gently to the E cover the fault, sealing it. No major movement has occurred along the El Bagual fault system segment S1 after the Upper Jurassic-Lower Cretaceous. Dotted line—bedding traces of major lava flows, note that bedding is flat lying; black line—fault, barb towards the downthrow block; thick black line—intrusive contact. Location of Figs. S10, S11, and S12 is shown.

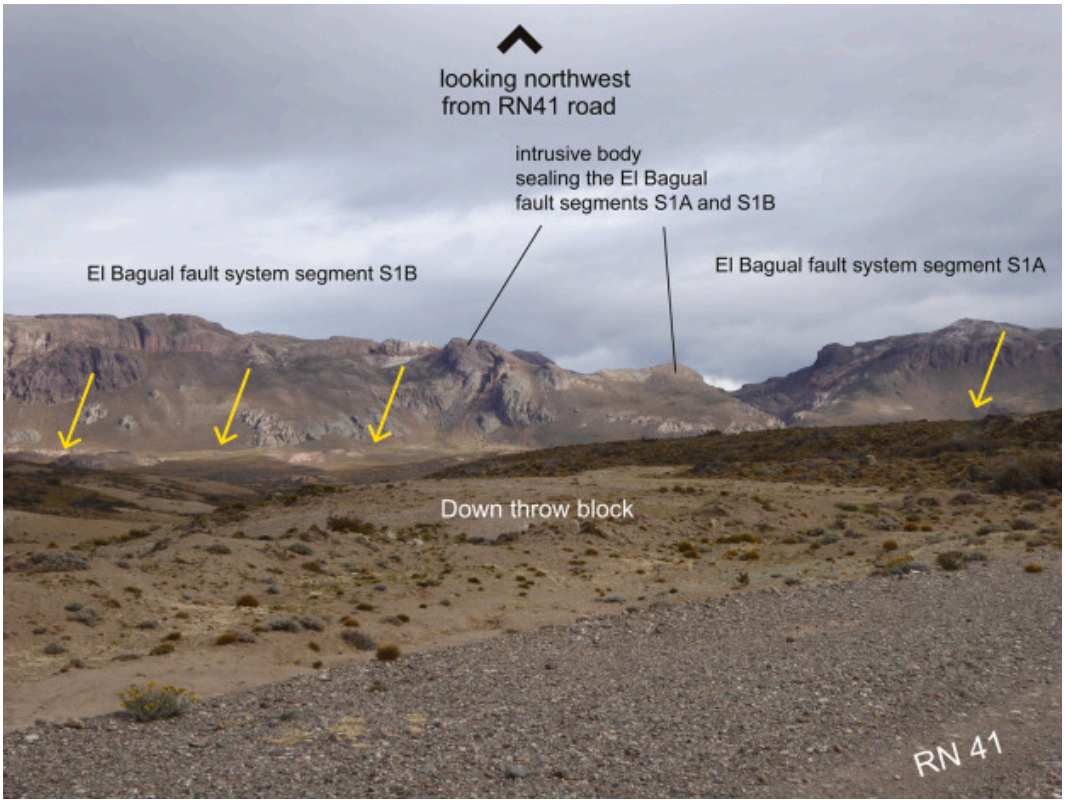

Figure S10. El Bagual fault system segment S1. In the center of the photo, intrusive body sealing the sub-segments S1A and S1B documenting no major movement occurring along the El Bagual fault segment S1 after the Upper Jurassic. Yellow arrows show the fault traces. Fig. S9 shows the shot site location.

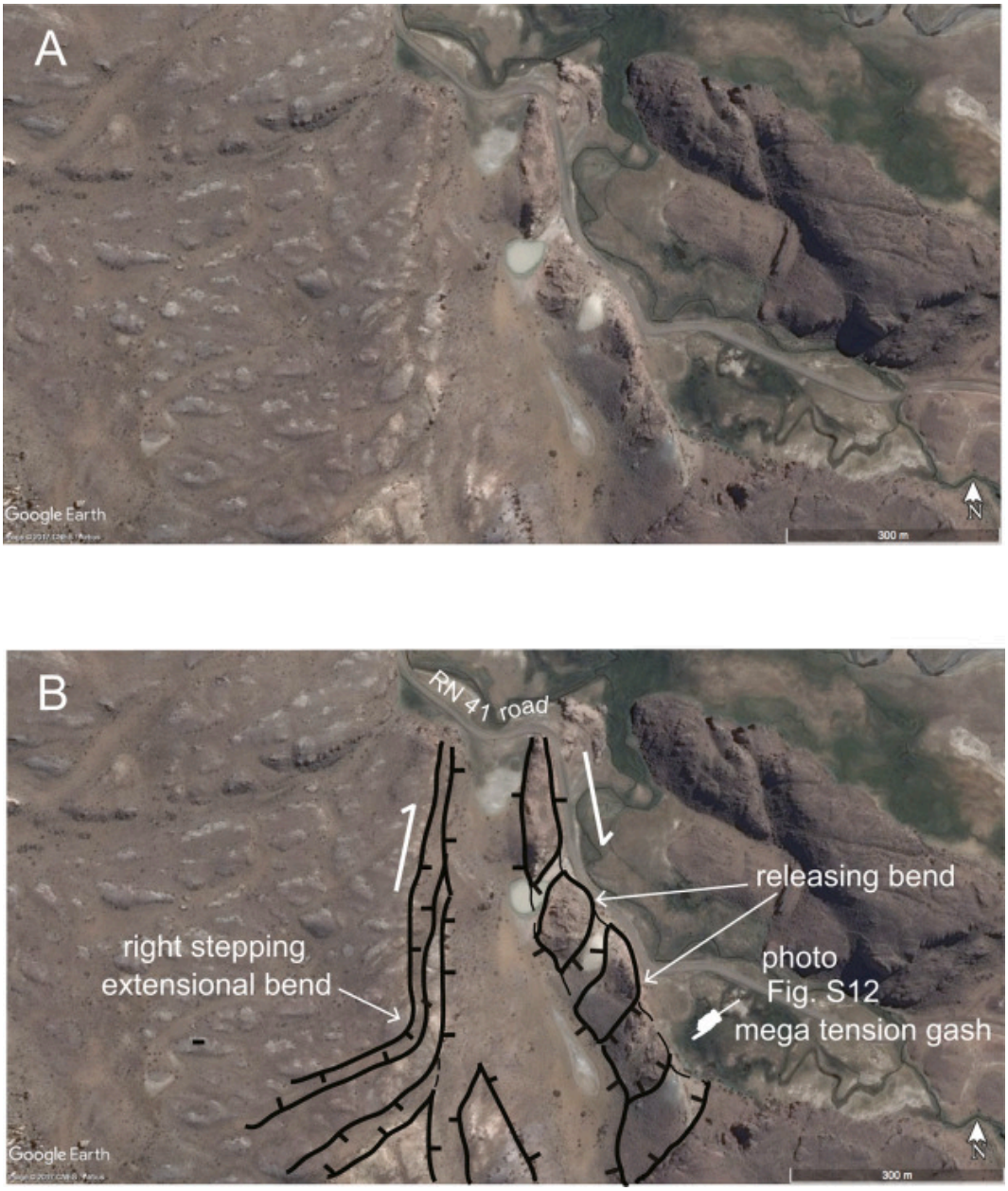

Figure S11. A: Google Earth image showing the northern tip of the El Bagual fault system (sub-segment S1A) exhibiting a N-S trending grabens. B: Line drawing of the major structures associated with the fault systems bounding the graben. Evidence documents transtensional right-lateral displacement. It includes right-stepping extensional bend and releasing bend structures bounding the graben to the W and to the E, respectively. The area shown underlain entirely by the Quemado Fm. The location of the mega tension gash (photo Fig. S12) is shown. Location Fig. S9.

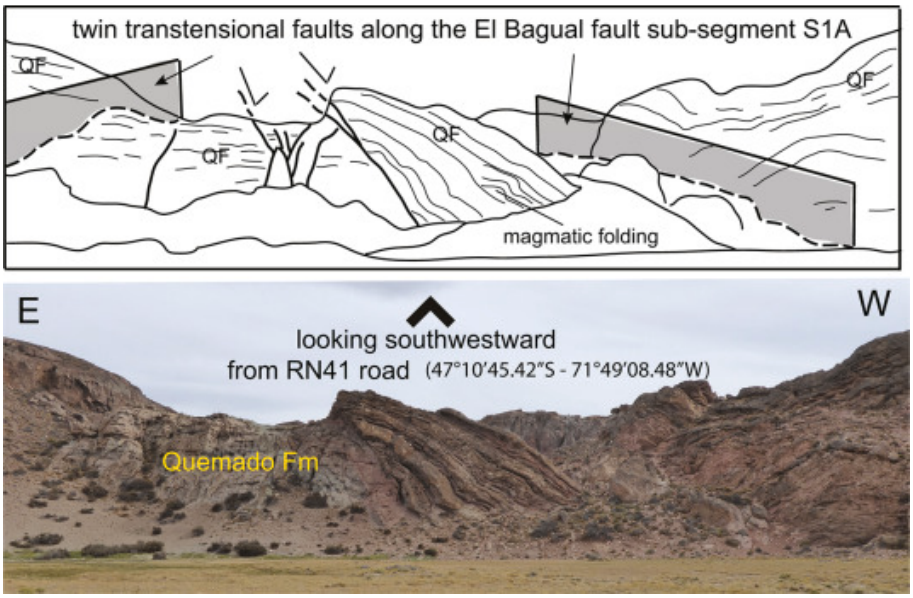

Figure S12. Mega tension gash trending N 45°-50° E associated with the right lateral component related to the tensional displacement along the main graben shown at Fig. S11 (northern tip of the El Bagual fault system, sub-segment 1A). QF–Quemado Fm. Location at Fig. S9 and S11.

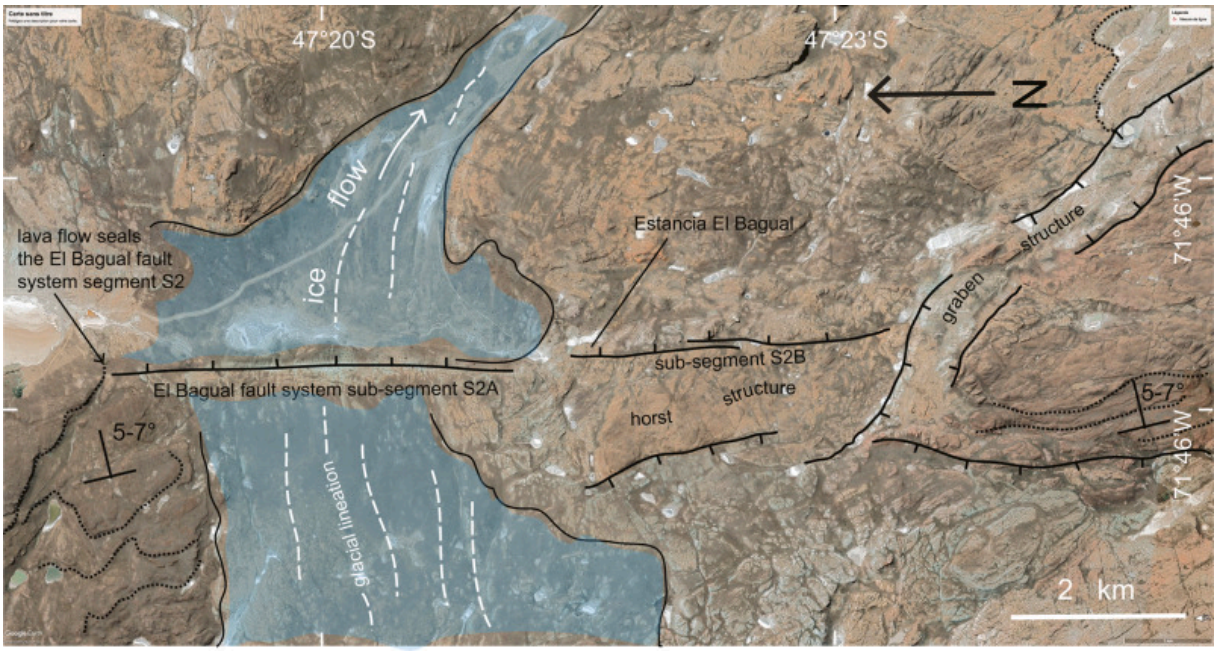

Figure S13. The El Bagual fault system segment S2 is a sub-vertical normal fault dipping 70-80° towards the E. At the northern tip of segment S2 thick lava flows (Quemado Fm) dipping

gently to the E are covering the fault. These lava flows seal the segment S2. No major movement has occurred along the El Bagual fault system segment S2 after the Upper Jurassic-Lower Cretaceous. Note that the glacial lineation follows the topography inherited from the Mesozoic tectonic deformation. Dotted line—bedding traces of major lava flows, note that bedding is flat lying; black line—fault, barb towards the downthrow block; blue color—glacial deposits and lineation.

Figure S14. High angle dip of volcanic breccias from the Ibañez Fm recording the transtensional displacement along the Paso Roballos fault. Location on Fig. 9 and S15.

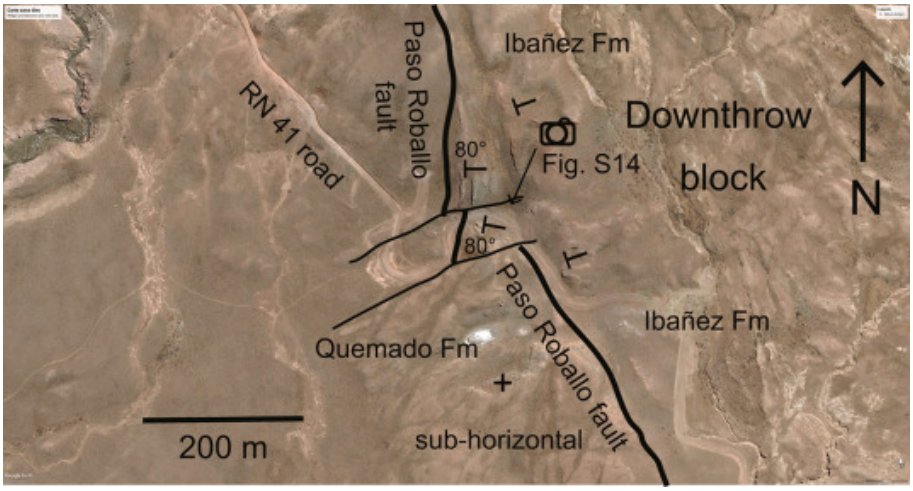

Figure S15. Detail map of the Paso Roballos fault showing the location of Fig. S14. Location on Fig. 9.

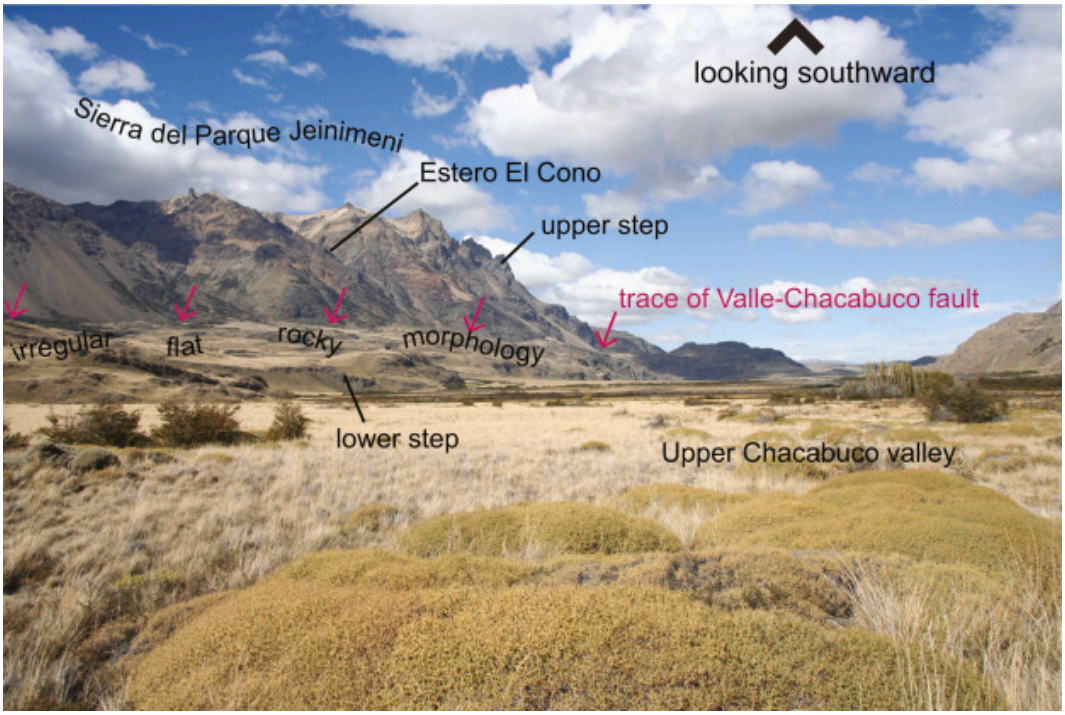

Figure S16. The Upper Chacabuco valley (Chile). It shows the morphological signature of the right-lateral strike-slip displacement of the Valle Chacabuco fault. Photo looking toward Argentina.

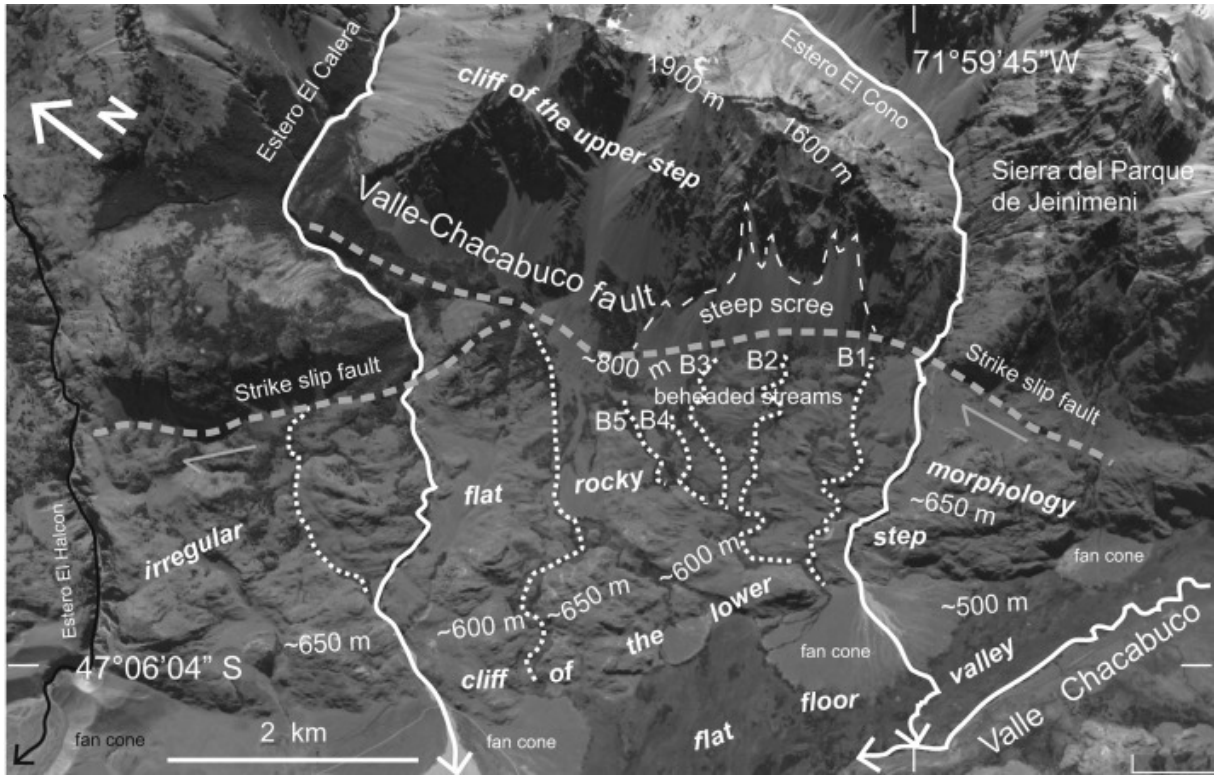

Figure S17. Valle-Chacabuco strike-slip fault at the upper Valle Chacabuco area (Chile). Beheaded streams (B1 to B5) document a right lateral displacement. The western block has moved several hundreds of meters to the NW during the past ~400 ka. See File S4 for more details.

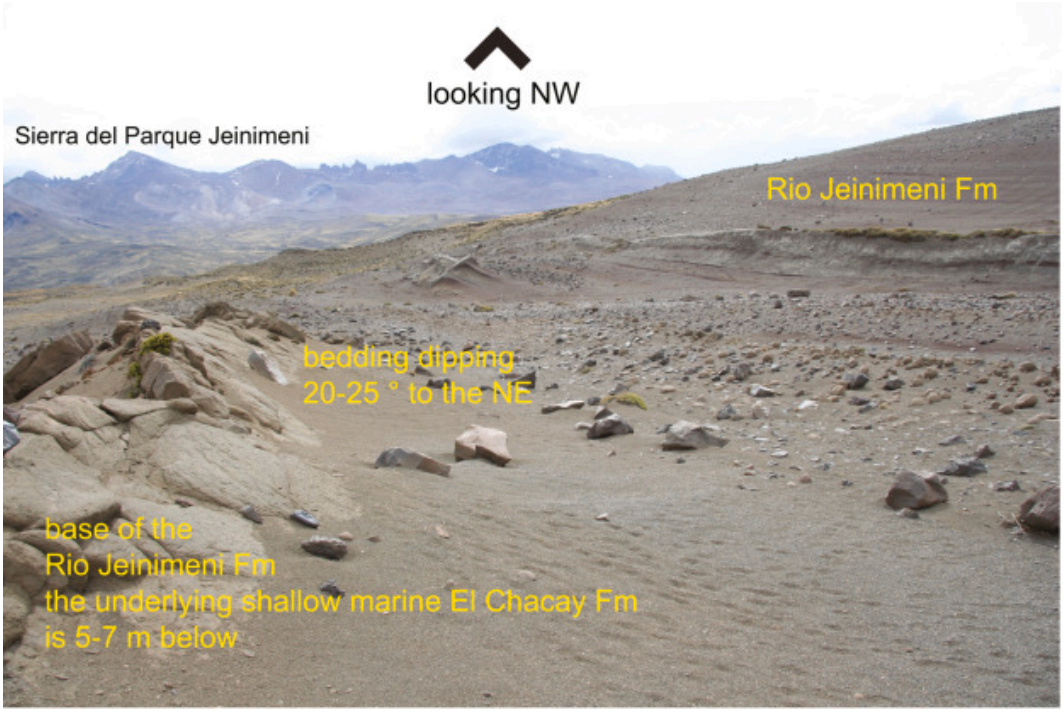

Figure S18. The Rio Jeinimeni Fm along the eastern side of the Alto Rio Ghio valley. This formation and the underlying shallow marine El Chacay Fm extend northwestward down to the valley floor, then extend across the other side of the valley until the morphologic frontline of the Andes (Sierra del Parque Jeinimeni). Note the 20-25° local dip.

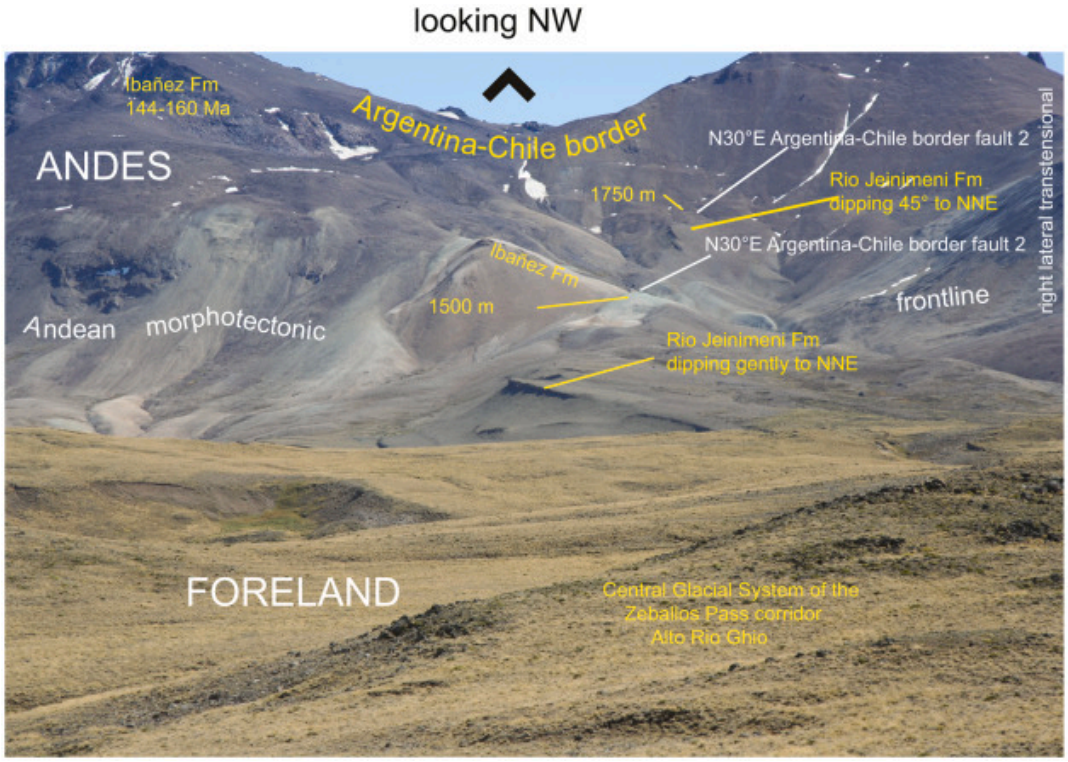

Figure S19. At midway between the lower Zeballos Pass corridor and the pass area, the lower Miocene of the Rio Jeinimeni Fm (younger than 18.1 Ma) exhibits sandstone beds dipping gently to the NNE. These beds extend continuously (with no interruption) from the Rio Ghio valley until the toe of the Sierra del Parque Jeinimeni –from point Y (1200 m) to point X (1500 m) on Fig. 11–. Trending direction of these beds (N60°W) is perpendicular to the Andean morphotectonic frontline. The Ibañez Fm is cropping out along the Argentina-Chile border. A prolongation of the lower Miocene beds –West of point X, Fig. 11– exists. Dip of these beds (1750 m in elevation) is 45-50° towards the NNE. These Miocene beds resting above the Ibañez Fm are the trace of a relay ramp between two overlapping transtensional faults: the Argentina-Chile border fault 1 and the Argentina-Chile fault 2. These two faults parallel to the Estancia Lago Bertrand fault are trending N30°E.

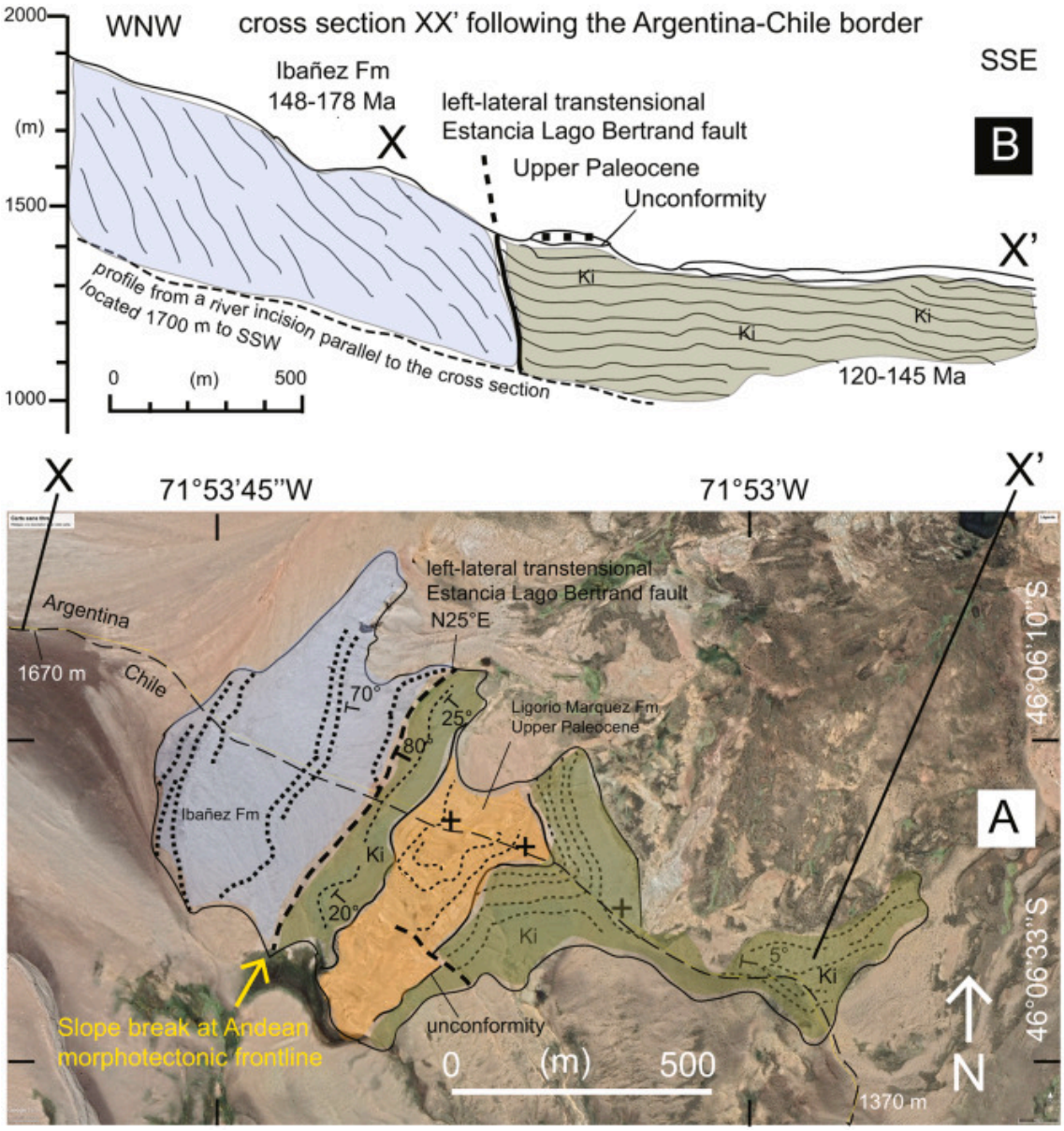

Figure S20. A–Andean morphotectonic frontline along the left-lateral transtensional Estancia Lago Bertrand fault. B–Cross section along the Argentina-Chile border. Location at Fig. 9.

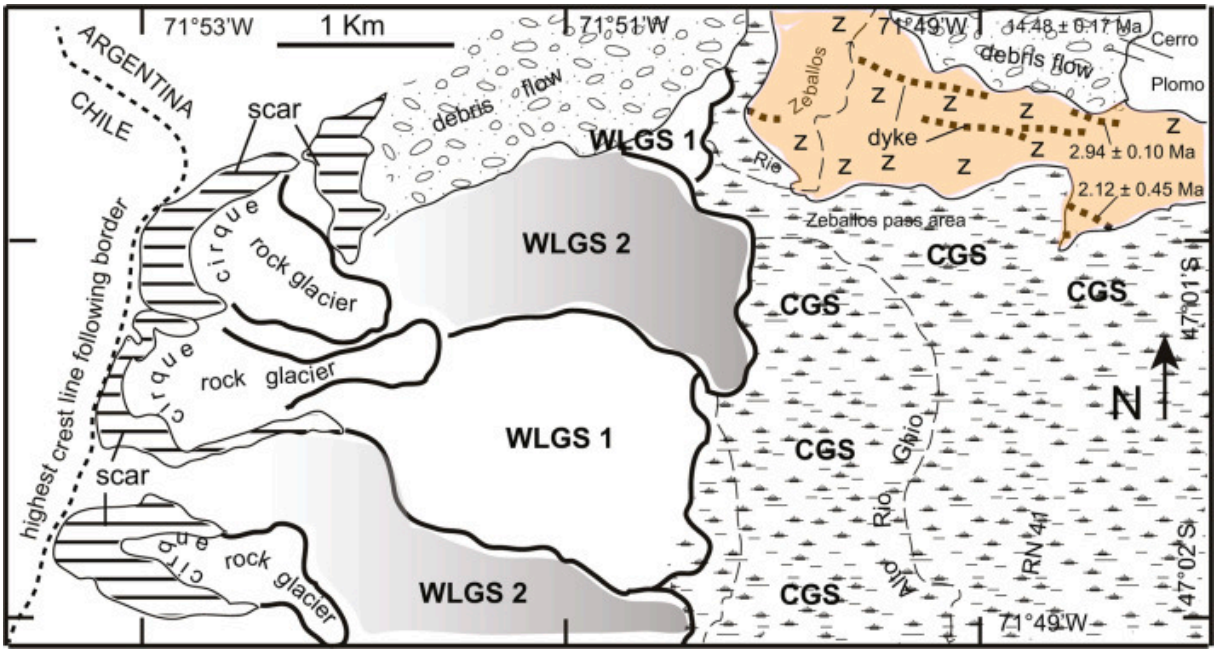

Figure S21. Geological map of the Zeballos pass area. Glacial deposits (till, moraine, stagnant ice sheet, outwash plain) overlying the basement rock are heavily blanketing this area. Cerro Plomo volcanic flow (14.48 ± 0.17 Ma) is overlying the fluvial sediment of the Zeballos Pass Fm. Glacial sediment of the CGS unconformably overlies a swarm of mafic dykes intruding into the Zeballos Pass Fm. One of these dykes is 2.12 ± 0.45 Ma constraining a maximum possible age for the CGS. West of the Zeballos Pass is the complex WLGS flowing from cirques located along the crest line following the Argentina-Chile border. Three retreat systems exist including WLGS 1, WLGS 2, and rock glacier from the oldest to the youngest. The WLGS unconformably overlies the CGS. Till and ground moraine that originated from stagnant ice sheet, cover the flat CGS hummocky area. CGS–Central Glacial System; WLGS–West Lateral Glacial System; Z–Zeballos Pass Fm older than ~16 Ma. See File S5 for more details.

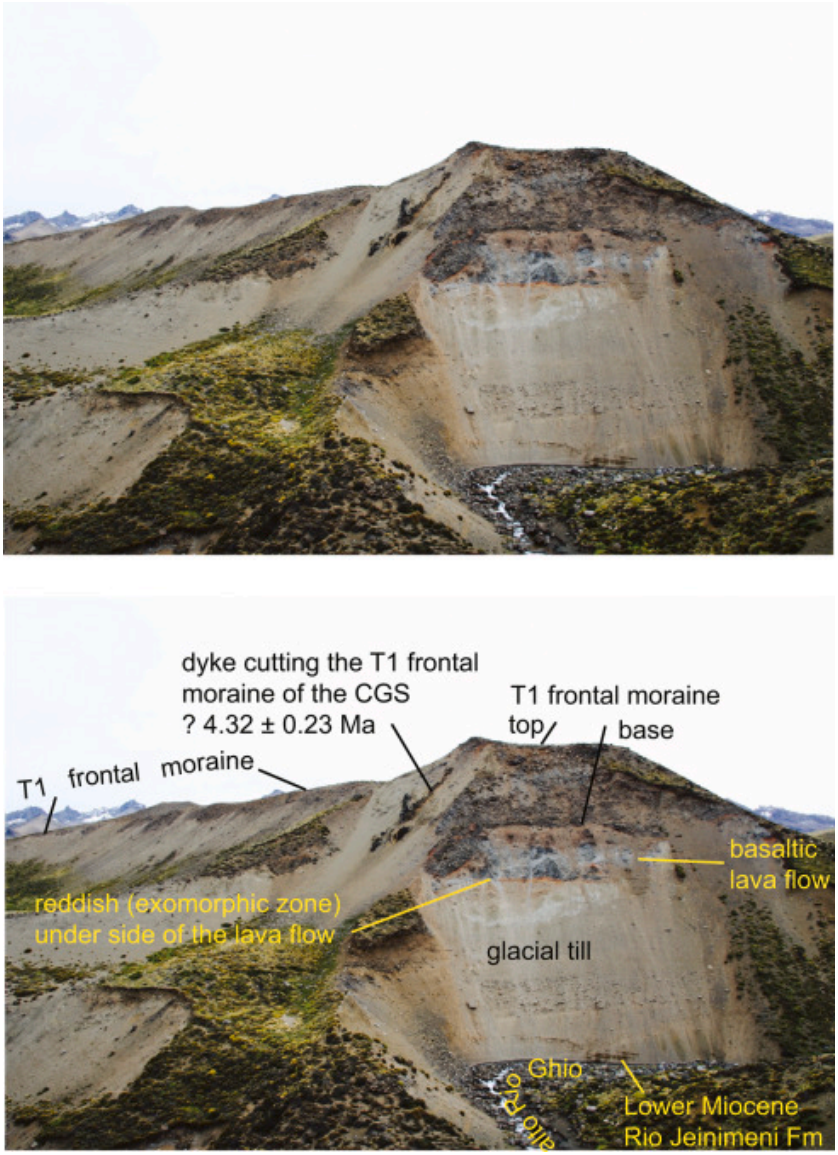

Figure S22. Scar located at point Y Fig. 11. The T1 moraine of the CGS is overlying a basalt lava flow that in turn covers a glacial till. See File S5 for more detail regarding the age of the dyke cutting the moraine. CGS–Central Glacial System. See File S5 for more details.

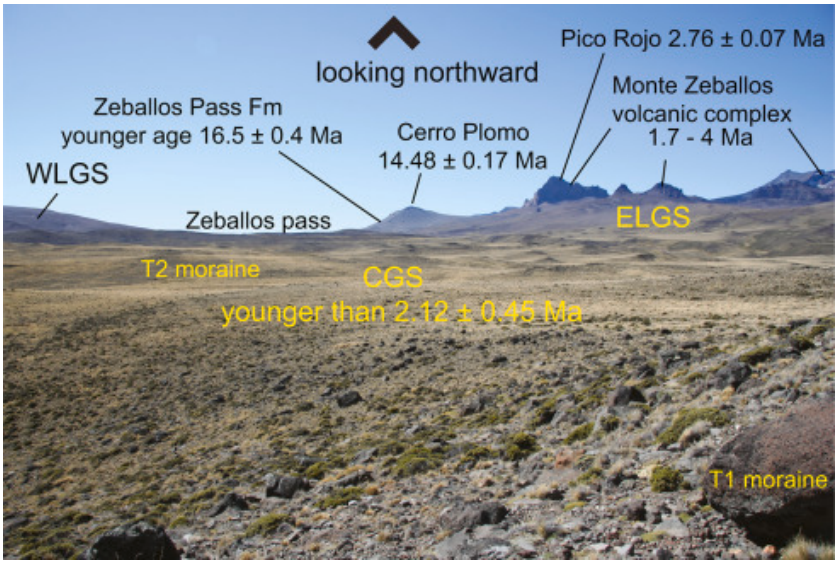

Figure S23. The flat hummocky glacial plain is the signature of the CGS covering the upper Ghio valley floor from the Zeballos pass to the southern front of the T1 moraine (Fig. 12). The ice flow was from NNE to S following the depression till the scar shown at Fig. S25. CGS–Central Glacial System; ELGS–East Lateral Glacial System; WLGS–West Lateral Glacial System. See also Fig. 13.

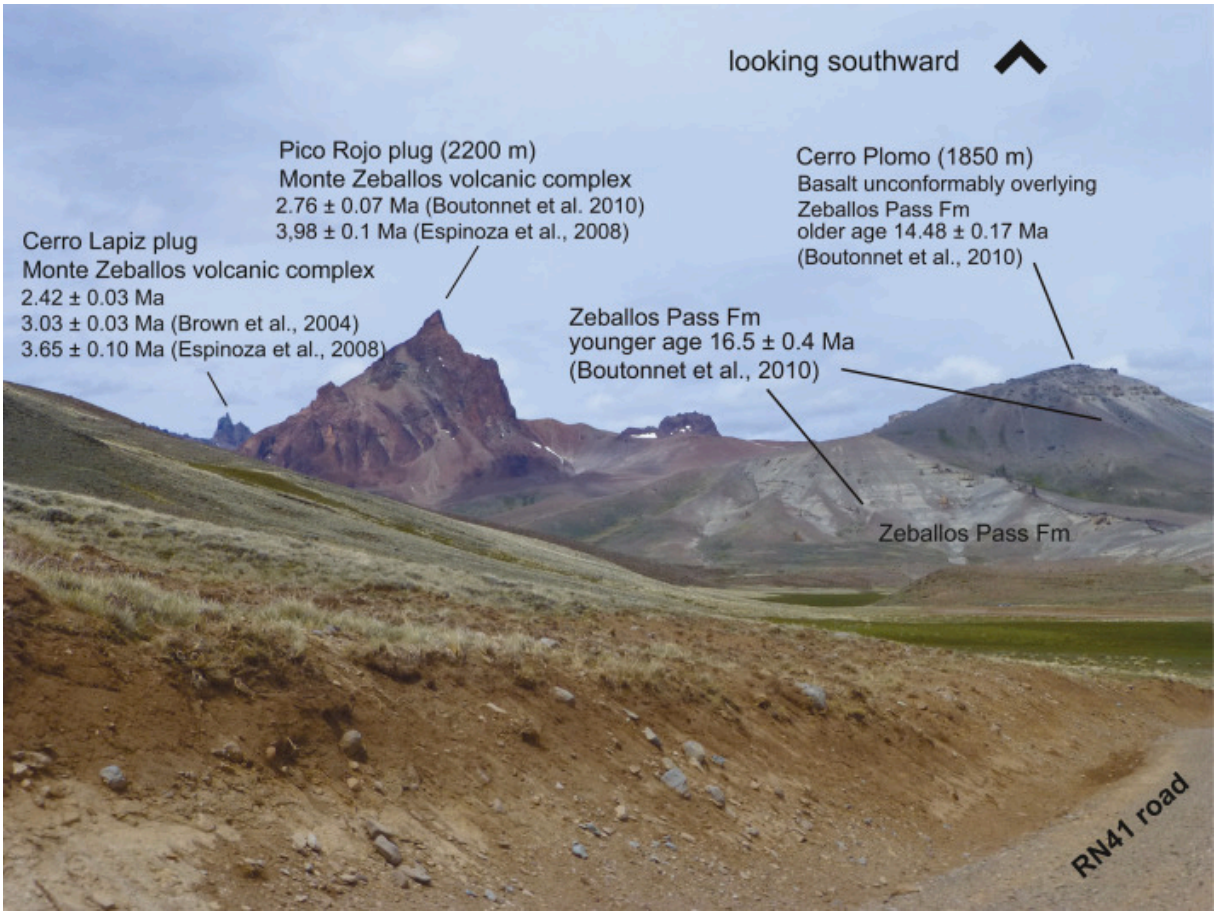

Figure S24. The east side of the Zeballos Pass corridor (photo from the RN41 at few km north of the pass). On the right is the Cerro Plomo volcanic flow resting unconformably on top the fluvial sediment of the lower Miocene Zeballos Pass Fm. On the left, a set of plugs intrudes the lower Miocene sediment. These plugs are volcanic features associated with the Mt Zeballos volcanic complex (1.7-4 Ma). The Mt Zeballos (2700 m) is behind the crest line.

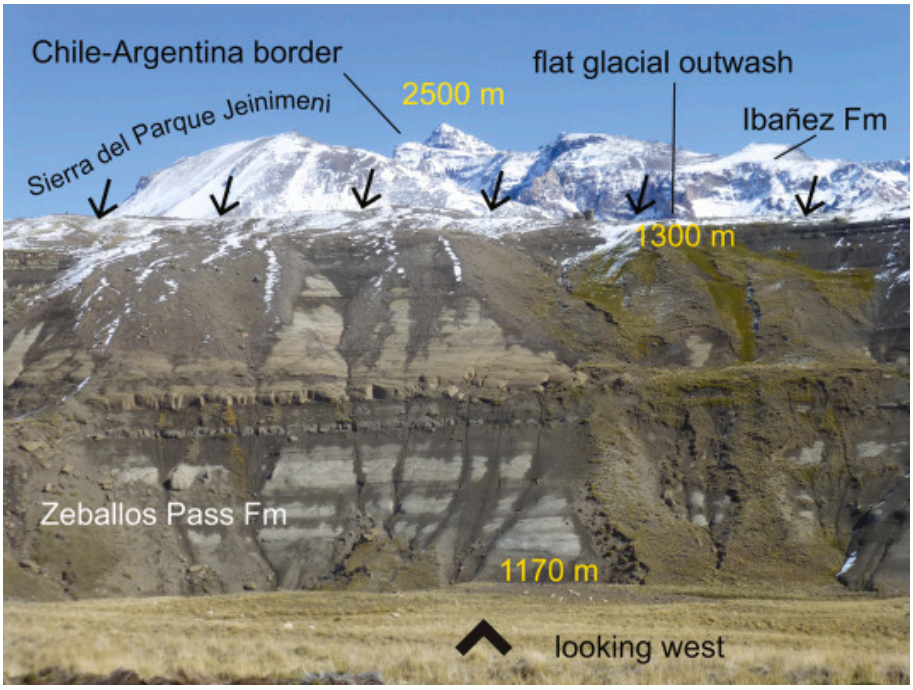

Figure S25. West side of the Zeballos Pass corridor, photo from RN41 (46°57'18"S-71°50'30"W at 6.5 km N of the pass). Zeballos River at the forefront. Background shows the Ibañez Fm. Between the riverbed and the toe of the Sierra del Parque Jeinimeni (Ibañez Fm) is the sub-horizontal Zeballos Fm of Lower Miocene age (younger age 16.5 ± 0.4 Ma). Total thickness of the outcropping section is ~130 m or so. At this site the lower Miocene is inferred sealing the tectonic front of the Andes. Arrows show the toe of the Andean morphotectonic fronline.

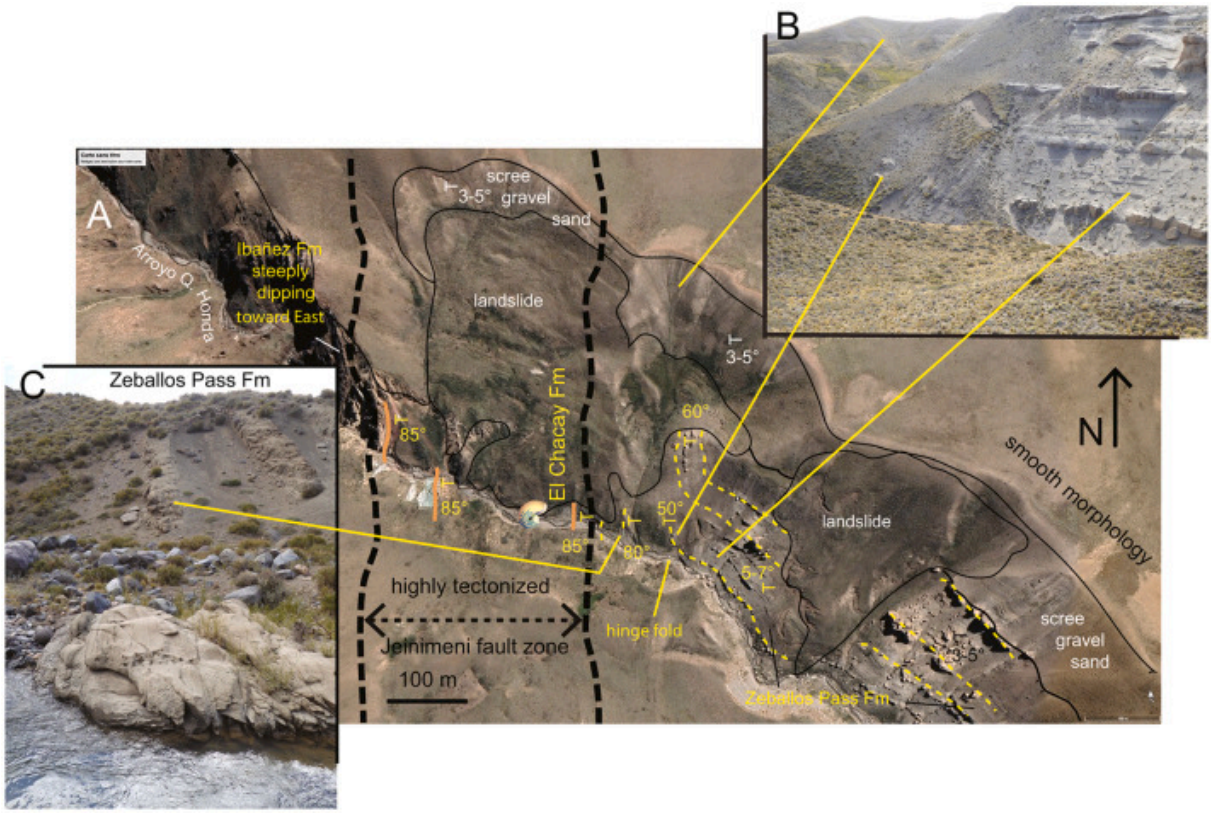

Figure S26. A- Detailled structural sketch of the Meseta de Chile Chico frontal area along the Arroyo Hondo river. To the west is the Ibañez Fm exposed along the eastern edge of the Meseta de Chile Chico. To the east is the Zeballos Pass Fm. In the center extends the highly tectonized Jeinimeni fault zone. An 80-85 m thick accumulation of scree, gravel and sand dipping gently to the east unconformably overlies the Jeinimeni fault zone (B Fig. 18). This formation exhibits a smooth morphology. B- Left bank of the Arroyo Hondo River shows the Foreland Zeballos Pass Fm dipping gently to the East. Close to the Jeinimeni fault zone the Zeballos Pass Fm exhibits beds dipping 60° towards the east. These beds connect to the flat lying beds through an open fold, which the hinge is well exposed close to the riverbed. C- Very close to the Jeinimeni fault zone detrital sequences of the Zeballos Pass Fm are dipping 80° to the east. Yellow dash line–Zeballos Pass Fm bedding; black dash line–Jeinimeni fault zone; orange color thick line–major tectonic sheet. See text for more details.

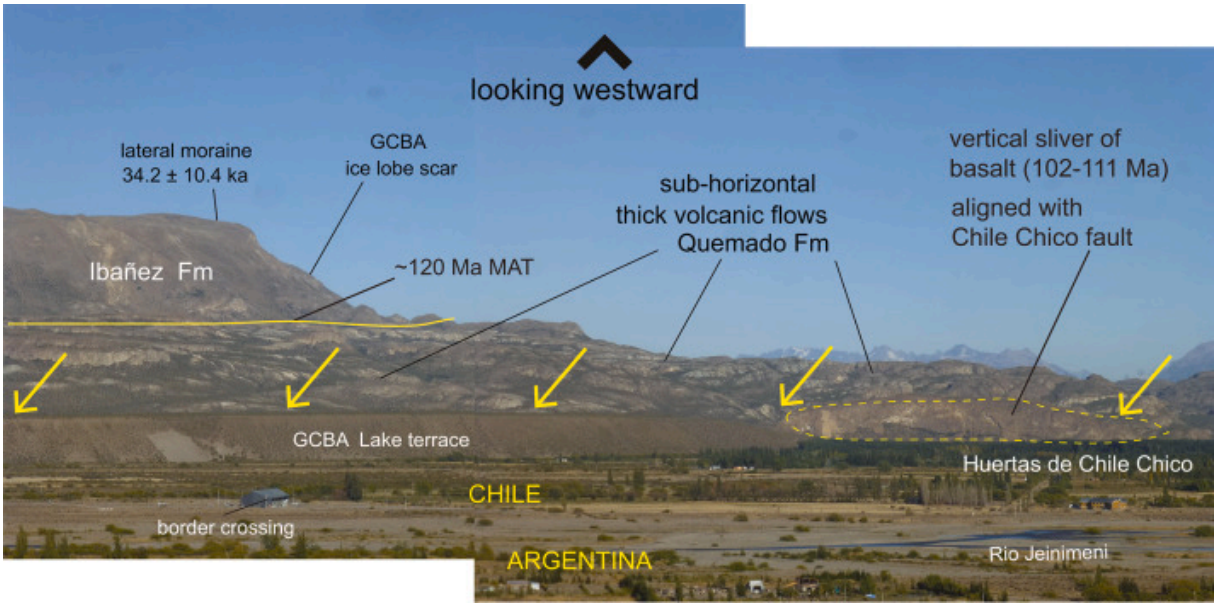

Figure S27. Photo from the Mirador de Los Antiguos (Argentina) looking towards the Andes. (Chile). Main morphological scarp is that of the GCBA glacial lobe. In the background is the NPI. The foreground shows a major GCBA terrace that obscures the Andean morphotectonic frontline between Chile Chico town and the Meseta de Chile Chico (MCC). The MCC frontal cliff follows a N-S trending vertical fault, the right lateral transtensional Chile Chico fault (yellow arrows). The ~120 Ma MAT is the main thrust fault bounding the Ibañez Fm (Meseta de Chile Chico, Upper Unit) and the Quemado Fm (Lower Unit).

Figure S28. Left bank of the Arroyo Marques river (46°36'04.56"S-71°43'21.87"W). A-The El Chacay Fm (18.1-20.3 Ma) dips 45-50° to the SE. At this site located along the morphological front zone of the Andes (left of photograph) the lower Miocene unconformably overlies the Ibañez Fm (Upper Unit) and the Quemado Fm (Lower Unit). The lower Miocene seals the 120 Ma MAT. B-Tectonic stretching features between beds suggest normal sliding toward N100-120°E (i.e. towards the Foreland area, right of photograph). Location on Fig. 19.

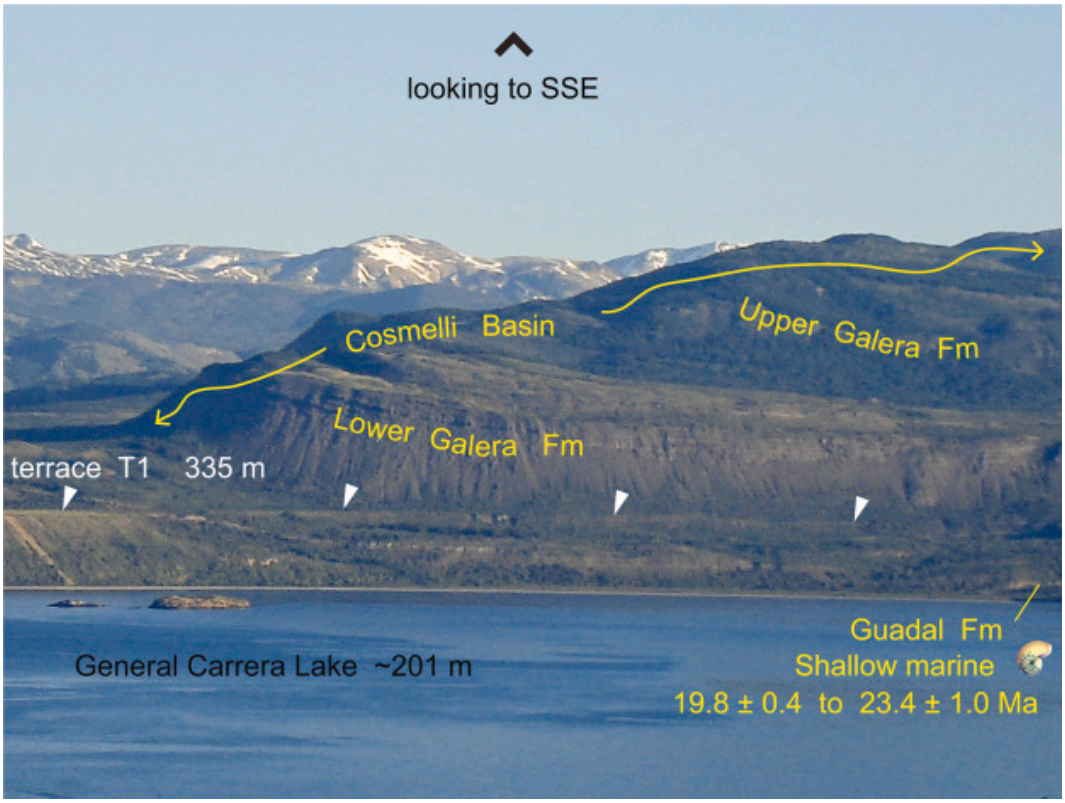

Figure S29. Northern Cosmelli basin. The shallow marine Guadal Fm of Burdigalian age is at 201 m elevation. Lower and Upper Galera Fm are fluvial deposits overlying the Guadal Fm. Terraces of the General Carrera Lake from Bourgois et al. (2016b). Background with snow–Sierra del Parque Jeinimeni.

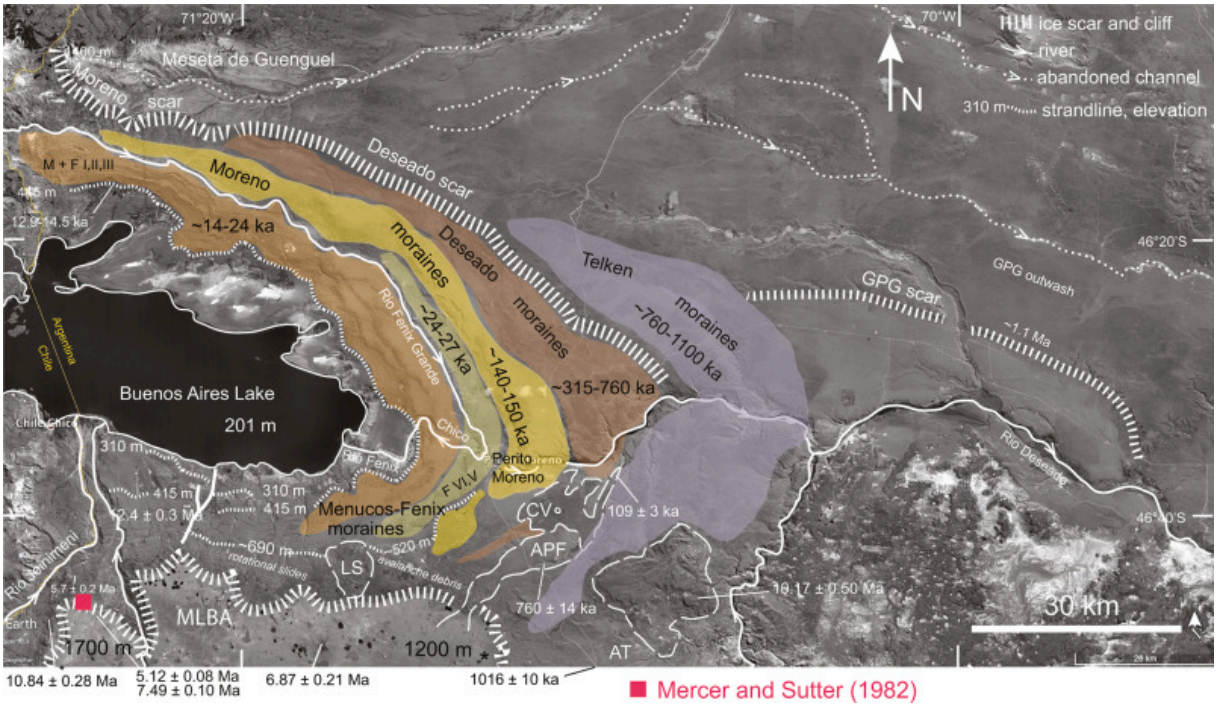

Figure S30. End Moraines at the Buenos Aires Lake (from Ackert et al., 2003; Kaplan et al., 2004; Singer et al., 2004; Kaplan et al., 2005; Douglass et al., 2006; Bourgois et al., 2016b). Red square shows location of the site studied by Mercer and Sutter (1982). Tills at that site are at 1500 m in elevation. From west to east end moraines include: M+FI, II, III–Menucos and Fenix I-III moraines (~14-24 ka); F V,VI–Fenix V and VI moraines (24-27 ka); the Moreno moraines (~140-150 ka), the Deseado moraines (315-760 ka), the Telken moraines (~760-1100 ka). Note that the Rio Fenix Grande branches the Rio Fenix Chico at Perito Moreno (392 m, elevation at the divide between Pacific and Atlantic) to feed the GCBA Lake. At Present, no connection exists between the Rio Fenix Grande and the Rio Deseado. A major scar located east of the Telken moraines is ascribed to the Great Patagonia Glaciation. APF–Arroyo Page basalt flow; AT–Arroyo Telken; CV Cerro Volcan; GPG–Great Patagonia Glaciation at 1.1 Ma; LS–landslide; MLBA–Meseta del Lago Buenos Aires.

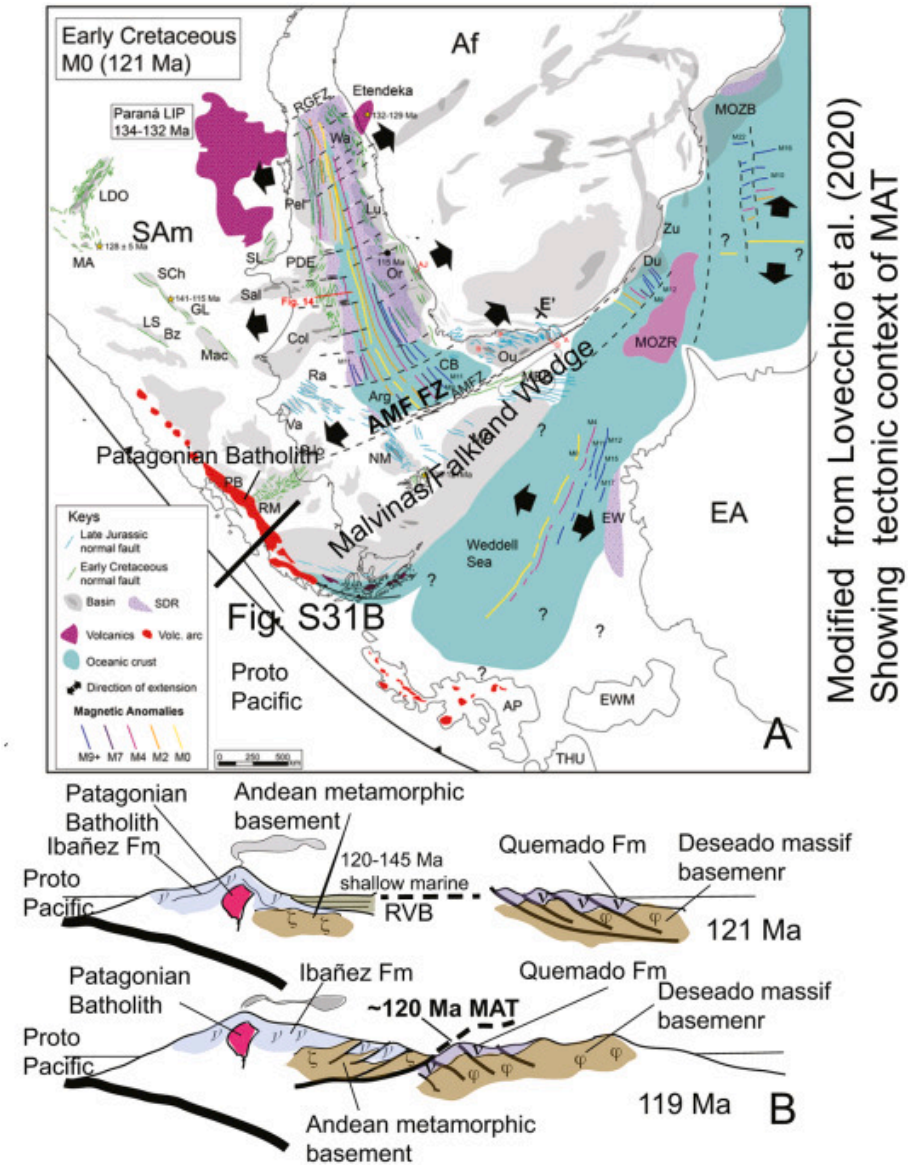

Figure S31. (A) Paleo-tectonic reconstruction of SW Gondwana land in the Early Cretaceous at 121 Ma (modified from Lovecchio et al., 2020). The Aguilhas-Malvinas (Falkland) FZ (AMF FZ) bounds the Malvinas/Falkland wedge showing tectonic context of the MAT to the N. To the west, the continental wedge the Patagonian batholith and associated Ibañez volcanic flows document Proto Pacific subduction. Thick black line shows the locations of Fig. 31B. (B) At 121 Ma the Rocas Verdes basin (RVB) has accumulated shallow marine sediment along the Ibañez back-arc area. To the East the Quemado Fm is the trace of the volcanic province related to the Atlantic rifting during the Middle and Upper Jurassic time. Major crustal shortening has occurred at ~120 Ma. The E-verging Main Andean Thrust (MAT) has

transported the Andean metamorphic basement onto the Quemado Fm volcanics. See main text for more details. Note that many abbreviation, illegible or not, are not mentioned in the legend. These are from the original Figure from Lovecchio and al. (2020), these are not directly related with the present work.

N°	Ref	Loc	Sample	Latitude	Longitude	rock	Age (Ma)	± 2σ
1	a	Avell.	Q387	46°25'19.74"	72°09'15.88"	lava	4.57	0.27
2	b	Nieves	CC-138	46°40'42.42"	72°04'41.59"	gran	3.20	0.40
3	c	MCC	PG 37	46°35'40.02"	71°49'06.02"	neck	4.63	0.13
4	c	MCC	PG 138	id	id	lava	4.46	0.22
5	c	MCC	FE01-11	46°44'27.60"	71°50'14.68"	lava	4.50	0.30
6	c	MCC	FE01-16	46°40'21.04"	71°48'15.44"	lava	4.60	0.20
7	c	MCC	FE01-36	46°37'57.14"	71°52'14.27"	lava	4.40	0.80
8	Unp	MCC	CC-270	46°38'15.40"	71°46'49.37"	lava	5.30	0.40
9	c	MCC	CC317-2	UBS		lava	7.60	0.40
10	c	MCC	CC-313	UBS		lava	8.20	0.50
11	c	MCC	FE01-23	UBS		neck	7.90	0.40
12	c	MCC	CC317-3	UBS		lava	9.80	0.10
13	c	MCC	FE01-29	UBS		lava	9.30	0.90
14	c	MCC	FE01-29	UBS		lava	13.10	1.90
15	c	MCC	FE01-39B		LBS	neck	40.70	1.40
16	c	MCC	PG-31		LBS	lava	42.80	2.00
17	c	MCC	PG-24		LBS	neck	43.50	2.00
18	c	MCC	CC-267		LBS	lava	45.70	1.50
19	c	MCC	CC-47		LBS	lava	46.50	1.70
20	c	MCC	CC-285		LBS	lava	48.60	1.60
21	c	MCC	PG-55		LBS	lava	49.50	2.40
22	c	MCC	CC-180		LBS	lava	53.40	1.80
23	Ba	MCC	P69			lava	52	
24	Ba	MCC	P71			lava	54	
25	Pa	East MCC	IBA6			gran	10	0.40
26	i	Ne Plomo	PA-06-03	47°00'32.40"	71°48'12.49"	dike	2.94	0.10
27	i	Plomo	PA-06-10	47°00'24.12"	71°47'55.25"	lava	14.48	0.17
28	i	Plomo	PA-06-11	id	id	lava	12.24	1.56
29	i	Pico Rojo	PA-06-12	47°00'26.71"	71°46'29.28"	dike	2.76	0.07
30	i	Pico Rojo	PA-06-13B	id	id	neck	–	
31	i	S PRojo	PA-06-15	47°00'50.98"	71°45'54.68"	dike	4.41	0.54
32	i	S PRojo	PA-06-16	id	id	lava	3.10	0.08
33	i	S PRojo	PA-06-17	47°01'14.63	71°46'01.56"	neck	4.48	0.14
34	i	S PRojo	PA-06-18	47°01'17.08"	71°46'17.87"	neck	3.23	0.08
35	i	SW PRojo	PA-06-19	47°01'02.68"	71°47'09.82"	neck	6.85	0.15

36	i	SW PRojo	PA-06-20A	id	id	dike	2.12	0.45
37	i	C. Plomo	PA-06-05	47°00’24.05”	71°48’02.77”	clast	16.73	0.21
38	i	C. Plomo	PA-06-06	id	id	clast	16.05	0.40
39	i	C. Plomo	PA-06-07	id	id	clast	16.98	0.36
40	i	Alto Ghio	PA-06-22	47°04’44.47”	71°49’30.00”	lava	6.44	0.56
41	i	Alto Ghio	PA-06-23	id	id	dike	9.42	1.42
42	i	Alto Ghio	PA-06-24	id	id	dike	–	
43	i	Alto Ghio	PA-06-25	id	id	dike	–	
44	i	Alto Ghio	PA-06-26	47°03’22.93”	71°49’10.85”	lava	–	
45	i	Alto Ghio	TM01	47°04’16.82”	71°47’10.57”	lava	4.17	0.16
46	i	Alto Ghio	TM02	47°04’11.68”	71°46’26.54”	lava	6.41	0.22
47	i	Alto Ghio	TM03	47°3’59.90”	71°46’04.12”	lava	–	
48	d	Alto Ghio	PG 65	47°04’00.08”	71°47’01.03”	lava	4.98	0.15
49	d	Alto Ghio	PG 67	47°04’00.08”	71°47’01.03”	lava	6.95	0.24
50	d	Alto Ghio	PG 69	47°06’44.78”	71°44’14.17”	lava	4.32	0.23
51	d	Alto Ghio	PG 70	47°04’00.08”	71°47’01.03”	lava	2.96	0.09
52	d	Alto Ghio	PG 72	47°04’00.08”	71°47’01.03”	lava	3.91	0.11
53	d	Alto Ghio	PG 75	47°03’00.61”	71°49’00.19”	lava	4.81	0.32
54	d	MLBA-NE	PG 44	46°52’24.02”	70°44’08.02”	lava	1.08	0.04
55	d	MLBA-E	PG-121	47°06’28”	70°59’16.50”	lava	1.19	0.08
56	d	MLBA-E	PG-116	47°04’29.20”	71°01’21.10”	lava	9.97	0.25
57	d	MLBA-E	PG-119	47°06’08”	70°59’59.06”	lava	10.71	0.29
58	d	MLBA-E	PG-120	47°09’32”	70°59’34.50”	lava	12.18	0.34
59	d	MLBA-SE	PG 116	47°09’29.16”	71°01’21.14”	lava	9.97	0.25
60	d	MLBA-SE	PG 119	47°06’08.03”	70°59’59.64”	lava	10.71	0.29
61	d	MLBA-SE	PG 120	47°05’24.00”	71°01’35.04”	lava	12.18	0.34
62	d	MLBA-SE	PG 121	47°08’07.01”	70°55’49.01”	lava	1.19	0.08
63	d	MLBA-SE	PG-52	47°20’15”	70°48’18”	lava	10.23	0.26
64	d	MLBA-S	PG 130	47°09’32.04”	71°33’15.01”	lava	3.44	0.11
65	d	MLBA-S	PG 132	47°09’28.01”	71°33’25.02”	lava	3.32	0.10
66	d	MLBA-S	PG 133	47°09’30.02”	71°33’19.04”	lava	3.64	0.11
67	d	MLBA-S	PG 134	47°10’27.01”	71°32’29.04”	lava	3.89	0.14
68	d	MLBA-S	PG-51	47°10’14”	71°32’22”	lava	3.44	0.10
69	e	C Lapiz	PAT-12	47°06’44.78”	71°44’14.17”	neck	3.65	0.10
71	e	Mifeldi	PAT-20	47°05’51.47”	71°43’53.04”	dyke	3.08	0.13
72	e	Mifeldi	PAT-22	47°05’04.49”	71°43’14.59”	lacc	3.28	0.10
73	e	Pico Rojo	PAT-27	47°00’46.62”	71°45’26.46”	lava	3.34	0.09
74	e	Pico Rojo	PAT-29	47°00’24.41”	71°45’41.18”	neck	3.98	0.10
75	d	MLBA-W	PG-113	46°46’47”	71°42’07”	lava	5.84	0.21
76	d		PG-114	46°46’33.60”	71°42’47.90”	lava	10.84	0.28
77	d	MLBA-NW	PG-105	46°43’33”	71°42’06’	lava	6.53	0.25
78	d	MLBA-NW	PG-108	46°44’00.56”	71°41’02.00”	lava	5.80	0.19
79	d	MLBA-NW	PG-109	46°44’01.90”	71°41’01.39”	lava	5.64	0.19
80	d	NW	PG-143	46°38’41”	71°28’08”	lava	12.36	0.33

		MLBA						
81	Unp	MLBA-SW	PAT-26	47°00’46.62”	71°45’26.46”	lava	4.52	0.16
82	f	Belgrano	PL9	47°49’07.93”	71°30’07.96”	lava	3.79	0.13
83	g	San L.	DW-38	47°30’55.22”	72°14’02.29”	bt	6.40	0.40
84	h	San L.	Q-379	47°36’25.92”	72°20’17.74”	bt	6.60	0.50
85	Br	MLBA-E	MLBA-98-21	46°49’12”	70°54’36”	lava	11.03	0.14
86	Br	MLBA-SE	MLBA-01-49	47°10’12”	70°58’48”	lava	10.12	1.35
87	Br	MLBA-SE	MLBA-01-58	47°12’00”	71°	lava	10.27	0.79
88	Br	MLBA Sello	MLBA-01-38	46°54’00”	71°18’00”	lava	7.86	0.16
89	Br	MLBA Sello	MLBA-01-31	46°54’00”	71°06’00”	lava	7.71	0.07
90	Br	MLBA NE	RIN-96-01	46°46’12”	70°48’36”	lava	7.69	0.16
91	Br	Cerro Overo	MLBA98-003	46°49’12”	71°10’12”	lava	6.87	0.21
92	Br	Pico Rojo	MLBA-01-55	47°	71°45’36”	dacite	3.29	0.22
93	Br	Cerro Lapiz	MLBA-01-57	47°07’12”	71°43’48”	neck	3.18	0.04
94	Br	Cerro Lapiz	MLBA-01-50	47°07’12”	71°43’12”	lava	3.03	0.03
95	Br	Cerro Lapiz	MLBA-01-51	47°07’12”	71°43’12”	lava	2.42	0.03
96	Br	Sello W	MLBA-01-36	46°58’12”	71°25’12”	lava	1.73	0.02
97	Br	Sello W	MLBA-01-34	46°54’36”	71°24’	lava	1.72	0.02
98	Br	Cerro Lapiz	MLBA-01-54	47°06’	71°45’	Lava	1.71	0.02
99	Br	Rio Pintura	MLBA-01-30	47°03’36”	70°49’12”	Lava	1.49	0.05
100	Br	Lag. Honda	MLBA-98-15	47°03’00”	71°03’00”	Lava	1.39	0.04
101	Br	Sello E	MLBA-98-13	47°	70°54’00”	lava	1.37	0.03
102	Br	Sello E	MLBA-01-40	46°54’00”	71°05’24”	lava	1.36	0.05
103	Br	Sello E	MLBA-01-41	46°57’00”	71°04’12”	lava	1.34	0.10
104	Br	Lag. Honda	MLBA-98-14	47°03’00”	71°03’00”	lava	1.34	0.03
105	Br	E. Vizcaino	MLBA-98-17	47°06’00”	71°	lava	1.31	0.03
106	Br	Casa Piedra	MLBA-01-27	47°07’48”	70°51’36”	lava	1.29	0.03

107	Br	E. Vizcaino	MLBA-98-18	47°06'36"	70°58'48"	lava	1.25	0.03
108	Br	C. Colorado	MLBA-98-11	46°54'00"	71°11'24"	lava	1.14	0.06
109	Br	L. Rincon	AT-98-02	46°54'00"	70°42'00"	lava	1.74	0.03
110	Br	Arr. Telken	AT-96-01	46°52'12"	70°44'24"	lava	1.02	0.01
111	Br	E. Paloma	AT-98-03	46°55'12"	70°48'00"	lava	0.99	0.03
112	Br	Sello E	MLBA-01-32	46°55'12"	71°06'00"	lava	0.75	0.11
113	Br	Arroyo Page	AP-96-01	46°42'00"	70°50'24"	lava	0.76	0.01
114	Br	Sello E	MLBA-01-39	46°54'00"	71°12'36"	lava	0.75	0.03
115	Br	Rio Pintura	MLBA-01-29	47°03'36"	70°49'12"	lava	0.74	0.01
116	Br	Cerro Leon	MLBA-98-10	46°58'12"	71°19'12"	lava	0.43	0.01
117	Br	Sello W	MLBA-01-35	46°57'36"	71°25'48"	lava	0.34	0.03
118	Br	Sello W	MLBA-01-37	46°58'12"	71°19'48"	lava	0.34	0.01
119	Br	Sello W	MLBA-01-33	46°57'00"	71°21'36"	lava	0.33	0.01
120	Br	Cerro volc.	CV-98-02	46°42'00"	70°45'00"	lava	0.11	0.01
121	Br	Rio Pintura	MLBA-98-20	47°06'00"	70°48'00"	lava	0.07	0.02
122	Br	Rio Pintura	MLBA-01-47	47°05'24"	70°50'24"	lava	0.07	0.01

Table S1. K/Ar and $^{39}Ar/^{40}Ar$ ages from Tertiary magmatic rocks located along the Eastern front of the Andes extending from 46°25' to 47°10'S. Ages from (a) Pelleter (2003); (b) Morata et al. (2002); (c) Espinoza et al. (2005); (d) Guivel et al. (2006); (e) Espinoza et al. (2006 and 2007); (f) Gorring et al. (1997); (g) Welkner (1999); (h) Suarez and De la Cruz (2000); (i) Boutonnet et al. (2010); (Br) Brown et al. (2004); (Ba) Baker et al. (1981); (Pa) Pankurst et al. (1999). Ref– Reference; Sample–Number as it appears in original works.

Avell.–Avellanos; Nieves–Rio de Las Nieves (W of MCC), MCC–Meseta de Chile Chico; Alto Ghio–Alto Rio Ghio; MLBA–Meseta de Lago Buenos Aires; San L.–San Lorenzo; Plomo–Cerro Plomo; Ne Plomo–Near Cerro Plomo; Ne Projo–Near Pico Rojo.

ACBFS	Argentina-Chile Border fault system
ACR	Antarctic Cold Reversal
AVZ	Austral Volcanic Zone
CB	Cosmelli Basin
CCP	Common Conversion Point
CGS	Central Glacial System
CP	Cochrane-Pueyrredon
GPG	Great Patagonia Glaciation
CPGL	Cochrane-Pueyrredon Glacial Lake
CTJ	Chile Triple Junction
ELGS	East Lateral Glacial System
FRTSS	Furioso River Thin-Skinned Structure
FZ	Fracture Zone
GCBA	General Carrera-Buenos Aires
GCBAGL	General Carrera-Buenos Aires Glacial Lake
GPG	Great Patagonian Glaciation
LOFS	Liquine Ofqui Fault System
LGM	Last Glacial Maximum
MAT	Main Andean Thrust
MCC	Meseta de Chile Chico
MLBA	Meseta del Lago Buenos Aires
MMCO	Mid Miocene Climatic Optimum

MU1	Main Unconformity 1
MU2	Main Unconformity 2
MZR	Monte Zeballos Ridge
MZPRS	Marques-Zeballos Pass Ramp system
NAZ	Nazca Plate
NPI	North Patagonia Icefield
PSW	Patagonia Slab Window
SAM	South American Plate
SAM MOHO P	South American Plate MOHO Plateau
SCR	South Chile Ridge
SCR 0	South Chile Ridge segment 0
SCR -1	South Chile Ridge segment -1
SPI	South Patagonia Icefield
SSVZ	Southern South Volcanic Zone
WLGS	West Lateral Glacial System

Table S2. List of Acronyms in alphabetic order